galaxies

MDPI

Review

Cosmic Ray Processes in Galactic Ecosystems

Ellis R. Owen [1,*], Kinwah Wu [2], Yoshiyuki Inoue [1,3,4], H.-Y. Karen Yang [5,6,7] and Alison M. W. Mitchell [8]

1 Theoretical Astrophysics, Department of Earth and Space Science, Graduate School of Science, Osaka University, Toyonaka 560-0043, Osaka, Japan
2 Mullard Space Science Laboratory, University College London, Holmbury St. Mary, Dorking, Surrey RH5 6NT, UK
3 Interdisciplinary Theoretical & Mathematical Science Program (iTHEMS), RIKEN, 2-1 Hirosawa, Saitama 351-0198, Japan
4 Kavli Institute for the Physics and Mathematics of the Universe (WPI), UTIAS, The University of Tokyo, Kashiwa 277-8583, Chiba, Japan
5 Institute of Astronomy, National Tsing Hua University, Hsinchu 30013, Taiwan
6 Center for Informatics and Computation in Astronomy, National Tsing Hua University, Hsinchu 30013, Taiwan
7 Physics Division, National Center for Theoretical Sciences, Taipei 10617, Taiwan
8 Erlangen Centre for Astroparticle Physics, Friedrich-Alexander-Universität Erlangen-Nürnberg, Nikolaus-Fiebiger-Str. 2, 91058 Erlangen, Germany
* Correspondence: erowen@astro-osaka.jp

Abstract: Galaxy evolution is an important topic, and our physical understanding must be complete to establish a correct picture. This includes a thorough treatment of feedback. The effects of thermal–mechanical and radiative feedback have been widely considered; however, cosmic rays (CRs) are also powerful energy carriers in galactic ecosystems. Resolving the capability of CRs to operate as a feedback agent is therefore essential to advance our understanding of the processes regulating galaxies. The effects of CRs are yet to be fully understood, and their complex multi-channel feedback mechanisms operating across the hierarchy of galaxy structures pose a significant technical challenge. This review examines the role of CRs in galaxies, from the scale of molecular clouds to the circumgalactic medium. An overview of their interaction processes, their implications for galaxy evolution, and their observable signatures is provided and their capability to modify the thermal and hydrodynamic configuration of galactic ecosystems is discussed. We present recent advancements in our understanding of CR processes and interpretation of their signatures, and highlight where technical challenges and unresolved questions persist. We discuss how these may be addressed with upcoming opportunities.

Keywords: cosmic rays; galaxy formation and evolution; interstellar medium; circumgalactic medium; outflows; inflows; star-formation; molecular clouds; feedback

Citation: Owen, E.R.; Wu, K.; Inoue, Y.; Yang, H.-Y.K.; Mitchell, A.M.W. Cosmic Ray Processes in Galactic Ecosystems. *Galaxies* **2023**, *11*, 86. https://doi.org/10.3390/galaxies11040086

Academic Editor: Alberto C. Sadun

Received: 16 June 2023
Revised: 11 July 2023
Accepted: 12 July 2023
Published: 16 July 2023

1. Introduction

Constructing a holistic scenario of the formation and evolution of galaxies requires the integration of information from macroscopic (e.g., dynamical and thermal) and microscopic (e.g., interaction and radiative loss) processes. One of the technical hurdles we face in achieving this is to resolve the multi-channel feedback processes operating between various internal and external components of galaxies, which themselves reside in a broad range of environments that evolve over cosmic time. Despite rapid progress, our current understanding of galactic feedback is still at an infant stage. Most existing work to date has been phenomenological. It mainly focuses on either thermo-mechanical and radiative effects. An example of the study of thermo-mechanical feedback is in the investigation of the energy of supernova (SN) explosions, where the inputs are based on theoretical and numerical modelling (e.g., [1–4]), and gauged against observational measurements [5–7]. An example of the study of radiative feedback is the investigation of star-forming cycles

regulated by stellar [8] or active galactic nucleus (AGN) activities (see, e.g., [9,10]). Radiative feedback played a particularly important role in the early Universe, influencing the modes and efficiency of star-forming episodes and their duty cycles [11].

Feedback dynamics in galaxies are intrinsically complex. They extend beyond the effects driven by SN explosions and stellar or AGN activities, which are essentially internal processes operating within or around a galaxy. A more complete scenario should encompass effects brought about by all agents that can facilitate the exchange of energy and momentum, including shared processes that operate between galaxies, their neighbours and their surroundings. Cosmic rays (CRs) serve this purpose well. They deposit energy and momentum as they traverse their parent galaxies, and they also deliver energy and momentum to neighbouring galaxies and their surrounding environments.

CRs interact with the magnetic and radiation fields of galaxies and participate in subatomic hadronic and leptonic processes. Their presence in galaxies is evident through observational signatures across the electromagnetic spectrum [12,13]. These CRs contain a substantial amount of energy, and their contribution to the energy budget in a typical galaxy is comparable to that contained by radiation, magnetic fields and thermal gas. They are therefore a significant ingredient in a typical galaxy, which can be amplified when CR accelerators are abundant (e.g., in star-forming galaxies; see [14]). Their presence not only modifies outflows from star-forming galaxies (see, e.g., [15]) but also drives global feedback processes within the broader galactic ecosystem (see [16,17]).

In this review, we provide an overview of the current state of understanding of CR processes in galaxies. We present a cross-section of recent progress in the field, particularly highlighting developments surrounding the feedback impact of CRs. We discuss the origins of CRs, their propagation through different components of galactic ecosystems, and their role in regulating thermal and hydrodynamic configurations of galactic environments. The scope of this paper focuses on scales from molecular clouds to the circumgalactic medium (CGM). We emphasize the implications of various CR process for galaxy evolution and star formation, examining the underlying interaction and propagation microphysics, as well as their observational signatures. This complements the recent review paper by Ruszkowski and Pfrommer [18], which provides a detailed introduction to the acceleration and transport physics of CRs, discusses their observable signatures and dynamical impacts, and includes a pedagogical review of the physics of CR feedback from the scales of individual SNe and molecular clouds to the CGM and galaxy clusters. Our focus is primarily on the effects of persistent sources of CRs in galaxies, with detailed discussion of hadronic (pp and pγ) interactions, including their application to stellar and galactic scale jet sources. We exclude burst-like or transient sources (e.g., neutron star–neutron star mergers, γ-ray bursts, fast radio bursts or tidal disruption events) and restrict the scope of our discussion to CR sources and processes up to the scale of individual galactic ecosystems. We therefore exclude larger structures such as groups, clusters, and large, strong AGN jets (weak jets in radio-quiet AGNs that terminate at the scale of a kpc are considered in Section 4.1).

This review is arranged as follows: Section 2 introduces the relevant CR physics that underlies the subsequent discussions. Section 3 discusses the origins and impacts of CRs within the interstellar medium of galaxies. Section 4 considers CR processes in high-energy environments, with a particular focus on systems associated with relativistic jets on galaxy scales or smaller. Section 5 discusses CRs in individual galaxies and galactic ecosystems, including the CGM. Finally, Section 6 presents our concluding remarks and discusses potential future research directions in light of new and upcoming observational and theoretical opportunities and developments.

2. Cosmic Ray Physics in Galaxies

2.1. Particle Transport

A simple prescription of CR transport that retains all essential physical aspects can be expressed in terms of the transport equation:

$$\left\{\frac{\partial}{\partial t} - \underbrace{\nabla\cdot[D\nabla - (u+\bar{v}_{\rm A})]}_{\text{Term 1}} - \underbrace{\frac{\partial}{\partial p}\left[p^2\mathcal{D}_{pp}\frac{\partial}{\partial p}\frac{1}{p^2}\right]}_{\text{Term 2}} + \underbrace{\frac{\partial}{\partial p}\left[\dot{p} - \frac{p}{3}\nabla\cdot(u+\bar{v}_{\rm A})\right]}_{\text{Term 3}}\right\}\psi_{\rm X} = \Gamma_{\rm X} - \Lambda_{\rm X}\psi_{\rm X}\,, \quad (1)$$

where the differential particle density of a CR species X per unit of momentum p is written as $\psi_{\rm X}$. $\Gamma_{\rm X}$ is a source term, describing the injection of CRs of species X. This may include primary CRs accelerated in a population of sources, or secondary CR species produced by interactions of parent nucleons. $\Lambda_{\rm X}\psi_{\rm X}$ is an absorption term. It describes stochastic interaction events that result in the destruction or absorption of a particle. It can also be used to describe catastrophic energy losses, where a substantial fraction of the energy of a particle is lost in a single interaction event.

Term 1 in Equation (1), accounts for the spatial transport of the CR distribution. This includes diffusion, specified by the spatial diffusion coefficient D. It also includes advection of CRs in a background bulk flow of velocity u. Under advection, the total propagation speed of the CRs is be $(u + \bar{v}_{\rm A})$. This is the sum of the background fluid velocity u that is carrying the CRs, and the effective velocity of CRs in their local medium. The main source of scattering between CRs and their surrounding plasma is their interaction with magnetohydrodynamic (MHD) waves. This is dominated by CR scattering in Alfvénic waves, which are driven by the CR gyro-resonant streaming instability. Assuming that the resonant waves are sufficiently energetic, the strong scattering of the CRs practically limits their velocity to the mean Alfvén speed $\bar{v}_{\rm A} \approx \langle|B_0|\rangle/\sqrt{4\pi n_i m_i}$, averaged over the direction of motion of the waves (see, e.g., [19]). This provides a good approximation to their local effective velocity. Here, n_i and m_i are the mass and number density of the background ions, respectively. *Term 2* describes the momentum diffusion of the CRs. This is usually dominated by diffusive re-acceleration, characterised by the energy-dependent momentum-space diffusion coefficient $\mathcal{D}_{pp}$. *Term 3* describes the momentum variation of CRs due to gains or losses, including those associated with the movement of the CR fluid and advection (e.g., adiabatic losses). In most galactic scenarios of interest we will discuss in this paper, this term is dominated by particle cooling processes.

The precise physics that is introduced to each of the terms in Equation (1) depends on the CR species being considered, X, and the exact configuration of the local medium. In the context of a galaxy, it is usually sufficient to consider only CR protons and electrons (including any collisional processes that convert one species into another—for example, hadronic interactions). Diffusive re-acceleration processes (term 2) may also often be neglected away from CR sources. Moreover, some parts of the interstellar medium (ISM) are not subject to significant bulk advective flows or strong turbulence (see [20] for examples of such simplifications). These factors allow for the considerable simplification of the transport equation. In many scenarios, analytic or semi-numerical solutions can often be constructed which offer a meaningful description of the dominant physics. In cases where more complex approaches are required to properly capture the subtle details of CR transport, more sophisticated numerical CR propagation and interaction codes are used to solve Equation (1) without invoking certain assumptions (e.g., see [21–24]). Many of the subtle effects handled by these codes fall outside the scope of this review. However, those that are essential to consider for the global evolution of galaxies are discussed in the following sections.

2.1.1. The Resonant Cosmic Ray Streaming Instability and Self-Confinement

In free space, CRs propagate by streaming at close to the speed of light c. However, in magnetized, ionized media, they are scattered by MHD waves. In the presence of CRs streaming at speeds faster than the local Alfvén speed, MHD waves become unstable to growth. Resonant wave modes corresponding to the gyro-radius of passing CRs are rapidly amplified. This is the resonant mode of the CR streaming instability [25].[1] It strengthens CR scattering effects leading to highly non-linear, and locally isotropic CR propagation. CRs are slowed down to the local Alfvén speed and efficiently confined (the self-confinement picture). A dynamical coupling between the CRs and their background plasma is also established, where the medium can be altered by non-thermal pressure gradients associated with the CRs. It can also be heated by CR energy transferred to MHD modes which then undergo damping (see Section 2.1.2).

In the Galactic context, the resonant CR streaming instability has been shown to produce observed breaks in the CR spectrum [20,26], while the self-confinement effect can set the CR transport physics within the Galaxy (for reviews, see [27,28]). An alternative model of CR transport has also been considered, called the extrinsic turbulence picture. In this scenario, CRs also interact resonantly with the turbulence. However, instead of scattering off waves that have been amplified by the resonant streaming instability, they scatter off pre-existing waves formed by turbulent cascades. In this picture, CR propagation is practically reduced to advection with the background gas, and results in no overall energy transfer between the CR and thermal fluids [29].[2]

2.1.2. Magnetohydrodynamic Wave Damping and Implications for Cosmic Ray Propagation

In the self-confinement picture, the growth of MHD modes is balanced against damping processes. If damping is severe, the growth rate of CR streaming instabilities is moderated. In extreme cases, damping can prevent the growth of MHD modes entirely. More typically, it operates to limit the CR streaming instability and regulates the amplitude of Alfvén waves that develop. This determines the strength of CR scattering and confinement, and sets the effective diffusion speed for CR transport [30]. The effectiveness of self-confinement and individual damping processes depend on the local conditions and CR energy. In the ISM, the main damping mechanisms often considered are non-linear damping, and ion-neutral damping. In non-linear damping, a turbulent cascade develops in wave-wave interactions, leading to dissipation at small scales. Ion-neutral damping instead arises from collisions between neutral particles in a semi-ionized medium, and the ions that are coupled to the MHD waves. Individual collisions transfer kinetic energy from the ions to neutral particles, which damps MHD waves and thermalizes their energy into the background medium.

Ion-neutral damping is more severe at longer wavelengths and in regions of higher density with a low ionization fraction. It is the dominant means of moderating the growth of MHD modes in most components of the ISM [20], with particular suppression expected in molecular clouds (except for waves that are resonant with CRs of very high energies, above a few TeV [20]). Other damping mechanisms have also been considered. For example, Coulomb collisions can affect MHD waves in ionized or partially ionized media. In highly ionized ISM phases, simulations have demonstrated they can suppress pressure anisotropies and boost the magnetic field amplification [31]. Dust grains in the ISM have also been shown to damp Alfvén waves. This is more severe in well-ionized parts of the ISM, where CR diffusion can be noticeably enhanced in the presence of dust compared to the standard self-containment picture [32].[3]

2.1.3. The Non-Resonant Cosmic Ray Streaming Instability

The non-resonant streaming instability (NRSI) arises when a flux of CRs passes through a plasma.[4] Their current generates magnetic perturbations, which impart a force into the background field. These drive velocity fluctuations and induce an electric field. The electric

field amplifies the magnetic perturbations, creating a feedback loop to cause MHD wave growth. The wavelengths most affected are generally much shorter than the CR gyro-radius. Their growth rate can be very large in some situations, particularly when the CR velocity or abundance is high or the magnetic field is strong. However, wave growth does not occur when the effective CR velocity is below a critical value, $v_{\rm NR} = cU_{\rm B}/U_{\rm CR}$ [20], where $U_{\rm B}$ and $U_{\rm CR}$ are the energy densities of the magnetic fields and CRs, respectively. The NRSI therefore only operates in certain situations. In typical ISM conditions it is inconsequential. However, it is important for shocks propagating in the cold ISM [34]. These may arise in an isolated SN remnant (SNR) during its first $\sim 10^4$ yr [35,36]. For SNR shocks propagating in a hot super-bubble, a modified form of the NRSI may also operate when CR densities are high (about 1000 times that of the Galactic ISM), or if the magnetic field in the bubble is below a few μG [37]. In this case, the growth of the non-resonant instability may be weaker [34,38,39].

Conditions where the NRSI is important are typical of those often associated with CR sources (see also Sections 3.1.1 and 3.1.3). The NRSI has been shown to be essential for accelerators to attain the maximum observed CR energies (see [40,41] for recent reviews). Specifically, it can account for the fast growth of MHD waves around SNR shocks [42], and can produce the inferred strong magnetic fields needed for CR acceleration up to PeV energies (see, e.g., [43], or [44] for a review). The wavelengths most strongly amplified by the NRSI are much shorter than the CR gyro-radius. This means they do not effectively scatter CRs, and cannot contain them to sustain their acceleration unless the waves amplified by the NRSI undergo an inverse-cascade to larger modes. The mechanism underlying such an inverse cascade is currently unsettled, although some proposals have noted that the dominant wavelength in the non-resonant instability increases with time, in proportion to $(\delta B/B_0)^2$ [45]. This could boost CR scattering and containment if the inverse-cascade timescale is shorter than advection.

The NRSI may operate in conjunction with the resonant streaming instability. For example, in the region surrounding CR sources, the excitation of both resonant and non-resonant modes enhances scattering and produces strong CR pressure gradients [46]. These pressure gradients can drive the formation of CR-dominated bubbles of gas and self-generated magnetic fields. They expand in to the ISM until reaching pressure balance with the surrounding medium, typically at sizes of a few 10s of pc [47]. Within the bubbles, CR diffusion is suppressed [46]. If this suppression is sufficiently severe, CRs can become trapped within these structures [48].

2.2. Particle Interactions

CRs are inhomogeneous collections of particles consisting of atomic nuclei, bare baryons and mesons, leptons and ultra-relativistic particles such as neutrinos. Here we put focus on the CR particles involved in collisional and/or hadronic interactions. This is because they carry the greatest energy density and momentum, and are most strongly engaged with feedback processes in galaxies. Leptonic CRs are primarily composed of electrons and positrons. Since both electrons and positrons undergo similar interactions, we refer to them collectively as "electrons" hereafter for convenience. Within galactic environments, electrons experience collisional ionization interactions, free–free cooling, and radiative cooling processes in photon and magnetic fields. Typically, electrons lose their energy rapidly and are less involved in transport throughout galactic ecosystems. Instead, they are more important in mediating energy deposition processes, such as thermalization.

Hadronic CRs are primarily protons, although heavier nuclei are also present. The dominant interaction mechanisms for heavy nuclei in galactic ecosystems are essentially the same as those for protons. At low energies, below a few hundred MeV, collisional and ionization processes serve as the predominant channels of interaction. However, at GeV energies and above, pγ (proton–photon) and pp (proton–proton) processes can become important. These processes result in the rapid production of electrons, neutrinos, and high-energy photons through pion formation. They play a role in transferring energy

from a non-thermal hadronic CRs to thermal gas by the formation and thermalization of secondary CR electrons (e.g., [14,49]). Hadronic CRs, from protons to heavy nuclei, are engaged in pion-producing interactions and Bethe–Heitler pair production in radiation fields. Despite the variations in the nuclei of a CR ensemble, their fundamental hadronic interaction processes remain the same. Therefore, without loss of generality, we illustrate these interactions using free protons (p) as a representative example of high-energy hadronic CR interactions in matter (baryon) and radiation (photon) fields.

2.2.1. pp Interactions

The pp interaction between CR protons and baryon leads to the following dominant pion production channels:

$$\mathrm{p}+\mathrm{p}\rightarrow\begin{cases}\mathrm{p}\Delta^{+}\rightarrow\begin{cases}\mathrm{pp}\pi^{0}\xi_{0}(\pi^{0})\xi_{\pm}(\pi^{+}\pi^{-})\\ \mathrm{pp}\pi^{+}\pi^{-}\xi_{0}(\pi^{0})\xi_{\pm}(\pi^{+}\pi^{-})\\ \mathrm{pn}\pi^{+}\xi_{0}(\pi^{0})\xi_{\pm}(\pi^{+}\pi^{-})\end{cases}\\ \mathrm{n}\Delta^{++}\rightarrow\begin{cases}\mathrm{np}\pi^{+}\xi_{0}(\pi^{0})\xi_{\pm}(\pi^{+}\pi^{-})\\ \mathrm{nn}2\pi^{+}\xi_{0}(\pi^{0})\xi_{\pm}(\pi^{+}\pi^{-})\end{cases}\end{cases}. \tag{2}$$

Here, ξ_0 and $\xi_\pm$ are the multiplicities for neutral and charged pions, respectively. The Δ^+ and Δ^{++} baryons are the resonances (see [50,51]). This interaction operates above a threshold energy of $E_{\mathrm{p}}^{\mathrm{th}}=(2m_{\pi^0}+m_{\pi^0}^2/2m_{\mathrm{p}})\mathrm{c}^2\approx 0.28$ GeV, which is the proton energy required for the production of a neutral pion through the channel $\mathrm{pp}\rightarrow\mathrm{pp}\pi^0$.

The branching ratios across all relevant channels for the production of each pion species $\{\pi^+,\pi^-,\pi^0\}$ is $\{0.6,0.1,0.3\}$ at 1 GeV. At higher energies, this levels out to $\{0.3,0.4,0.3\}$ [52]. Overall, approximately 30 percent of the total interaction energy is transferred to neutral pions, while the remainder goes to charged pion production. The neutral pions predominantly decay into two photons through an electromagnetic process:

$$\pi^{0}\rightarrow 2\gamma\,. \tag{3}$$

It has a branching ratio of 98.8 percent and occurs over a timescale of 8.5×10^{-17} s [53]. The charged pions decay into electrons and neutrinos through a weak interaction:

$$\begin{aligned}\pi^{+}&\rightarrow\mu^{+}\nu_{\mu}\rightarrow\mathrm{e}^{+}\nu_{\mathrm{e}}\bar{\nu}_{\mu}\nu_{\mu}\\ \pi^{-}&\rightarrow\mu^{-}\bar{\nu}_{\mu}\rightarrow\mathrm{e}^{-}\bar{\nu}_{\mathrm{e}}\nu_{\mu}\bar{\nu}_{\mu}\,.\end{aligned} \tag{4}$$

These channels have a branching ratio of 99.9 percent and occur over a timescale of 2.6×10^{-8} s [53]. Around 3/4 of the energy is inherited by neutrinos in these decay processes. The remainder is transferred to the secondary electrons.

The total inelastic cross-section and formation of secondary products in the pp interaction has been extensively investigated. Monte Carlo (MC) event generators have been developed, which simulate high-energy collision events to give a precise description of hadronic interactions in light of new accelerator data, including from the Large Hadron Collider (LHC). These generators handle complex calculations and predict many quantities that show good agreement with experimental data (e.g., [54]). Several classes of these MC event generator codes exist. General purpose examples include `HERWIG` [55], `SHERPA` [56], `GEANT4` [57–59] and `PYTHIA` [60–62], which include both Standard Model and beyond Standard Model physics. Other codes include particularly sophisticated high energy hadronic physics models. These include `Phojet` [63], `DPMJET` [64] and `EPOS` [65]. Other types of MC codes specialize in air shower simulations, and are particularly concerned with high energy secondary particle production. These include `SIBYLL` (e.g., [66–69]) and `QGSJET` [70,71], and can be widely useful to inform models of secondary particle production in astrophysical applications.

To reduce computational requirements, parametrizations based on pp interaction MC event generators have also been developed. These provide analytical descriptions of key quantities such as the total inelastic cross-section and γ-ray production spectra [72]. Some parametrizations also include inclusive production spectra of secondary electrons and neutrinos [73,74], making them versatile alternatives to expensive numerical computations. Interpolated codes have also been created to provide these parametrizations as user-friendly computational tools (e.g., [75,76]). While these parametrizations are suitable for use in a wide range of astrophysical settings and bypass the need to conduct intensive numerical calculations for pp collisions, they are also inherently limited. In particular, they integrate out intermediate particles in interaction and decay chains, and so do not accurately capture rapidly time-varying systems or situations where conditions lead to noticeable cooling of secondary intermediaries. Therefore, careful consideration should be given to the suitability of these parametrizations in more extreme or highly transient situations.

2.2.2. pγ Interactions

pγ processes are less straightforward to model. In many astrophysical environments, the contribution of the target photon field to the total interaction energy cannot be neglected. As such, pγ interaction calculations depend on both the energy of the CR protons involved in the interaction, and the energy distribution of the target photon field. pγ interactions can be categorized into photo-pion production and Bethe–Heitler pair production interactions. Photo-pion production, similar to pp interactions, can generate various hadrons, including charged and neutral pions, neutrons, and protons. On the other hand, photo-pair production predominantly results in the formation of electron–positron pairs. It can also produce higher-energy lepton pairs such as muons and anti-muons. These higher-mass lepton pairs can subsequently decay into electrons and positrons, with neutrinos as a by-product.[5]

Photo-pion production occurs when incident protons collide with the photons of a radiation field. The dominant interactions in photo-pion production are resonant single-pion production, direct single-pion production, and multiple-pion production [78]. Although other processes such as diffractive scattering can arise, they are generally less significant. The total cross-section of photo-pion production is therefore the sum of the cross-sections of these three main interactions. Resonant single-pion production occurs through the formation of Δ^+ particles. These decay through two major channels that produce charged and neutral pions (see [79]):

$$\mathrm{p}\gamma \rightarrow \Delta^+ \rightarrow \begin{cases} \mathrm{p}\pi^0 \rightarrow \mathrm{p}2\gamma \\ \mathrm{n}\pi^+ \rightarrow \mathrm{n}\mu^+\nu_\mu \\ \qquad\quad \hookrightarrow \mathrm{e}^+\nu_\mathrm{e}\bar{\nu}_\mu \end{cases} . \tag{5}$$

The branching ratios for the $\Delta^+ \rightarrow \pi^0$ and $\Delta^+ \rightarrow \pi^+$ channels are 2/3 and 1/3, respectively. Direct pion production is less efficient. While single-pion production dominates at lower energies, at higher energies multi-pion production becomes important (see [78]).

Some neutrons form in the process as given by Equation (5). These have a half-life of about 880 s [80]. If they do not first collide with other particles or photons, they undergo β^--decay, $\mathrm{n} \rightarrow \mathrm{pe}^-\bar{\nu}_\mathrm{e}$. They may instead undergo further interaction with the radiation field. This leads to additional p and π^- production,

$$\mathrm{n}\gamma \rightarrow \Delta^0 \rightarrow \begin{cases} \mathrm{p}\pi^- \\ \mathrm{n}\pi^0 \end{cases} , \tag{6}$$

with branching ratios of 1/3 for the $\Delta^0 \rightarrow \pi^-$ channel, and 2/3 for the $\Delta^0 \rightarrow \pi^0$ channel [81]. When taking the additional charged pions produced in the residual interactions into account (including $\mathrm{p}\gamma \rightarrow \Delta^{++}\pi^-, \Delta^0\pi^+$), each of the pion species are produced in roughly equal proportion (e.g., [82]).

pγ interactions in astrophysical settings can be accurately modeled using MC event generator software, such as SOPHIA [78,83]. This provides a comprehensive framework to thoroughly study pγ interactions, taking into account detailed cross-section data. Alternatively, to alleviate computational demands, self-consistent models are available that simplify the treatment of interaction kinematics, but adopt the same underlying particle physics as SOPHIA [81]. These models account for the production of the Δ-resonance and higher resonances, multi-pion production, and direct pion production. By separately calculating the contributions of pion intermediaries without integrating out secondaries, they preserve the essential particle physics involved. In situations where the retention of this detail is unnecessary and computational efficiency is a priority, analytical parametrizations for pγ interactions have also been developed (e.g., [84]).

2.2.3. Comparison between pp and pγ Channels in Galactic Environments

In Figure 1, the relative importance of pp and pγ interactions is estimated by comparing the energy loss path lengths of CR protons in different galactic environments. These environments are characterized by parameter values listed in Table 1, and include various components of the ISM of our Galaxy, as well as average conditions expected in starburst galaxies, cosmic noon galaxies, and high-redshift protogalaxies. In all of these cases, it can be seen that pp interactions dominate over pγ interactions at most energies. The pγ channel only becomes important at CR energies above $\sim 10^7$ GeV, with the exact transition energy being strongly influenced by the specific physical conditions. The number of CRs at these energies is generally very low. It may therefore be considered that the pγ interaction only has a negligible involvement in CR feedback in galaxies. Instead, the pp interaction is most involved in regulating the impacts of hadronic CRs in galactic ecosystems.

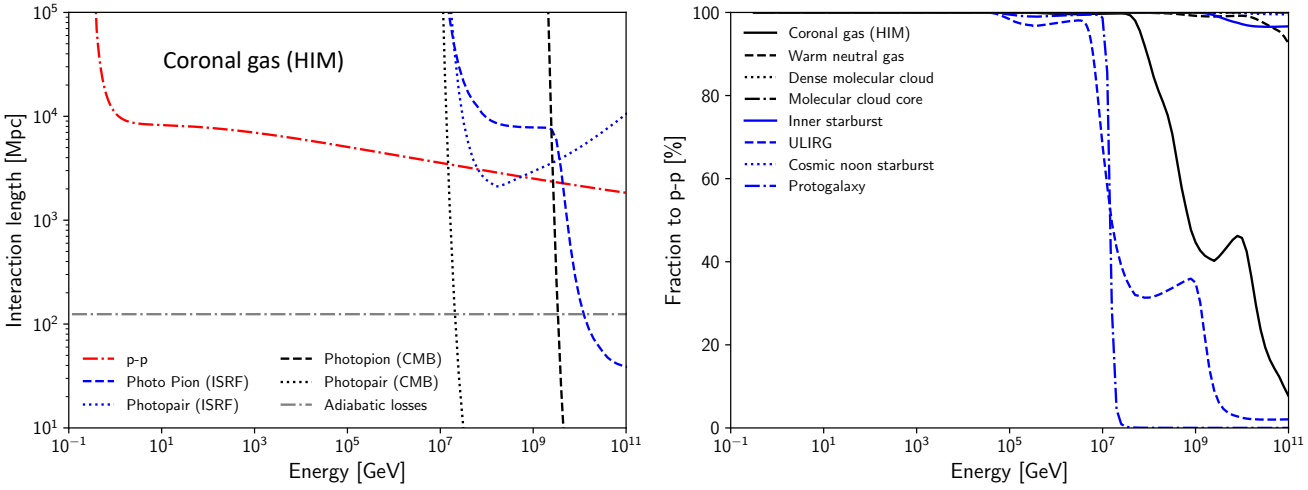

Figure 1. (**Left**) CR proton losses in terms of effective interaction path lengths for conditions representative of the hot ionized medium (HIM). Losses shown are due to pp interactions, pγ (photo-pion and photo-pair) interactions in interstellar radiation fields, pγ interactions in the cosmological microwave background (CMB), and adiabatic losses due to the expansion of the Universe. pγ processes are inconsequential below energies of $\sim 10^7$ GeV, with pp processes in this hot rarefied gas also being relatively unimportant. The pp interaction rate scales with gas density, and so would become much more severe in warm neutral gas or dense molecular clouds (cf. Table 1). (**Right**) Fractional energy transfer in hadronic collisions to the pp channel. At lower energies, pp losses entirely dominate hadronic processes. At higher energies, hadronic CRs are more likely to engage in pγ interactions in environments with strong radiation fields. The pγ path lengths shown here are computed using analytic approximations rather than by full numerical calculation. This can differ from a thorough treatment by as much as an order of magnitude [82], but is not consequential for the conclusions here.

Table 1. Summary of parameters adopted for galaxy and ISM conditions in hadronic pp and pγ path length calculations, as shown in Figure 1.

Model	ISRF Energy Density		ISRF Radiation Temperatures		Gas Density	Redshift
	Stars	Dust	Stars	Dust		
Coronal gas/HIM [a]	0.66	0.31	3000	17	0.004	0
Warm neutral gas [a]	0.66	0.31	3000	17	0.6	0
Dense molecular cloud [a]	–	–	–	–	10^3	0
Molecular cloud core [a]	–	–	–	–	10^6	0
Inner starburst [b]	79.2 [d]	1.5×10^6	18,000 [e]	135	6.5×10^5	0.018
ULIRG [c]	673	310	18,000 [e]	135	0.1 [f]	0.64
Cosmic noon starburst [g]	2630	1230	18,000 [e]	57	10^4	2.33
Protogalaxy [h]	2.77	1.30	18,000 [e]	40	0.0003 [i]	9.11

Notes: [a] Densities for the phases of interstellar gas and Galactic ISRF properties adopted from [85]. For the dust component of the ISRF, we adopt the properties of the dominant component, although note that around 1/3 of the total dust emission power is thought to be emitted by polycyclic aromatic hydrocarbons (PAH) which would not strictly emit radiation of the indicated temperature. [b] Nearby inner starburst parameters are adopted to emulate the inner circum-nuclear disk of Arp 220. Values taken from [86]. For dust emission properties, these values were originally derived from [87,88]. [c] ULIRG parameters are adopted to emulate the nearby Hyper Luminous IR galaxy (HyLIRG) IRAS F14537+1950, where the ISRF intensity is scaled by bolometric luminosity compared to the Galaxy, from [89]. Dust temperatures are assumed to be the same as the central nuclear disk of Arp 220, as heating by intensive star-formation activity would be similar. [d] Interstellar radiation field (ISRF) stellar energy density is scaled from that of the Milky Way by star-formation rate, assuming a rate of 120 $M_\odot\,yr^{-1}$ for Arp 220 (following the estimate by Ref. [86]). [e] Temperature of starburst galaxy stellar radiation field component adopted from [90], see also [91]. [f] Estimated from the Galactic column density towards F1437+1950 from Ref. [92], assuming a kpc sized galaxy. [g] Properties based on the Eyelash galaxy, SMM J2135-0102 [93]. This is a lensed, dusty cosmic noon submillimeter galaxy where ISRF intensities are scaled against the Milky Way. [h] Based on the properties of the lensed high-redshift galaxy MACS 1149-JD1, with physical parameter choices informed by Ref. [94]. The ISRF energy densities are scaled by star-formation rate against Milky Way values. [i] Based on the dust mass obtained by [94], assuming a standard gas-to-dust ratio of 100 [95].

3. Cosmic Rays in the Interstellar Medium

3.1. Origins of Cosmic Rays in Galaxies

CRs originate in violent, magnetized astrophysical environments. Within galaxies, core-collapse (CC) supernovae (SNe) and their remnants have traditionally been regarded as the dominant factories of CRs (see [96]). This view has been particularly motivated by energy budget arguments, with SNRs among only a few candidate source types that can sustain the observed energy flux of CRs in our Galaxy (e.g., [97,98]). In recent years, the SNR source paradigm has been increasingly challenged. The capability of stellar end products to inject Galactic CRs with the required spectra and chemical abundances to match the observed properties of CRs has become less certain. Moreover, the lack of clear detections at the highest energies in γ-rays casts doubt on the capability of SNRs to supply all of the observed CR flux detected on Earth (for an overview of these challenges, see [99]). New types of object have therefore been considered, including star-forming regions and star clusters. These have enjoyed an increasing bank of recent observational support. They have been firmly established as the origins of at least some CRs in galaxies, and have even been proposed as an alternative to SNRs as the dominant source in the Milky Way. Our understanding of the origins of CRs in galaxies has developed considerably in recent years. This section provides an overview of the current status of the field, including the main CR source candidates being discussed and developments arising from new observational insights at near-PeV energies.

3.1.1. Stellar End-Products

SNe in our Galaxy occur at an approximate rate of once per ∼35 years [100] and are natural candidates as CR sources. CC SNe harbor particularly favourable conditions for

particle acceleration. These include strong, fast magnetized shocks and an abundance of seed particles in the ionized circumstellar medium (CSM). If invoking SNe and their remnants as the only source of CRs in the Galaxy, they must convert around 10 percent of their energy into CRs to sustain the observed level of the Galactic CR "sea" (e.g., [101]). This required efficiency is relatively high. However, it has been shown to be feasible under strong diffusive shock acceleration scenarios (e.g., [40]). CC SNe produce fast shocks that interact with the dense CSM of the progenitor star. Accelerated CRs may be accumulated at these shocks, where they can strengthen magnetic fields through streaming instabilities ahead of the shocks. The NRSI (see Section 2.1.3) can be particularly important to amplify magnetic fields in the up-stream region. This mainly happens within a few days of the shock breakout [102,103]. The strengthened up-stream magnetic fields boosts CR containment and acceleration efficiency [102]. SNe classes hosting extended shocks, for example type IIb SNe, can experience particularly strong magnetic amplification by this mechanism.

The maximum energy CR acceleration processes can attain in an expanding SN shell may be estimated from the shock velocity $v_{\rm sh}$, the size of the shell $r_{\rm sh}$, and its mean magnetic field strength, $\langle |B| \rangle$:

$$E_{\rm max} \sim 1 \left(\frac{r_{\rm sh}}{\rm pc} \right) \left(\frac{v_{\rm sh}}{1000 \ {\rm kms}^{-1}} \right) \left(\frac{\langle |B| \rangle}{\mu {\rm G}} \right) {\rm TeV} \, , \tag{7}$$

(e.g., [99,104]). This indicates that SN shells can accelerate CRs to 1–10 TeV energies with typical CSM magnetic field strengths and shock velocities. To reach energies in excess of 1 PeV, fast ($v_{\rm sh} \sim 10^4$ km s^{-1}), extended shocks pervading a dense CSM are required. Resonant [25,105] and non-resonant [42,106–108] CR streaming instabilities can then build-up the magnetic field to 10 s of μG ahead of the shocks in these circumstances. Such strengths have been observed in young SNR shells (see [109] for a summary). These requirements highlight type IIn SNe as viable candidate accelerators capable of operating up to PeV energies [102,110]. In these systems, CR acceleration would start before the shock breakout. A radiatively dominated shock is initially launched through the hydrostatic core of the progenitor. This propagates outwards to the outer layers of the stellar core, where radiatively dominated shock is replaced by a collisionless shock [111–114]. Diffusive shock acceleration is then possible. However, it has been considered that the formation of a collisionless shock occurs significantly before breakout in some optically thick winds [115] for particles with gyro-radii greater than the shock width [116,117].

Remnants of SN explosions have also been regarded as an important source of CRs in galaxies. In SNRs, CRs can be accelerated to a few PeV at the transition between the free expansion phase and the Sedov-Taylor phase, within 100–1000 yr after the explosion (corresponding to the Sedov time; see [118]).[6] Particle escape generally arises from the slow-down of the SNR shocks as circumstellar gas is swept up during the expansion. As the shock becomes slower, it eventually falls below the diffusive propagation speed of the CRs. The CRs then begin to diffuse away upstream ahead of the shock, and the probability of their return from the upstream direction for further acceleration gradually reduces. Eventually the CRs are no longer coupled with the shock [120]. As particle diffusion is energy-dependent, more energetic CRs diffuse faster and escape from the SNR earlier. Evidence of this can be seen in spectral breaks from SNRs observed in γ-rays (e.g., [121]). From Equation (7), it can be seen that the maximum energy an SNR can attain will reduce over time as the shocks slow down.

The accumulated swept-up CSM gas can form a massive shell around the SNR. The dense gas in the shell acts as a target for pp collisions with the accelerated CRs. This can generate γ-ray production from the decay of neutral pions that form in pp interactions (cf. Section 2.2), which has been detected around some SNRs (e.g., [121,122]). However SNe with such a dense CSM that can be detected in γ-rays may not be common [123]. The high-energy emission from many SNRs is often instead attributed to the interactions of escaping CRs with nearby molecular clouds (e.g., [124–129]). Observations of SNR shells at other wavelengths are more informative. In addition to γ-rays, hadronic pp interactions

also generate secondary leptons. These radiate synchrotron emission [130,131]. Together with contributions from primary electrons accelerated by the SNR shocks and/or by turbulent magnetic fields that develop in the vicinity of the shocks [96], this emission has been detected at high radio frequencies through to X-rays around young and middle-aged SNRs [43,96,132].

3.1.2. Star-Forming Regions, Star Clusters and Super-Bubbles

Recent studies have put a renewed focus on systems other than SNe and isolated SNRs as the origin of CRs in galaxies. This is motivated by differences between the spectra of accelerated particles at SNR shocks and the observed CR spectrum on Earth, as well as difficulties in accounting for the CR electron-to-position ratio under an SNR source scenario (for reviews, see [99,133,134]). Star-forming regions, including young massive stellar clusters and associated super-bubbles have emerged as particularly promising candidate source populations. Star-forming regions hosting massive stars can develop powerful winds. Their massive stellar populations can also rapidly produce SNe. The wind termination shocks, and the shocks associated with the SNe can act as CR accelerators. Star-forming regions have been recently observed in γ-rays. The Cygnus region has taken centre-stage in many of these observational enquiries, and has perhaps provided the strongest evidence to support hadronic CR acceleration in stellar clusters (e.g., [135–138]). Particularly notable is the emission associated with Cygnus X. This region includes many young star clusters and OB associations [137], and hosts the *Fermi* Cocoon super-bubble which has been detected up to $\sim$1.4 PeV [135,136,138,139] with the Cygnus OB2 star cluster likely being the origin of the CRs that produce this emission [109]. Additional studies include observations towards W43 [140], Westerlund 1 [141,142], Westerlund 2 [143], the Carina Nebula Complex [144], the Aquila Rift and some giant molecular clouds hosting star-formation in the Gould Belt [145] (ρ Ophiuchus and Cepheus). These studies confirm the role of stellar clusters and star-forming regions as particle accelerators, and demonstrate their capability to operate up to energies well-above a TeV.

The confluence of the shocks and dense winds in tight clusters of star-formation can be particularly important CR factories [146,147]. In younger stellar clusters, where an SN event has yet to occur, CR acceleration arises at wind termination shocks. If the cluster is compact, the confluence of winds is decelerated at a spherical termination shock. In looser clusters, this confluence does not generally arise, and each star develops its own wind termination shock. Older stellar clusters are expected to accelerate CRs through a radically different mechanism. They reside in a super-bubble, which is subjected to the recurrent SNe from the stellar cluster. These super-bubbles are regions of hot ($T > 10^6$ K), low-density ($n < 10^{-2}$ cm^{-3}) highly turbulent gas carved out by the winds and SN explosions of associations of OB stars, surrounded by a dense communal shell of swept-up ISM gas. The gas internal to the bubble is a combined mixture of chemically enriched SN ejecta and stellar wind material, as well as residual ISM gas [148]. Within these super-bubbles, particles are accelerated more intermittently, and the process can be more complex than in isolated sources. Acceleration happens either in the collective stellar winds, in individual SNe and SNRs [149,150], at the confluence of the shocks and weak reflected shocks from SNRs, in the turbulent medium[7] inside the bubble [149,151–155], or at the boundary of the bubble. Winds from Wolf–Rayet (WR) stars may also contribute [156,157], with enriched WR wind material being accelerated at stellar wind termination shocks [158]. The wind termination shocks in super-bubbles have been shown to be capable of accelerating particles up to PeV energies [153,159,160].

Stellar clusters as CR sources provide a more natural explanation of CR chemical composition trends in the ISM (for brief reviews, see [134,161]). Notably, they produce elemental abundances consistent with a mixture of primordial and enriched material. This is thought to originate from a seed ISM composed of primordial solar composition material enriched with material from stellar outflows and ejecta [162] and a parent plasma of hot gas [163]. More subtle indications from CR abundance measurements also lend support

to a super-bubble origin. For example, the high abundances of CR refractory elements compared to volatile elements [162,164,165] is consistent with dust grains being entrained from the ISM, as would be expected around super-bubbles. These undergo very effective acceleration at shocks due to their typical high charge to mass ratio. Dust erosion by sputtering at high velocities releases refractory species into the shock. These have the same velocity of the primary dust grain, and are injected directly into the acceleration process independently of their mass-to-charge ratio [166,167]. A super-bubble origin also provides more consistent predictions for the abundance ratio of B and Be in the observed composition of CRs. If their origin is associated with the ISM, these elements are expected to increase in proportion to metalicity (traced by O abundance), following general enrichment trends of the ISM driven by SNe. However their observed increase with the square of O abundance is instead consistent with Be and B being produced by spallation reactions with CRs accelerated out of the ISM, and then interacting with the ISM itself [168–170].[8]

3.1.3. Searching for *PeVatrons*

The identification of Galactic CR origins above a PeV presents a particular challenge. Around this energy, the CR flux we receive on Earth transitions from mainly Galactic in origin, to extra-galactic. This is marked by a steepening of the CR spectrum at a few PeV (the so-called *knee* [171,172]; for an overview of efforts to resolve this spectral feature, see [173]). It is unclear whether this observed steepening is due to the extra-galactic source transition, the effects of different convolved source spectra, or a feature resulting from the competition of different energy-dependent transport effects (e.g., [174–176]). Moreover, it may be dependent on the CR species, with recent indications that a knee arises for lighter CR species at slightly lower energies of around 0.7 PeV [177]. However, the existence of a spectral feature marking the transition to extra-galactic CRs is theoretically expected. This can be understood by a comparison between the size of the Galactic halo size or disk thickness (of order a few kpc) with the CR gyro-radius in a $\sim$1 μG magnetic field, characteristic of the average magnetic field strength in the ISM. At a few 10 s of PeV, this gyro radius is $r_{\rm gy} \sim 1.1 \left(E_p/10\,\mathrm{PeV}\right)\left(B/1\,\mu\mathrm{G}\right)^{-1}$ kpc. CRs of lower energies than this would mainly be confined within the Galaxy by its magnetic field. This means that the bulk of observed CRs up to the knee must be supplied by sources within the Milky Way.

A range of plausible candidate source populations can be considered as the potential origins of Galactic PeV CRs (cf. the Hillas criterion [104]). These meet the requirement of being able to accelerate CRs to a PeV. However, this is not sufficient to claim that they are the origin of the bulk of the PeV CRs we observe on Earth. Indeed, nearby well-studied pulsar wind nebulae systems like the Crab nebula have been found to accelerate CR particles to PeV energies [178], yet it remains unsettled whether systems like the Crab could be a dominant source of most of the hadronic Galactic CRs at 10–100 PeV (see [178–180]). This has motivated the search for CR accelerators operating to PeV energies, called *PeVatrons*, which are capable of sustaining the detected abundance of PeV CRs.

Without an unambiguous determination of the dominant population of Galactic PeVatrons, several possibilities have been considered. Some of these are supported by observational studies, indicating that SNRs (originally proposed by [181]), the supermassive black hole in the Galactic Center (see, e.g., [182]), pulsars (e.g., [183]), highly collimated micro-quasar jets [184], and young massive stellar clusters (e.g., [154,185]) could all be plausible PeVatrons. Interest has particularly increased recently in young star clusters due to the steady increase in the observed associations between star clusters/super-bubbles and high energy γ-ray sources [136,137,140,186–188]. It has been suggested that these sources may even be a dominant source population for the highest energy Galactic CRs [185]. Acceleration in fast SNR shocks expanding in the collective wind of a compact cluster may be one mechanism to reach energies well above a PeV [189]. However, sufficiently powerful SN explosions to yield the necessary fast SNR shocks in these systems are rare [190] (see also the overview in Ref. [161]), and it remains unsettled whether CR energies can be attained that are sufficient to account for the Galactic CR flux above a PeV [150,160]. Shocks around

isolated SNe have also been considered. However, the requirement for shock velocities of around 40,000 km/s [191] to reach PeV energies is challenging to achieve. Moreover, it remains unclear whether the non-resonant instability can sufficiently amplify the CSM magnetic field up-stream of most CC SN shocks to sustain PeV CR acceleration.

When discerning the origin of Galactic CRs, the search for hadronic PeVatrons is arguably more pressing than leptonic ones. This is because most of the Galactic CR flux is comprised of hadrons. Moreover, leptons typically experience severe energy losses and generally would not be able to survive substantial propagation through the ISM to sustain a CR sea. This makes their origin a more local question.[9] Hadronic CR accelerators should yield signatures in γ-rays persisting to higher energies (from π^0 decays) and neutrinos (from $\pi^{\pm}$ decays), while leptonic accelerators can only produce electromagnetic emission. It is likely that neutrino emission from hadronic PeVatrons arises at levels that are below detection thresholds of current instruments (for discussion, see, e.g., [193]). Firmly establishing source candidates as hadronic will therefore rely on neutrino detections with up-coming and proposed facilities [194–197]. Present observational efforts to discriminate between hadronic and leptonic PeVatrons instead focus on their γ-ray emission above $\sim$50 TeV. At these energies, Klein-Nishina suppression considerably reduces the efficiency of leptonic γ-ray emission. To date, a number of γ-ray sources have been detected in this energy range. Tibet-ASγ has reported γ-rays with energies between 100 TeV and 1 PeV in the Galactic disk [198], and nine sources have been detected above 56 TeV with the High Altitude Water Cherenkov Observatory (HAWC), including three up to 100 TeV, and 12 above 100 TeV with the Large High Altitude Air Shower Observatory (LHAASO; [136]).[10]

The 12 LHAASO sources detected above 100 TeV (which include the three detected above 100 TeV by HAWC) have been considered as PeVatrons [200]. The majority of them have plausible associations with energetic pulsars ($\dot{E} \gtrsim 10^{36}$ erg/s) and known counterpart very-high-energy (VHE) sources. Pulsar wind nebulae are predominantly leptonic accelerators, for which the Klein-Nishina effect causes an abrupt cut-off at the highest energies [201]. However, it has been demonstrated that the energy density of high radiation environments can compensate this effect somewhat, such that even leptonic scenarios may account for γ-ray emission at $\sim$100 TeV [202]. LHAASO J2032+4102 associated with the Cygnus region is a promising case as evidence for PeVatron activity by young stellar clusters, laying claim to the highest energy photon measured at 1.42 ± 0.13 PeV. The vicinity of the Boomerang nebula, LHAASO J2226+6057 (also detected by Tibet-ASγ [203]) was recently studied in detail with the MAGIC telescopes, exhibiting intriguing energy-dependent morphology. As the location of the emission seems to shift within the SNR G106.3+02.7 with energy, there are indications to support a scenario where high energy particles escape the source and travel further in the surrounding medium [204].

Two sources that do not appear to have a known energetic pulsar counterpart are LHAASO J1843-0338, plausibly associated with the SNR G28.6-0.1, and the enigmatic source LHAASO J2108+5157; the only source to be first discovered at the highest energies. To date, coincident molecular material as been found at the location of the latter [205,206], potentially indicating that energetic particles are hadronic in nature, yet no accelerator has as yet been identified in the vicinity [207].[11] Within a scenario whereby the particles accelerated to the highest energies escape the accelerator, travel through the intervening ISM and subsequently interact with target material such as molecular clouds, one may anticipate a population of such 'passive' sources emerging at the highest energies. Future studies from surveys at the highest energies, including LHAASO, HAWC and the forthcoming Southern Wide-Field Gamma-Ray Observatory (SWGO) covering the Southern sky, may be able to shed further light on these phenomena [209].

Detected γ-ray sources may not (yet) be able to account for the full budget of Galactic CRs and may not even be hadronic (e.g., [210]). Indeed, it has recently been speculated that some hadronic PeVatrons may not yield observable γ-ray signatures at all. Instead, Ref. [211] discussed how they may be too thin in column density for CR hadronic interactions to take place within them at detectable levels. The accelerated CRs then simply

escape without local interactions or discernible electromagnetic signatures. Alternatively, they may be too thick in matter or radiation density that CRs cannot escape. In this case, the CRs may be attenuated locally by pp or pγ interactions (see also Section 2.2), or γ-rays are produced but are attenuated by pair-production with low energy photons in the SN photo-sphere (e.g., [212–214]). However, it is possible that a larger population of weaker hadronic PeVatrons falls below detection limits for current γ-ray observatories, and more sources will emerge as integration times increase—particularly with the advances to be made in the 100 TeV domain using the new generation of γ-ray facilities.

3.2. Cosmic Rays in Diffuse Interstellar Media

3.2.1. Magnetohydrodynamic Mode Damping and Implications for Cosmic Ray Propagation

In conditions typical of the Milky Way's hot ionized medium (HIM), the resonant CR streaming instability operates efficiently. However, the growth of MHD waves driven by CRs of energies up to a few GeV is roughly balanced by damping processes [20]. For these modes, a steady state MHD wave amplitude is established. The CRs driving them will then experience diffusive propagation constrained roughly to the local Alfvén speed (cf. the self-confinement view; Section 2.1.1). This self-regulated view of CR transport coupled to MHD fluid treatments has been widely adopted in CR propagation simulations. Such studies can recover the characteristics of macroscopic CR transport in a steady-state limit [19], and have been used to inform larger scale simulations of galaxies (e.g., [215,216]). Some developments take additional consideration of CR transport variation in different ISM phases [216], where the dominant processes damping MHD wave modes may differ. For example, turbulent damping can dominate in the warm ionized medium, but ion-neutral damping is usually operates more quickly in weakly ionized molecular clouds [217]. This can lead to strong suppression of MHD turbulence [218] and less diffusive [219,220], faster CR propagation in these settings. However, recent γ-ray studies have demonstrated that the situation may be more complex (see also Section 3.3.1). They have introduced new evidence that diffusive CR propagation persists within molecular clouds, at least down to the sub-pc clump scale below 10 GeV energies [221]. This may suggest damping processes operate less efficiently than expected in ISM molecular complexes, or that MHD wave amplification is more severe.

3.2.2. Cosmic Ray Heating Processes in the Ionized Interstellar Medium

The ISM of galaxies is inhomogeneous. The largest component is the HIM. This fills about half of the ISM volume in the Milky Way [85]. In other galaxies, it also comprises a substantial fraction of the ISM, but the exact filling fraction may differ according to local conditions [222]. HIM heating is generally efficient. It is driven mainly by starlight and shocks from SN explosions to sustain a temperature above $\sim 10^{5.5}$ K and a high ionization fraction. By contrast, the low gas density means that cooling is inefficient, operating over timescales of Gyrs. The HIM of most galaxies is therefore in a runaway thermal state. The HIM of galaxies hosting a rich reservoir of CRs can be subjected to particularly powerful heating. If mediated by hadronic collisions, Coulomb thermalization of CRs can dominate [14]. By this channel, CRs can have a significant role in setting the thermal history of galaxies and their evolution (e.g., [223]).

The other major ionized component of the ISM is the warm ionized medium (WIM). In the Milky Way, this occupies around 10 percent of the ISM volume. In other galaxies, this fraction can be higher. It depends on local thermal conditions [222], and can be affected by CR pressure and transport [49]. The WIM is comprised of photo-ionized, photo-heated HII gas. It is typically held at a temperature of around $\sim 10^4$ K, with cooling operating relatively slowly via optical line emission and free–free emission. Heating is supplied by photo-electrons and CRs, with CRs believed to be dominant. Their role in maintaining the thermal balance of the WIM has been considered in several recent works. This operates through Coulomb collisions of low energy CRs, below $\sim$100 MeV [224],

Coulomb thermalization of secondary electrons via hadronic collisions [14,49], and the dissipation of MHD waves [224–227].

3.2.3. Cosmic Ray Effects on the Structure of Interstellar Media

CR pressure gradients and transport effects can modify gas structures within the ISM. This can have consequences for galaxy evolution, as the capability of dense star-forming clouds to develop can be changed. Resolving the relevant CR processes that regulate the phase configuration of a galaxy is therefore essential to properly establish their global feedback impacts. CRs have not been found to play a significant role in stellar cluster formation [228], and their direct impact on star-formation in molecular clouds is unsettled, with some studies reporting relatively moderate effects (over 100 Myr timescales [228]), while others have found more severe impacts may be possible in certain settings (e.g., in starburst galaxies [229,230]). Less direct effects on star-formation have been shown to be more consequential. For example, self-generated magnetic fields around CR sources can reduce CR diffusivity in large CR-inflated bubbles [46]. The accumulation of CRs and strong local pressure gradients prevent the formation of massive gaseous clumps in these regions [231] and a smoother ISM [232]. This frustrates the development of future stellar nurseries.

CR propagation through an established multi-phase ISM can also modify the potential for star-formation by disrupting the configuration of existing clouds. For example, CRs may propagate less diffusively in dense, relatively neutral structures like clumps and molecular clouds. As CRs decouple and experience higher streaming speeds in the semi neutral gas, the local CR energy density drops. This creates a CR pressure gradient at the cloud-ISM interface (sometimes referred to as the CR 'traffic jam' effect; e.g., [233]). This can be sufficient to collisionlessly generate waves that are able to overcome local damping mechanisms (e.g., ion-neutral damping) and exert a force on the cloud. It can accelerate [234–236] and reshape the cloud [233], and may even boost the gravitational instability to induce earlier collapse and trigger star-formation. Cloud compression can also be induced by the Parker instability,[12] which is more severe and arises more frequently in the presence of CR streaming and self-confinement [237] (although the effects can be different depending on the CR transport model adopted [238]). This may increase star-formation. Conversely, the Parker instability is less severe if adopting an extrinsic turbulence model for CR transport [237], leading to suppressed star-formation and a more puffed-up ISM overall. These effects are expected to be particularly strong in starburst galaxies, where the Parker instability can grow more quickly [237].

3.3. Cosmic Rays in Molecular Clouds

3.3.1. Propagation

CR propagation in the ISM can generally be described as a combination of diffusion, ballistic streaming and advection (see Section 2.1). The balance of these processes depends on local conditions. In molecular clouds, advection in bulk flows is usually negligible. However, diffusion and streaming are important. In the warm, ionized envelopes around ISM clouds, CR diffusion can be highly variable. Coefficients have been inferred observationally to span at least four orders of magnitude in the Galaxy (e.g., [229,239,240]), with simulations indicating that no single value is suitable for different locations or for CRs of different energies [216]. In molecular clouds, clumps and cores, ion-neutral damping can be strong (see Section 3.2.1), with small-scale resonant MHD turbulence being damped entirely in dense cores (e.g., [241]). CR transport should therefore revert increasingly to ballistic streaming in these structures [219,220], which increases their effective speed. A local reduction in CR density and pressure then emerges [218,242,243], producing a CR deficient zone. Effects including modulation by electric fields from charges deposited by CRs (especially in regions of high electron-dominated ionization; see [244]) and magnetic mirroring [218,245–249] can then reduce CR density further, especially in multiple-peaked magnetic field structures (where mirroring and focusing effects do not cancel out [250]).

Although CR-deficient zones due to fast, less-diffusive propagation can account for observed trends in molecular clouds (e.g., anti-correlated CR ionization rate with density [251]), other possibilities have also been considered. Slow CR diffusion in dense star-cluster-forming clumps where stronger magnetic fields sustain turbulent motions [252] would also create a local deficiency of CR density if severe enough. In this scenario, the CR-deficient regions would be more accurately described as exclusion zones, as it is harder for CRs to penetrate into them. A different possibility is that MHD turbulence on larger clump-scaled structures may support more moderate diffusive CR propagation. Such a scenario is not implausible. Below ∼100 MeV, CR absorption due to ionization processes can be severe, particularly on the scale of dense cores [253]. The CR flux in cloud interiors can therefore be severely reduced, by as much as two orders of magnitude, with the CR electron flux being especially affected [254]. The CR flux leaving a clump or core can then be much lower than that entering it. This introduces a flux difference able to sustain MHD turbulence and the generation of Alfvén waves via the streaming instability (e.g., [241,243]), which can be sufficient to enable some scattering and diffusive propagation. At >GeV energies, attenuation by hadronic interactions is possible. Gas densities associated with clouds are sufficient to cause strong CR attenuation (see Section 2.2). This leads to a reduction in CR density overall and is able to account for the γ-ray 'holes' observed with *Fermi*-LAT below 10 GeV [221]. This level of attenuation may also be sufficient to sustain MHD turbulence at a level where some diffusive propagation is possible. A further possibility is that CR propagation may instead be suppressed in a small envelope region separating dense clumps from the larger diffuse cloud due to self-generated MHD waves [241,255,256]. This would hinder their penetration into the cloud, but boost signatures of their effects in the envelope region. Such an envelope may be challenging to be disentangle observationally.

3.3.2. Cosmic Ray Interactions in Molecular Clouds and Observable Signatures

CRs interact with molecular clouds through multiple channels, each of which can have distinct physical effects and produce different observable signatures. The dominant interaction process depends on the CR species, its energy and the local physical conditions within a cloud. Collisional ionization processes are caused by CRs of all species, and are particularly important at energies between 10 and 100 MeV [257]. They can modify the physical and chemical conditions deep inside clouds by maintaining a low level of ionization through the dense gas. This ionization sustains a coupling between the gas and magnetic field, with implications for the cloud dynamics [258]. It also drives rich astrochemical networks, initiated by the production of H^+ and H_2^+ ions. These lead to the formation a wide selection of molecular ion species that have accessible transition lines at sub-mm wavelengths.

H_2^+ rapidly reacts with H_2 to produce the H_3^+ ion. This can be directly detected to infer the local CR ionization rate along a line of sight (e.g., [259–261]). By using this ion, observations with the Atacama Large Millimeter/Sub-Millimeter Array (ALMA) have recently been able to produced intricate maps of CR ionization through molecular cloud complexes [262], allowing new tests of CR propagation models with unprecedented clarity. Other molecular ions, such as ArH^+ [263–266] and HCO^+ [258], can also be used as probes to measure CR ionization. These are less direct tracers than H_3^+, and require additional chemical modeling. This can introduce uncertainties when interpreting data, but provides observational flexibility. For example, in cases where H_3^+ emission or absorption lines are not detectable with current instruments, or limitations make detection impractical for a particular target (e.g., a requirement to have a suitable background early-type star to obtain an estimate for the column density of the target species (e.g., [260,267]), other chemically related species may be accessible instead. Relating observations of indirect tracers to the underlying CR ionization rate can often be achieved by simplified gas-phase chemical networks.[13] Figure 2 demonstrates an example of an oxygen (O) network which shows how typical observable species like OH^+ and H_2O^+ can be connected to the CR ionization

rate. These reduced networks allow relatively simple analytic relations to be derived that relate the abundance of a target species (e.g., OH^+) to the CR ionization rate [271,272].

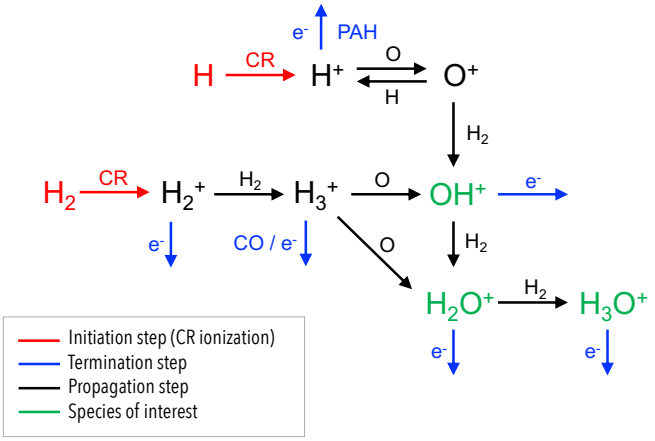

Figure 2. Standard simplified network of chemical processes driven by CR-induced ionisation of H and H_2 in a molecular cloud. Pathways leading to the formation of OH^+, H_2O^+ and H_3O^+ are shown. Termination steps are caused by neutralisation with electrons (which may be ambient free electrons, or even low-energy CRs) within the cloud are indicated in blue. It is also possible for polyaromatic hydrocarbons (PAHs) or carbon monoxide (CO) to facilitate some termination processes, as noted. Adapted from Ref. [273].

OH^+ and H_2O^+ are often used as tracers of CR ionization in diffuse molecular clouds, where their abundances are strongly affected by the ionizing CR flux. Other tracers, such as H_3O^+, DCO^+, HCO^+, N_2H^+, N_2D^+ and their associated isotopologues, are selected depending on the required physical conditions of the target region within a particular cloud complex. Observations using these tracers have provided new information about the CR ionization rate at different locations in the Galaxy, with a few hundred diffuse molecular clouds analyzed so far. These observations have revealed broad variations in the ionization rate at different locations throughout the Milky Way, ranging from $\sim 10^{-18}\,s^{-1}$ to $\sim 10^{-14}\,s^{-1}$ [267,274–283]. The ionization rate at a particular cloud column density depends on the propagation model and irradiating CR spectrum adopted [284,285]. Local factors, such as magnetic field strength and structure (including magnetic mirrors [218,247]), also impact the capability for CRs penetrate and ionize interstellar cloud. However, the magnitude of the variation of CR ionization inferred for different molecular clouds far exceeds the variation typically attributed to these local factors. Instead, the broad variation of CR ionization rates throughout the Galaxy indicates a highly non-uniform irradiating flux of low-energy CRs throughout the ISM.

Many chemical signatures of CR ionization associated with molecular ions are accessible in the sub-mm band, with instruments such as ALMA. However, their ionizing impacts can also be detected in other parts of the electromagnetic spectrum. In particular, MeV CR protons (and heavier species) can collide with neutral to low-ionized Fe atoms in ISM clouds to produce FeI Kα X-ray line emission at 6.40 keV [286]. Such emission results from the removal of a K-shell electron by a CR ionization event, with the vacancy filled rapidly by an electronic transition from the L shell. These collisions result in shifts of characteristic X-ray line energies and distinctive spectral structures, making it possible to study the properties and composition of CRs irradiating molecular clouds [287].

CRs do not only cause ionization when they collide with the gas in molecular clouds. They also excite electronic and ro-vibrational energy levels of H_2 [288]. Primary CRs propagating into a molecular cloud with energy spectra peaking between 10 s of keV to a few MeV can produce secondary CR electrons of energies of order 10 s of eV [285]. These efficiently excite ro-vibrational transitions of H_2, particularly to the first vibrational state ($\nu = 1$). The subsequent relaxation leads to the emission of photons that can be detected

in infrared (IR) using instruments including the Very Large Telescope (VLT), or the Near InfraRed Spectrograph (NIRSpec) on the *James Webb* Space Telescope (*JWST*). Four lines in particular, (1-0)O(2), (1-0)Q(2), (1-0)S(0), and (1-0)O(4) at 2.22, 2.41, 2.63 and 3.00 μm, respectively, have been identified as transitions where CR excitation dominates over competing processes like photo-excitation [288]. These transitions are therefore viable tracers of CR activity. Recent advancements of this technique have demonstrated that cloud density variations affect the penetrating capability of CRs according to their energy [285]. This means that, by measuring ro-vibrational line intensities and H_2 column densities towards a molecular complex, the low-energy CR ionization rate, CR spectral index, and spectral normalization can all be deduced. This provides a novel means of studying the variation of CRs of different energies throughout the Milky Way's disk [289,290]. In the era of *JWST*, this is a powerful new tool for studying CRs.

High-energy interactions provide an opportunity to study CRs in molecular clouds at energies far above those involved with ionization and ro-vibrational excitations. At $\gtrsim$GeV, CR protons and electrons are subject to different interaction pathways that generate different signatures. For instance, when the energy of a CR proton exceeds a threshold of about $\sim$0.28 GeV, it can undergo pion-producing interactions with gas nuclei in clouds (see Section 2.2). These interactions release γ-rays (e.g., [291]) and neutrinos (e.g., [292–295]) from the decay of neutral and charged pions, respectively. These interaction products can be used as a tracer of CR engagement in molecular clouds in violent environments, such as the vicinity of a CR source like an SN remnant or pulsar wind nebula [293,296,297]. We can gain insight into the properties and composition of the CRs escaping from these sources by studying the emission associated with CRs interacting in these so-called *active* clouds (see also Section 3.4).

High energy CR electrons can drive synchrotron emission when they interact with the magnetic fields of clouds and cores. These magnetic fields can be substantially stronger than the ISM average (for a review, see [298]). The CR electrons driving this emission can be primary CRs, irradiating a cloud from the ISM. However, given their fast cooling times, they are often secondary CRs, produced from the decay of the charged pions produced in hadronic collisions. Detection of synchrotron emission from CRs in molecular clouds can be challenging, and is thought to be very low in some clouds, e.g., the Sgr B2 complex [239]. A particular issue is the thermal emission (including that caused by enshrouded stars), which can overwhelm non-thermal emission signatures from the cloud. Despite this, previous studies have reported non-thermal radio emission from starless infrared dark clouds, such as G0.216 + 0.016, where contamination from thermal radiation is less severe [299]. This emission is consistent with the radiation produced by secondary CR electrons, with a suppressed diffusion coefficient (by a factor of 0.1–0.01) and substantially enhanced local magnetic field of 470 μG [300]. Other studies have reported correlations between Galactic (e.g., [301]) and extra-galactic (e.g., [302]) CO emission with radio emission, suggesting the radio emission is synchrotron that originates in molecular clouds. Future facilities such as the Square Kilometer Array (SKA) may be able to detect synchrotron emission from CRs in a wide range of Galactic molecular complexes [284,303], especially those irradiated by nearby energetic sources such as SNRs [304]. Such radio observations would provide the opportunity for more spatially resolved observations than is possible with other signatures.

3.3.3. Molecular Clouds as Cosmic Ray Barometers

Molecular clouds can serve as CR barometers. When CRs interact with them, the resulting products (photons and neutrinos) can be used as observable tracers of the CR distribution throughout the Galaxy. *Passive* molecular clouds are irradiated by CRs from the interstellar distribution, or the CR 'sea', rather than a nearby source. γ-ray studies have established the use of these clouds as barometers to measure the variation in the CR 'sea level' throughout the ISM [256,291,305–308]. They find significant variation in different parts of the Galaxy. This is consistent with the large spread of CR ionization rates determined for molecular clouds throughout the Milky Way (e.g., [267,274,309]), which

indicate that clouds in some parts of the ISM are irradiated by a CR spectrum two orders of magnitude more intense compared to that detected at Earth [310]. This variation may be due in part to the discrete nature of CR sources, which have been shown to produce a distribution of intensities with an expectation value that is not representative of the CR spectrum throughout the Galaxy, but has a median compatible with the CR proton and electron data obtained with *Voyager* [311].

Studies of CR ionization rates in clouds have also established a trend with Galactic radius. As seen in Figure 3, the density of CR protons tends to increase towards smaller Galactic radii, although a significant reduction is observed towards the inner ∼2 kpc of the Galaxy [305]. Indeed, reductions of CR abundance in the central molecular zone (CMZ) have been reported [312]. It has been suggested this may arise due to variations in CR propagation due to, e.g., suppression of the diffusion parameter or the presence of a 'barrier' formed by the self-excited MHD turbulence at the edges of clouds [313] or trapping of CRs in outer cloud layers.

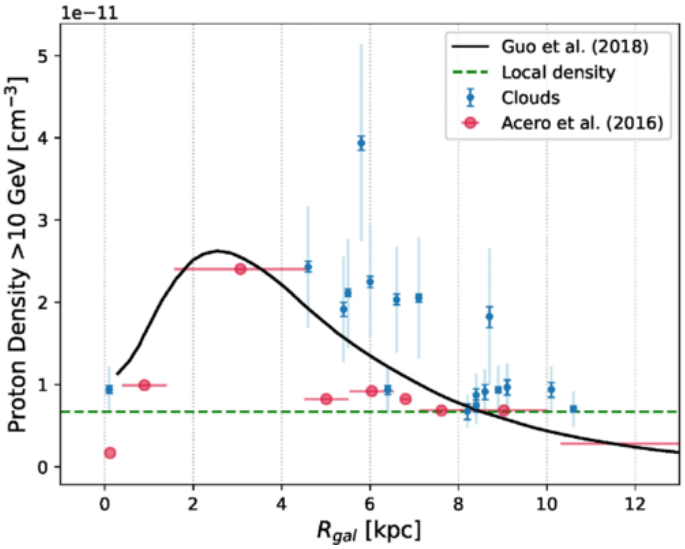

Figure 3. Energy density of CR protons above 10 GeV as a function of distance from the Galactic Centre (GC). Estimates obtained from passive clouds are shown, with statistical (thick lines) and systematic (thin lines) errors shown by the error bars. Energy density of protons derived above 10 GeV. For each cloud are indicated the and the error bars. The data points from Ref. [314] are shown in red. The model adopted from [315] is shown by the black line, while the local proton density derived from the measurements of [175] is shown by the green dashed line for reference. Figure reproduced from Ref. [305].

In the GC, the trend of declining CR ionization of clouds appears to reverse. This is likely due to the presence of nearby CR accelerators, rather than a global change of the CR sea level [316]. The GC increase has been studied with GeV-TeV γ-rays, ionization signatures (probed with H_3^+, for example) and the X-ray Fe I Kα line [259], targeting cloud complexes such as Sgr B2 (which may vary over time [317]) and the Arches [318–320]. The latter of these is located near a cluster of young massive stars near the GC region. It has been found to have time-variable ionization [321], which has been shown to be in agreement with a CR origin [322,323]. These findings complement earlier results obtained with iron Kα lines in the Galactic ridge, where the line profile was indicative of molecular cloud bombardment by an MeV proton flux [324].

3.3.4. Thermal Balance and Star-Formation

CR heating is an important factor in setting the thermal balance of the WIM of galaxies (see Section 3.2.2). It also plays a role in regulating the thermal structure of molecular clouds. The effective power supplied by CR heating is determined by the mechanisms

responsible for CR thermalization. These depend on the energy distribution of the CRs and the local conditions. Molecular clouds have a complex hierarchical structure (as show in Figure 4). Different CR heating processes dominate in various regions of the cloud, and the overall efficiency of heating can vary dramatically in each of the components.

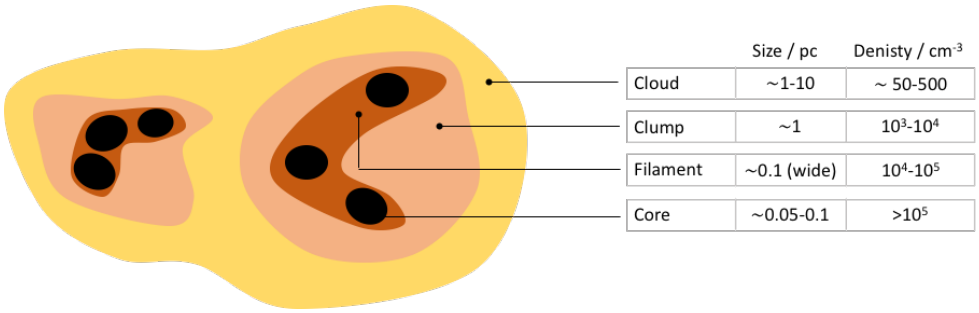

Figure 4. The hierarchical density structure of molecular clouds, ranging from diffuse regions to small dense cores where star-formation can occur [325]. From large to small scales, temperatures vary from a few 10s of K to a few K, and ionization fractions range from nearly $x_i \approx 1$ to $x_i \approx 10^{-7}$ [85]. CR propagation in the clouds is primarily diffusive, becoming less diffusive as higher neutral fractions damp MHD waves [219,220]. The continuous substructure of molecular clouds cannot be fully captured by a simple hierarchy of just a few distinct elements [326], and alternative distinctions between cloud components are equally valid (e.g., [327]) (Figure from Ref. [273]).

In the most dense, neutral regions of clouds, collisional ionization is likely to be important in driving CR thermalization [328] (see also [329]). This process can be caused by CR protons or electrons, including secondary electrons produced in hadronic collisions. When they collide with gas and cause an ionization event, the electrons released (called 'knock-on' electrons) thermalize via electron-neutral collisions and Coulomb scattering. The effectiveness of this process depends on the ionization fraction, x_i, of the gas. A more direct form of this mechanism can also operate, with lower energy CRs directly undergoing Coulomb and collisional scattering with the cloud medium. This is more important for CRs below 100 MeV, in regions with non-negligible ionization fractions [14]. Another heating process is the excitation and damping of MHD waves, driven by the local CR pressure gradient. This channel is associated with all species of CRs. Strong ion-neutral damping suppresses MHD waves in the densest regions of clouds. However, these waves can still be excited by CR pressure gradients in dense regions of clouds with strong magnetic fields and/or high ionization fractions. They are damped rapidly so are not usually sufficient to affect CR propagation. Instead, they mediate thermalization from the CRs to the cloud medium with an efficiency that is strongly dependent on the local magnetic field configuration [229].

The efficiency of CR thermalization is set by the balance between CR interactions that lead to thermalization, and those where energy is radiated away as photons. The CRs irradiating ISM clouds are mostly energetic protons (e.g., as may be inferred from the local CR spectrum, [330]). They do not thermalize efficiently. Heating instead relies on inelastic hadronic collisions that produce secondary CR electrons. Figure 5 shows the typical CR electron spectrum that would be generated by hadronic collisions from an irradiating power-law CR proton flux. These secondary electrons engage more strongly in thermalization. However, their production introduces losses to neutrinos and γ-rays in the pp decay chain. This limits the maximum efficiency of CR heating via pp collisions to around 15 percent (see, e.g., [14]). The secondary electrons would experience radiative losses, mainly by synchrotron and free–free emission. This further limits their thermalization efficiency. The exact fraction of their energy available for heating the cloud medium is subject to more complicated dependencies on the local environment. This is illustrated by Figure 5, which shows how efficiency of thermalization varies through the density structure of a cloud. This simplified model adopts an empirically informed relation between cloud density

and magnetic field strength from Ref. [331] to determine the synchrotron loss rate, while the ionization fraction of the gas follows from Ref. [332]. Typically around 50 percent of secondary CR energy can go into heating background gas, which can increase to 90 percent in certain conditions. The overall thermalization fraction of primary CR protons therefore varies between ∼5 and 15 percent.

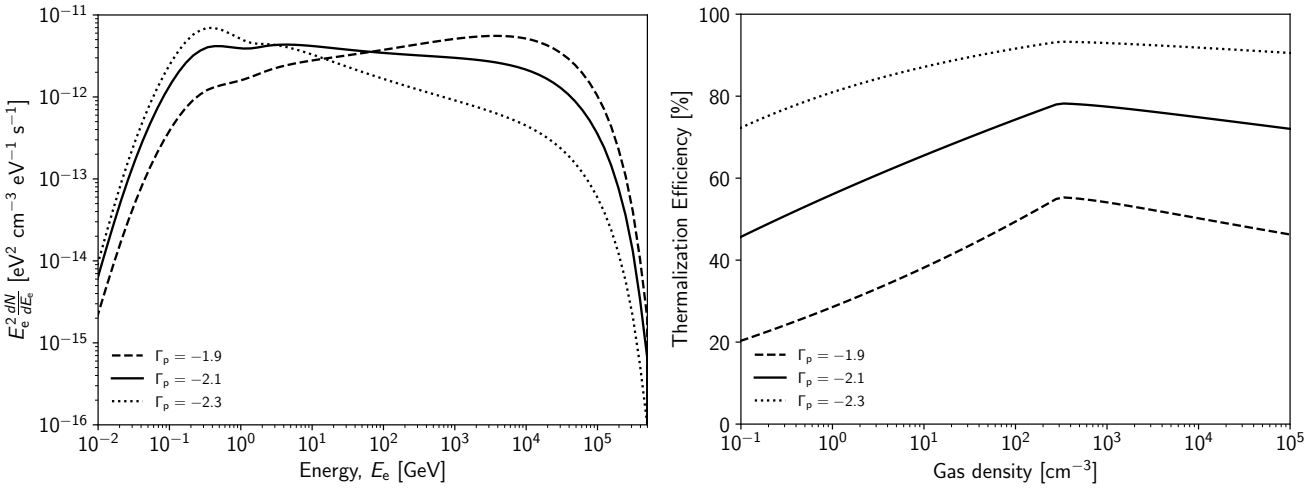

Figure 5. (**Left**) CR secondary electron spectra produced by CR protons interacting with gas of density $n_H = 1.0$ cm^{-3}. Proton spectra are defined between 100 MeV and 1 PeV and normalized to an energy density of 1.4 eV cm^{-3}. Three power-law indices are considered, as labelled. Harder spectra transfer more power to higher energy secondary CRs. (**Right**) Efficiency of energy transfer from CR secondary electrons to gas heating over a range of densities found in molecular clouds. Free–free and radiative synchrotron emission are considered as losses, while heating is driven by ionization and Coulomb interactions. The efficiency depends on the local magnetic field structure and is highest at gas densities of $n_H \sim 10^3$ cm^{-3}, corresponding to clumps in Figure 4. Softer CR primary proton spectral indices lead to higher heating efficiencies. This is because more electrons are produced at lower energies where thermalization channels are favoured. Heating by thermalization of MHD waves is not considered. It can vary substantially depending on local magnetic field configurations within individual molecular cloud complexes.

If CR heating is severe, it can elevate the temperature of a cloud. Observations have found that clouds experiencing significant CR ionization are warmer [333,334]. Theoretically, elevated temperatures of 30–50 K have been estimated for molecular clouds with CR ionization rates increased by around $\sim 10^3$ times that typical of the Galaxy [333], or ∼50–100 K for CR energy densities increased by $\sim 10^3$–10^4 [230]. Warmer clouds are subject to more thermal pressure support against gravitational collapse. This makes star-formation less favourable. The exact effect this has on star formation, quenching (e.g., [223]), clustering [229] and the initial mass function (IMF) [230] remains unclear. This is partly because the exact temperature increase experienced by a cloud is uncertain. It is strongly dependent on local conditions, model configuration (including the CR transport and interaction micro-physics; see also Section 5.3.7) and the level of CR bombardment in different regions of a cloud. Some studies have explored these dependencies explicitly, reporting equilibrium temperatures up to ∼40 K and varied temperature distributions throughout cloud under different CR irradiation intensities [335]. More conservative temperature increases ranging from ∼6 to ∼21 K have also been reported [336,337], with slightly higher values possible in the external layers of clouds [338] and strongly heated skins at the boundaries of cold clouds [242]. Other studies did not find an increase in temperature at all in some clouds under Galactic conditions [229], with CR heating power in diffuse clouds not even being competitive against thermal condition of heat from the hot ambient ISM plasma [242].

3.4. Clouds and Diffuse Media Associated with Stellar Remnants and Supernovae

Molecular clouds and diffuse ISM structures surrounding stellar remnants and SNe provide an opportunity to study CRs in the vicinity of their sources. Sometimes referred to as *active* molecular clouds, they are natural laboratories to investigate CR acceleration, propagation, and the feedback impacts CRs can deliver into the dense phases of the ISM. γ-rays provide information about CR interactions in molecular clouds near SNRs at energies above a GeV [124–129] (for early pre-*Fermi* era propositions and reviews, see [306,339]). The 6.4 keV neutral iron Kα line also traces MeV CRs in molecular clouds [340], as demonstrated by X-ray studies of known molecular clouds around SNRs [341–347]. Complementary information about the engagement of 10–100 MeV CRs can be obtained from molecular ion emission or absorption lines (e.g., [260]). Using multiple tracers sensitive to CRs of different energies opens a broad view of the CR spectrum in different parts of the Galaxy, and enables the study of relevant transport and interaction physics involved in CR feedback. For example, diffusive propagation of CRs away from their sources may be slower at lower energies. This can enhance the intensity of CR ionization and Iron Kα line signatures from the medium near SNRs, but may have less effect on γ-ray emission from the same region. To properly resolve the feedback impact CRs have in galaxies, a thorough understanding of their inhomogeneous distribution at different energies is required. Of particular importance is variation of the CR distribution with respect to ISM structures like molecular clouds, where CRs deliver feedback. This is set by the CR propagation physics, and the spatial correspondence between clouds and CR source locations.

Within the Milky Way, Ref. [348] showed that SNRs and molecular clouds occupy a volume fraction of the ISM of 0.01 percent and 0.25–3.3 percent, respectively. As the volume occupied by SNRs is much less than molecular clouds, the number of clouds in very close proximity to an SNR is low. OH maser measurements suggest only around 15 percent of core collapse SNe interact with dense molecular gas directly [349]. Notable exceptions have been studied. These may be identified from increased cloud temperatures due to shock heating, or high levels of turbulence within a cloud and offset γ-ray emission away from the cloud direction. There are several examples of SN shocks interacting directly with molecular clouds (e.g., HESS J1825-137, W49B, and the Boomerang nebula/SNR G106 region; see [203,204,350–352]). However, direct interaction of SN shocks, or the associated injection of CRs accelerated by shocks passing through molecular clouds statistically the less common scenario [348]. Instead, hadronic and leptonic CRs accelerated in SN shocks propagate diffusively through the ISM for some distance before encountering a molecular cloud. Non-linear effects, such as the build-up of low-energy ($<$10 GeV) CRs around sources could lead to self-confinement. In this scenario, the overabundance of CRs generates turbulence that scatters particles. This can lead to the suppression of the diffusion coefficient by up to 2 orders of magnitude [353]. γ-ray observations surrounding an SNR shell [122], and from hadronic γ-ray emission from molecular clouds in a range of CR-irradiated environments [124,156] have shown indications of such suppression of CR diffusion.

3.5. The Interstellar Medium of Starburst Galaxies and Implications for Cosmic Ray Feedback

The discussion in this section has focused on our local Galactic neighbourhood. However, in starburst galaxies, the configuration of the ISM and its components is different. Firstly, the overall energy budget of CR feedback in a starburst galaxy is larger than that of the Milky Way (e.g., [14,16]). They have more energy to deposit into their host's ISM, where their impacts can be stronger. In addition to this, the efficiency by which their feedback is delivered may also be greater. This is because of the closer spatial correspondence between sites of CR acceleration and the locations where feedback delivery would affect star-formation. For example, massive molecular cloud complexes are common in starburst galaxies [354], but not in the Milky Way. These clouds develop into massive stellar clusters, which are important CR accelerators (Section 3.1.2). Consequently, the fraction of CR sources interacting closely with molecular clouds is higher in starburst galaxies. More-

over, the prevalence of interactions between super-bubbles or SN remnants and clouds is likely to be much higher in intensely star-forming galaxies. This is indicated by the increased volume filling fraction of hot gas, which tracks the SN rate [355]. Additionally, the volume-filling fraction of SN remnants in the ISM will be increased (e.g., perhaps up to 8–9.5 percent in starbursts like M82 and NGC 253 [356]), making cloud-SN remnant interactions much more widespread. This is supported by observations, as the total γ-ray emission of starburst galaxies has a strong dependency on the star-formation rate. By contrast, γ-ray emission from clouds in the Galaxy shows a strong dependency on mass. This suggests that the γ-ray emission from star-forming galaxies originates mainly from CRs that are accelerated by local active sources [357]. These differences imply that CR feedback power is delivered more efficiently in starburst galaxies compared to the Milky Way, as the sources of CRs are generally much closer to the sites of star formation.

4. High-Energy Environments

Several nearby galaxies exhibit a γ-ray flux that exceeds the calorimetric limit of their star formation activity associated with SNRs [358,359]. This section is dedicated to discussing alternative, persistent CR production sites within galaxies.

4.1. Active Galactic Nuclei, Jets and Outflows

A sizeable fraction of galaxies are found to harbour an AGN or show a certain degree of AGN-like activities [360,361]. These galaxies, in particular those possessing jets, may have multiple sites of continuous CR production. Several scenarios have been proposed. They invoke either pγ or pp interactions as the mechanisms shown in Figure 6, or their combination in some situations. As the theme of this *Review* concerns CRs at the galactic scale (i.e., $\lesssim$10 kpc), we exclude systems with large-scale relativistic jets that extend far beyond the host galaxy. The discussions here therefore focus instead on radio-quiet systems, if there is AGN activity in their galactic centre.

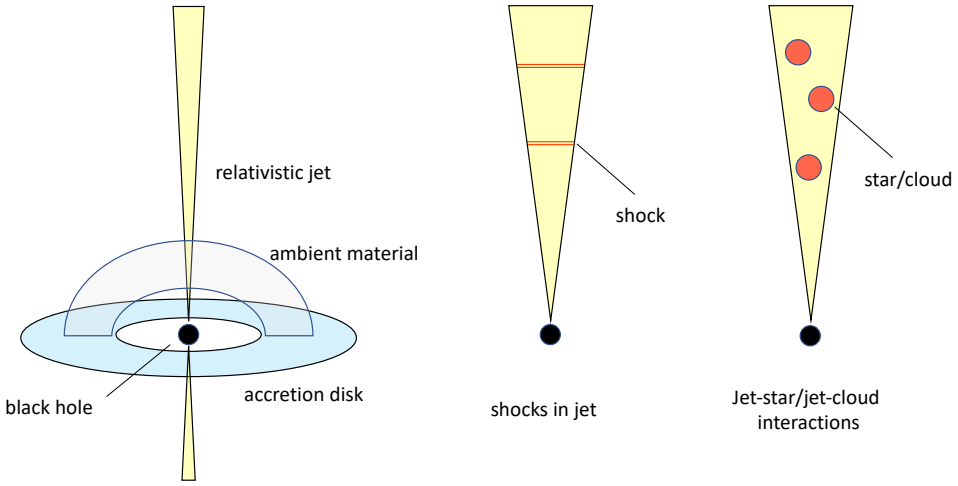

Figure 6. Illustrations of some possible scenarios for hadronic processes in galactic-scale environments associated with jets in a weak AGN (not to scale). (**Left**) The energetic particles in the jets interact with the ambient material, e.g., the ISM, near the central black hole. (**Middle**) Particles are accelerated and/or energised by the shocks formed inside the jet. (**Right**) The AGN jet interacts with stars or clouds trespassing into it.

Weak jets in radio-quiet AGNs that are CR source candidates would terminate at the scale of $\sim$ kpc (see, e.g., [362]). A recent ALMA observation toward NGC 1068 (a radio-quiet Seyfert galaxy) unveiled CR production activity, likely at the 'head' of the jet, $\approx$670 pc away from the supermassive black hole (SMBH) [363]. The CR power in the jet is estimated to exceed that expected from activity directly associated recent star formation episodes in this galaxy.

Wind outflows from the accretion disk are believed to be able to produce CRs. Ultra-fast outflows (UFOs) are the most powerful among variants of AGN disk winds. They are also fastest, and their velocities can reach 0.1 c, i.e., 10 percent of the speed of light [364,365]. This translates to a large kinetic power, as high as $\sim$5 percent of the bolometric luminosity of these systems [365,366]. They are a power bank that feeds the CR production processes. Current observations indicate that UFOs are present in roughly 40 percent of nearby AGNs [365]. However, possible mechanisms to transfer the kinetic energy carried in UFOs efficiently into CR energy are yet to be resolved. Nonetheless, there is no dispute, in terms of energetics, that UFOs, which share some similarity with relativistic jets, and that it is possible for them to produce high-energy CRs (see [367–371]).

The solar corona is known to produce particles of energies many orders of magnitude higher than the photons from the photosphere, through thermal emission process. The energetic particles arise as a consequence of a variety of sequences of eruptive magnetic coronal activities, field reconnection, shock formation, flaring emission and plasmoid ejection (see [372,373]). Such activities could also arise in corona above accretion disk in AGNs. As a consequence, energetic non-thermal particles are produced through macroscopic and microscopic plasma processes or different combinations of both in a multi-stage sequence, cf. coronal mass ejection and the associated acceleration of particles. Thus, accretion disk corona in AGNs are expected to be CR production sites (e.g., [374–379]); see also [380] for low-luminosity AGN cases). This scenario is supported by the recent IceCube observations, which identified a neutrino hot-spot (with a significance level of 4.2 σ) located in the direction of NGC 1068 [381], which is a known γ-ray emitter [382–384]. Production of VHE neutrinos in astrophysical systems is thought to arise through pion production channels (see Section 2.2). There is an equal chance that each of the three pion species (π^0, π^+ or π^-) are produced in a hadronic interaction. This implies that neutrino sources would also be intrinsic sources of γ-rays. Moreover, the intrinsic luminosity of the neutrino emission would not significantly exceed the that of the γ-rays, unless processes are present within the interaction sites that suppress charged pion production compared to neutral pion production. IceCube observations of NGC 1068 imply that the neutrino flux is greater than the GeV γ-ray flux [381,385]. This would require a suppression of neutral pion production, which is not easy to achieve. An alternative explanation is the significant attenuation of GeV γ-rays. One possible process to achieve this is the interaction of GeV γ-rays with strong radiation (or matter) fields.

Studies of X-ray binaries (XRBs) have shown them to be X-ray bright with a luminous accretion disk in a high-soft state, and latent jets. Taking accretion disks and jets in XRBs as a reference, it can be taken that accretion disks in certain AGN could produce a strong radiation field and that their jets are present but not prominent. While weak jets may be radiatively inefficient and are confined near the galactic centre, they would still be capable of accelerating particles. These energetic particles would undergo interactions within the strong radiation from the accretion disk, leading to the development of a particle cascade through the pγ interaction. In this scenario, γ-rays would arise from decay of neutral pions formed by CR interactions near the acceleration site, the magnetic disk corona. They would be attenuated when the accretion disk is luminous enough to create a dense radiation field (see [386–388]).

4.2. X-ray Binaries

Compact objects as individual systems, (e.g., isolated pulsars and magnetars [389–392]) or in binaries (e.g., cataclysmic variables (cf. [393–395]), XRBs [396] and millisecond pulsar binaries [397,398]) could produce photonic and non-photonic particles with energies greatly exceeding tens or hundreds of MeV. However, we do not discuss these sources here. Instead, we mainly consider microquasars, which are stellar-scale and share similar characteristics to AGN. One of these characteristics is their relativistic jets, which are powered by secular and episodic mass accretion. We put focus on SS433 and Cyg X-3, and their probable counterparts in early Universe, i.e., Pop III microquasars.

4.2.1. SS433

Highly collimated jets are expected to be efficient particle accelerators, and microquasars (XRBs with jets) are often considered as potential CR sources [184]. SS433 is one of the most investigated microquasars. It has a pair of well defined jets [399] and contains a compact object. This may be a black hole [400], accreting material from a probable super-giant star [401,402]. Polarisation observations have indicated that the magnetic field of the jets have helical structures [403,404]. They are embedded with the binary in the nebula W50, implying that there would be interaction between the jets and ambient nebula material.

Observations with the High-Altitude Water Cherenkov Observatory (HAWC) have detected of $\gtrsim$25 TeV γ-rays from the jets of SS433 [405]. The emission regions are $\sim$30 pc away from the location of the binary. Both the eastern and western emission lobes are found to coincide with these regions, from which X-ray emission is non-thermal [406–411]. These observations suggest that the jet downstream regions are sites of high-energy particle acceleration that produce the TeV γ-rays and non-thermal X-rays [412,413].

As illustrated in Figure 7, extragalactic microquasars, similar to SS433, may be associated with expanding bubbles with a velocity that can reach 80–250 km s^{-1} [414,415]. These expanding nebulae provide suitable conditions for particle production and CR acceleration, especially through a sequence of processes triggered by an initial hadronic interaction. It was shown in Inoue et al. [416] that nebulae with fast expansion velocities $\gtrsim$120 km s^{-1} are capable of accelerating charged particles up to $\sim$100 TeV, making them viable UHE CR sources.

4.2.2. Cyg X-3 and Related Systems

Cyg X-3 is an XRB with an orbital period of 4.8 h [417,418]. It contains a compact object, which is likely to be a black hole, although the possibility of it being a neutron star has not been ruled out. The compact object is accreting from a companion star, commonly identified as a WR star [419] from the characteristic broad emission line features and lack of Hydrogen lines in the optical spectrum. These features make Cyg X-3 unusual among the Galactic XRBs, both in terms of its evolution and orbital dynamics (see, e.g., [420]). Cyg X-3 spends most of its time in a hard X-ray spectral state. Although its radio emission may be relatively latent at that time, it occasionally shows episodic relativistic ejection and giant radio flares [421]. When it is radio active, Cyg X-3 is the brightest radio source among the Galactic XRBs (see, e.g., [422]).

The detection of a one-sided jet in Cyg X-3 [423,424] implies that the jets are highly relativistic and that the jet axes are sufficiently aligned with the line-of-sight (with a viewing angle probably $< 15^\circ$, see, e.g., [423]). Cyg X-3 is among the very few XRBs that have been detected in γ-rays [425–427]. As such, it has been considered as a potential CR source. How particles are accelerated in Cyg X-3 is still unresolved. It is also unknown if the material in the Cyg X-3 jets has a substantial amount of baryons. With the strong wind from the WR star, Cyg X-3 should be enveloped by a cocoon of dense wind material (see Figure 7). When the jets of Cyg X-3 encounter dense materials, shocks can be formed. These shocks will in accelerate charged particles, whether they are leptons or baryons. These energetic particles are CRs, and their interaction with the WR wind envelope would lead to the production of high-energy photons and particle cascades if there are substantial amounts of baryons in the jet material. The subsequent decay of the pions in the particle cascades will give rise to neutrino and γ-ray emission.

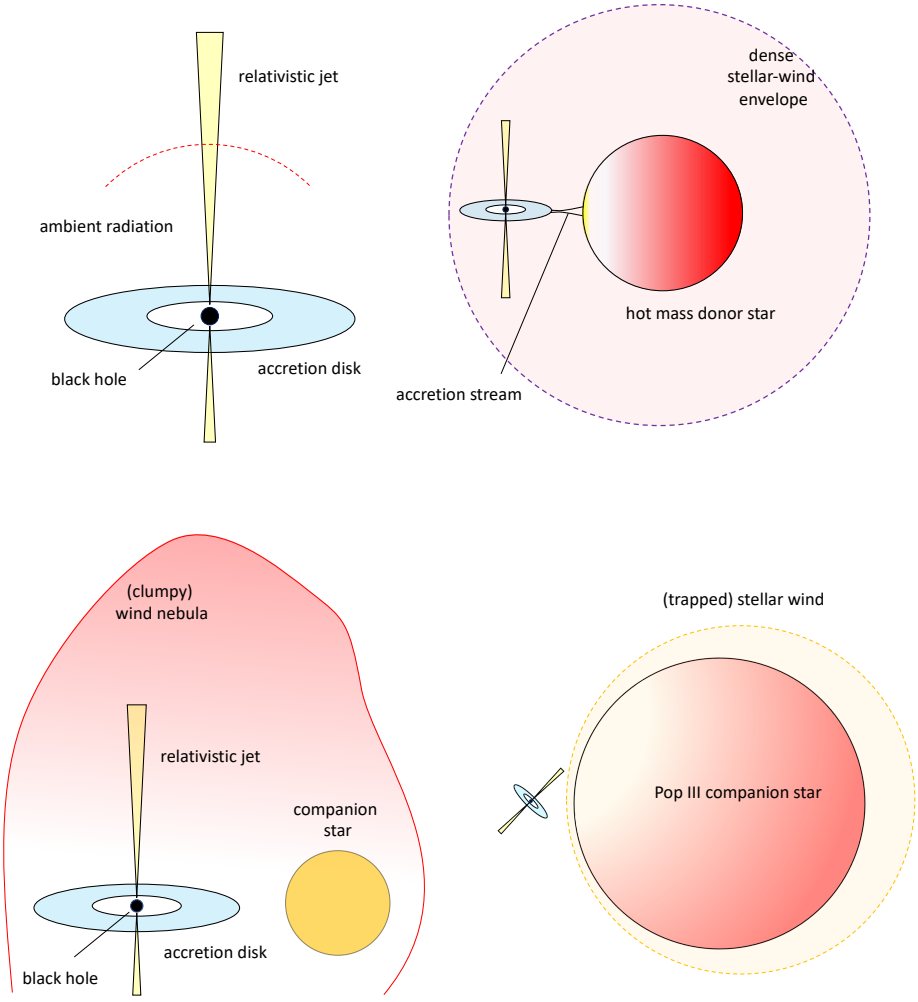

Figure 7. Illustrations of example scenarios for hadronic interactions in stellar-scale accretion-powered jet sources (not to scale). (**Top left**) A strong radiation field is present near its central engine, the black hole. The energetic particles in the jets interact with the photons in the ambient radiation field, leading to photo-hadronic processes. (**Top right**) The binary system is embedded within a circum-binary envelope formed from the dense wind of a Wolf–Rayet star. The energetic particles in the jets interact with the baryons in the circum-binary material, through pp processes. (**Bottom left**) The binary system resides inside a wind-blown nebula bounded by neutral or lowly ionised ISM. The nebula could be clumpy, and contains substantial non-thermal particles, which can be hadronic or leptonic. Shocks may arise when the jets propagate through the nebula, which leads to particle acceleration and re-energisation. The energetic particles originally in the jets, and/or accelerated/re-energised in the shocks interact with the nebula material as well as the ISM interfacing with the nebula medium through pp processes. (**Bottom right**) A Pop III XRB consists of a compact object accreting material from a very massive companion star. The companion star is expect to drive a wind. This wind is relatively weak compared to line-driven winds from massive stars with high metalicity. The wind material could be somehow trapped near the star. If the jets are not perfectly aligned with the orbital rotational axis, they will be intercepted by the trapped wind envelope or even the companion star itself.

4.2.3. Pop III X-ray Binaries

Pop III stars could have masses in excess of 100 $M_\odot$ (see [428,429]). They are short-lived and evolve rapidly. Some of them would end up forming black holes, through direct collapse or pair-instability SNe (see [430,431]). A Pop III star paired with a black hole forms a Pop III XRB, when the Pop III star begins to transfer material to the black hole (see [432]). Pop III binaries are often considered as counterparts of Galactic high-mass X-ray binaries

(HMXBs) in the early Universe. However, Pop III stars are metal poor and would not have a strong dense wind driven by large metal line opacity. Pop III XRBs are therefore different to present-day HMXBs. The mass transfer in Pop III XRBs, at least for X-ray luminous systems, would not be mediated by the accretion of the stellar wind onto the black hole. The mass transfer would instead be facilitated by Roche-lobe overflow or focused wind flows near the critical Roche surface and is probably driven by the nuclear evolution of the Pop III mass donor star, instead of orbital shrinkage caused by the loss of orbital angular momentum of the binary (see, e.g., [433]). Thus, Pop III XRBs are semi-detached binaries. Some Pop III XRBs would possess a pair of relativistic jets, which are sites of particle acceleration. These Pop III XRBs are microquasars, and are potential CR sources.

The mass ratio ($q = M_2/M_{\rm bh}$, where M_2 is the mass of the Pop III mass donor star) of Pop III XRBs would be around 20–40, if considering that the mass of their black holes is $M_{\rm bh} \sim (3-5)\,{\rm M}_\odot$. We may obtain the Roche-lobe radius $r_{\rm L}$, in terms of the orbital separation a for semi-detached binaries using the expression given in Ref. [434]. The ratio $r_{\rm L}/a$ is only weakly dependent on the mass ratio q. For the parameters of Pop III XRBs considered here, $r_{\rm L}/a \approx 0.6$, over the range of $q \sim$ (20–40). This almost constant value of $r_{\rm L}/a$ implies that a jet/outflow with a 45° half-cone opening angle will hit the atmosphere of the Pop III star (see illustration in bottom right panel in Figure 7), if the symmetry axis of the jet/outflow has a tilting angle of $>8°$ with respect to the angular momentum vector of the binary.

While such a jet-tilting angle is not expected to be commonly found in the Galactic microquasars, which are mostly low-mass X-ray binaries (LMXBs) and have evolutionary time scales of order hundreds of Myr, it would not rule out the possibility of such jet orientations to occur in Pop III XRBs. However, little is known about the evolutionary trend of the progenitors of the Pop III XRBs. It is unlikely that Pop III XRBs would go through the same evolutionary channels that produce Galactic HMXBs and LMXBs (see, e.g., [435,436]). The short-lived nature of Pop III stars implies that Pop III XRBs are all extremely young systems. The black holes in Pop III XRBs would not have sufficient time for their spins to align with the orientation of the angular momentum of the binary orbit. The accretion torque would instead drive the black hole spin axis and the jet axis into precession and nutation. If the jets have a substantial amount of protons, the atmosphere of the Pop III star will act as a target for energetic protons in the jet. This leads to hadronic pp interactions, which generate cascades of descendent pions and leptons. This scenario of CR production does not require the presence of material outside the binary.

There are more conventional views for CR production where Pop III XRBs are practically direct counterparts of the Galactic microquasars, except that the mass donor star in a Pop III XRB is a massive and ultra-metal-poor Pop III star. Thus, the particle acceleration and production scenarios are the same as those proposed for the Galactic XRB jet sources (see, e.g., [437,438]), using the same prescription developed for CR production in AGN jets (see, e.g., [439,440]). The energetic particles that result from acceleration in the jets, presumably through shocks, would interact with the ambient radiation field through pγ interactions, or pp interactions with baryonic matter in the cocoon/envelope close outside the binary, or in a nebula at a larger distance (see, e.g., [441]) (see Figure 7). In this scenario, particle acceleration and hence CR production and interactions in the Pop III XRBs are analogous to those in the microquasars SS433 and Cyg X-3 described earlier in this section.

Compared to low-mass Galactic microquasars, Pop III XRBs might be more likely to reside in crowded young multiple-star environments. The evolutionary timescale of Pop III XRBs is expected to be shorter than the dynamical time scale of their host galaxies. Thus, Pop III XRBs would not have sufficient time to disperse from their birth places (cf. the distribution of the HMXBs and LMXBs in the Galaxy). This also implies that Pop III XRBs might cluster in close proximity to each other. When an ISM is bombarded collectively or continually by energetic CR particles and and irradiated by intense radiation from a cluster of Pop III XRBs, it would inevitably be heated. This in turn will affect subsequent episodes of star formation and, hence, the next generation of stars and early-Universe XRBs.

5. Cosmic Rays in Galaxies and Their Circumgalactic Environments

5.1. The Milky Way

The distribution of CRs within and around the Milky Way can be measured using γ-rays. High quality all-sky data obtained with *Fermi*-LAT now allows a detailed view of CR engagement within the Galaxy to be constructed (see Figure 8; for a review of interstellar γ-ray emission studies and its implications for the distribution of CRs in the Galaxy, see [442]). One of the most striking signatures in the γ-ray sky above 1 GeV is the Galactic plane itself. Intricate emission structures, which trace the underlying gas distribution, emerge as bright extended diffuse emission. This covers the entire galaxy, while less bright extended emission reaches several degrees above and below the plane. Hadronic CRs are contained within the Galactic ISM by the interstellar magnetic field. They interact with the ISM gas by inelastic pp collisions (see Section 2.2). The resulting decay of neutral pions, produced in these interactions, generates the observed emission. The intensity of the emission is proportional to the product of the local gas density and the CR density. Thus, the distribution of CRs can be recovered where high-resolution gas maps using an appropriate tracer are available. Some of the more reliable dense gas tracers are CS and dust. However, they do not always agree, and they are not guaranteed to provide the same information about the precise ISM gas distribution (e.g., [443,444]). This can lead to substantial differences in inferred CR distribution estimations.

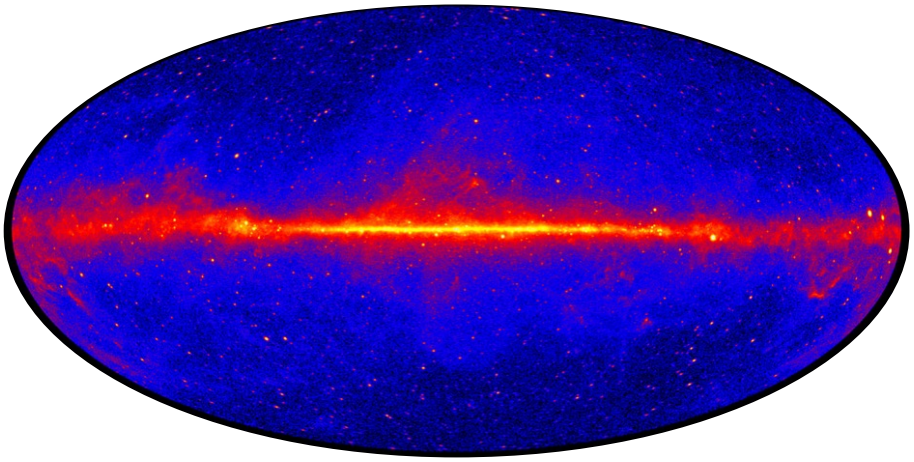

Figure 8. Full sky as seen with *Fermi*-LAT at energies above 1 GeV over 12 years of observations (Hammer projection). The Milky Way dominates the emission, and the Galactic Plane appears across the middle of the image as a bright diffuse glow. The Galactic interstellar diffuse γ-ray emission originates from hadronic CR interactions with gas and leptonic interactions with the interstellar radiation field. It provides a clear signature for the presence of CRs. Image credit: NASA/DOE/*Fermi*-LAT Collaboration. Reproduced in accordance with NASA Media Usage Guidelines.

γ-ray emission features in the Galactic plane are particularly strong around the GC. The CMZ is located in the middle of the central bright peak. The origin of this γ-ray emission is unclear. While it is likely both a hadronic and leptonic component would be present, the relative importance of each is unsettled. Strong radio emission has been observed in this region [445]. It has been suggested this originates from predominantly leptonic primary CRs in intense GC magnetic fields. These CRs could also contribute significantly to the γ-ray emission through inverse Compton scattering [445]. An alternative scenario has also been considered, motivated by the strong magnetic fields (up to 100–250 μG [446,447]) and concentrated molecular gas content in the GC. These conditions resemble those typically found in starburst galaxies (see [446], also Section 5.2.3), leading to the proposition that the CR population could have a significant hadronic composition [446]. In this scenario, the CRs experience cooling and advective losses within a single-zone three-phase ISM, including diffuse, hot gas, ionized gas, and dense molecular gas. This can provide a plausible

explanation for the TeV emission from the CMZ and account for the radio emission via synchrotron radiation from primary and secondary CR electrons. However, the GeV γ-ray emission in this scenario is under-predicated and much more difficult to reconcile with observations. This suggests a need for an additional CR component, or a population of unresolved γ-ray sources. The precise details of the CMZ emission require further investigation. However, it is evident that a significant population of CRs exist in that region. They could be supplied by a hidden population of pulsars (as has recently been proposed by several studies, including, e.g., [448]), pulsar wind nebulae, processes associated with the Sgr A* supermassive black hole, or SN remnants arising due to the elevated local star-formation rate.

Above and below the CG, extended diffuse γ-ray structures can be seen (these can be discerned faintly in Figure 8). These so-called *Fermi* bubbles extend to heights of 50° above and below the GC, with a total 1–100 GeV power of $>10^{37}$ erg s^{-1} and a spectral cut-off at around 110 GeV [449] (for a review, see [450,451]). The origin of these structures is unsettled, and their non-thermal composition could be hadronic (e.g., [452,453]) or leptonic (e.g., [454–456]). One possibility is the presence of a galactic outflow driven by feedback from concentrated star-formation activity around the GC [452]. This outflow could serve to channel hadronic CRs from the ISM into the Galactic halo and CGM. This may also be achieved by subsonic breezes [457]. These breezes, although slower, can have a similar role in CR circulation through a combination of advection and diffusion. They have been shown to be capable of supplying CRs several kpc into the CGM, where they can sustain CR energy densities as high as a few percent as that in the ISM [457,458]. Alternatively, the CRs could be supplied by past jet activity of the Sgr A*, where the CR electrons are rapidly transported to high Galactic latitudes before they cool [454,459,460]. This leptonic jet model has been shown to reproduce the spatially uniform γ-ray spectrum [461] as well as the recently discovered X-ray *eRosita* bubbles [462].

The presence of CRs in galactic halos has been investigated for some time. This interest stems from observations of kpc-scale synchrotron halos around edge-on galaxies (e.g., [463]), as well as simulation work indicating a significant population of CRs reside in the CGM of Milky Way mass galaxies [464–466]. Recent studies have reported detections of extended halo emission around M31 in γ-rays. It extends up to 200 kpc from the center [467]. It is possible that some of this extended emission originates from bubbles analogous to the Galactic *Fermi* bubbles [468], but most can be attributed to M31's CGM. The exact origin of this emission remains unsettled, however leptonic models with in situ CR acceleration in the acceleration shock due to in-falling matter [467], hadronic models involving CR advection [126] and hadronic models including both CR advection and diffusion have been considered [469]. The presence of CRs in the CGM of the Milky Way has also been observationally confirmed. Studies using γ-rays emitted from High and Intermediate Velocity Clouds (HVCs and IVCs) at heights ranging from hundreds of pc to a few kpc [470][14] showed their emissivities to exhibit a significant decrease with distance from the Galaxy, up to $\sim$2 kpc [470,474]. This is caused by a decreasing CR density with distance. It has been suggested that the emission from CRs interacting within the Milky Way's halo gas may contribute to the isotropic γ-ray background [467,475,476], and these interactions may also account for some of the diffuse flux of neutrinos observed by IceCube [477] (although this contribution is likely sub-dominant [478]).

The existing observations have provided important insights that allow effective CR transport models in the Galactic halo to be constrained. However, upcoming instruments like the Cherenkov Telescope Array (CTA), with its increased sensitivity, will enable the detection of more HVCs, IVCs, and halo gas in γ-rays. With the data to be obtained from these next-generation instruments, it will be possible to conduct more thorough tests of CR transport models within the CGM. Efforts have already begun to model CR diffusion in the CGM context more rigorously, in order to relax the approximations associated with effective transport treatments. In particular, consideration has been made of the non-linear interaction of CRs with MHD waves excited through the CR streaming instability [479–481], and their

interplay with fast-mode turbulence [482], or advection from the Galactic disc [483]. These models allow the role of CRs in CGM ecosystems, and their influence on the evolution of central galaxies, to be explored more thoroughly by reducing model uncertainties and establishing more reliable treatments of CR transport.

5.2. Studies of Cosmic Ray Effects in Individual Galaxies

5.2.1. Cosmic Ray Containment, Calorimetry and Galactic Magnetic Fields

CRs emerge as an inevitable consequence of star-formation in galaxies, regardless of the underlying source type or acceleration mechanism (see Section 3.1). Starburst galaxies are therefore rich in CRs. These CRs are scattered in galactic magnetic fields (Section 2.1), and typically experience a diffusive propagation regime. They are confined by their host galaxy and leak out gradually through a combination of diffusion and advection, or undergo attenuation and/or complete energy loss through cooling before they can escape. A CR confinement scenario can develop quickly in a starburst galaxy. It is controlled by the magnetization of the ISM, which is believed to arise early in its evolution. It has been proposed that the growth of magnetic fields in galaxies may be closely connected to their star formation activities. In this scenario, a saturated μG magnetic field can develop within a few Myr after the onset of star formation, if driven by a turbulent dynamo mechanism [484]. This is consistent with observations, which indicate early magnetic field growth in galaxies. In particular, high-redshift galaxies have generally been found to harbor well established ISM magnetic fields with strengths comparable to those in local galaxies (e.g., [485,486]).

The degree of CR confinement a galaxy can practically achieve is set by several factors. In some galaxies, a calorimetric limit can be reached where CRs are completely absorbed, or lose all their energy before they can escape. This results in the conversion of a very high fraction CR energy to ISM heating or non-thermal radiation and neutrinos. The degree of calorimetry varies with CR energy and species, with electron calorimetry generally being more achievable than proton calorimetry. While main sequence or relatively quiescent galaxies like the Milky Way may have low calorimetric fractions, starbursts like NGC 253, Arp 220, or M82 can exhibit very high calorimetry [356]. This is because their strong magnetic fields and dense interiors are very effective in containing, cooling and/or absorbing CRs.

In highly calorimetric settings, close correlations are expected between CR injection rates (estimated by tracers of a galaxy's star formation rate, e.g., its far-IR luminosity) and signatures for CR activity. Thus, starburst galaxies not dominated by AGN emission generally exhibit strong correlations between their far-IR, γ-ray, and radio luminosities (e.g., [12,358,487–491]).[15] Electron calorimetry can naturally explain the tightness of the far-infrared (FIR)–radio correlation. However, its validity has been questioned due to conflicts in the observed radio spectral indices for normal galaxies [493,494] and difficulties to reconcile the inferred CR diffusive escape time in the Milky Way with the typical estimated synchrotron cooling time [495]. These tensions have motivated the development of modified calorimeter models for normal galaxies that include CR escape over comparable timescales to electron cooling [496] and invoke SN remnants as a cause of a flattened radio spectrum (e.g., [497]). Other approaches have proposed to move away from the calorimeter model entirely (e.g., [498,499]), but these often require some sort of 'conspiracy'[16] to maintain the tightness of the FIR–radio correlation, given the enormous dynamic range in physical properties of galaxies that obey it.

More recent studies have considered sophisticated analytical models of turbulent clumpy star-forming galactic disks [495] or detailed numerical simulations to investigate the physics and development of the far-IR-radio and far-IR-γ-ray relations relations in various situations. These include evolving protogalaxies [501], Milky Way-like galaxies [502] and isolated galaxies over a broad range of halo masses [503,504]. These studies show that the relations can start to break down for low IR luminosity quiescent galaxies [505], where CR escape can become more severe [506]. For example, even though Milky Way-like galaxies are believed to be reasonably efficient electron calorimeters (e.g., [507]), they are not likely

to be proton calorimeters [505] and are not guaranteed to closely follow either the far-IR-radio or the far-IR-γ-ray relation [506]. In very extreme galaxies such as Arp 220 or the Circinus galaxy, calorimetry may exceed 100 percent. This could be due to highly efficient CR acceleration, systematically more energetic SN explosions, or contamination from AGN emission or other γ-ray sources [505].

The multi-scale configuration of the magnetic field of a galaxy regulates effective CR propagation parameters (see Section 2.1). This sets the distribution and confinement of CRs, and governs their calorimetry and feedback patterns. On macroscopic scales, CR propagation is fundamentally anisotropic (e.g., [508,509]). Modeling it as an isotropic process on the scale of galaxies can distort our qualitative understanding of the resulting CR feedback effect. For example, invoking isotropic CR diffusion in models can lead to stronger galactic outflows [510], weaken the development of the Parker instability [511], or significantly affect outflow wind launching and mass loading factors [512]. To properly establish an effective prescription for large-scale anisotropic CR propagation through a galaxy, a thorough understanding of the large-scale magnetic field structure is needed. In recent years, it has become possible to measure this using instruments like the High-Angular Wideband Camera Plus (HAWC+) on the Stratospheric Observatory For Infrared Astronomy (SOFIA) [513] and POL-2 on the James Clerk Maxwell Telescope (JCMT) [514].

From these studies, it has been shown that the large-scale structure of the magnetic field of a galaxy is strongly influenced by its dynamical situation. For example, barred-spiral galaxies, such as NGC 1068 (Figure 9, left panel), have exhibited an organized magnetic field patterns that align closely with their spiral arms. This alignment would direct CR diffusion along the spiral pattern, thereby influencing CR feedback patterns. Moreover, this alignment may also enhance CR calorimetry on a global scale throughout the galaxy. Anisotropic diffusion of CRs along the arms is favored over inter-arm diffusion, leading to longer propagation distances for CRs and an increased likelihood of cooling or absorption before escaping the galaxy. This effect becomes particularly significant if CRs are predominantly injected into the spiral arms. Indeed, this would be expected in a density-wave origin for the spiral pattern, where the arms represent regions of intensified star-formation and, consequently, higher CR density.

Figure 9. (**Left**) Magnetic fields in NGC 1068 shown as streamlines, measured using SOFIA's HAWC+ instrument using polarized far-IR emission to observe dust grains aligned perpendicular to their local magnetic field vector. They are plotted over an X-ray/visible composite image (from *HST*, *NuSTAR* and SDSS). Magnetic fields follow the spiral arms, where elevated star-formation is taking place. The spiral arms in this galaxy will be the main source of CRs, and the magnetic fields aligned with them will preferentially channel CRs. This may introduce distinctive feedback patterns. Image credit: NASA/SOFIA; NASA/JPL-

Caltech/Roma Tre Univ. Reproduced in accordance with NASA Media Usage Guidelines. (**Right**) Magnetic fields in Antennae galaxies probed at 154 μm, overlaid onto an *HST* image (from [515]). This system is undergoing a collision, with two cores (NGC 4039 below and NGC 4038 above). The magnetic fields roughly align along a tidal tail to the west of the system, and the two cores show inter-connecting magnetic fields. A relic spiral arm persists to the North-East, associated with NGC 4038, which retains some magnetic field alignment. The correspondence between the magnetic field and density/relic spiral structures elsewhere has been completely disrupted. The resulting configuration of the system could channel CRs between the two cores, or release CRs along the tidal tail into the intergalactic medium (IGM). This may reduce CR containment in the individual components of this system. Figure adapted from Lopez-Rodriguez et al. [516].

Elevated star-formation levels in galaxies can disrupt the alignment between magnetic fields and spiral arms. This is due to winds and ISM bubbles caused by feedback processes (e.g., [517]). The disruption becomes even more pronounced in chaotic systems such as the colliding Antennae galaxies (Figure 9, right panel). In this case, the magnetic field is primarily influenced by the interactions between the galaxies themselves, and is stretched between them. The strong disruption of magnetic fields during the collision phase of these galaxies would initially release confined CRs into the intergalactic medium. However, as interconnected magnetic fields formed between the interacting galaxy cores after the initial collision, CRs would begin to channel between them. CR channeling between the interacting galaxies would become established over a diffusion timescale (a few Myr). This is much shorter than the typical timescale of galaxy interactions, which is on the order of several hundred Myr [518]. Consequently, intense episodes of star formation in one galaxy can exert a feedback impact on the other galaxy in this pair. This illustrates the interconnected nature of CR feedback effects in galaxy interactions.

5.2.2. Cosmic Ray Pressure Support in Individual Galaxies and the Eddington Limit

CR feedback in galaxies can be invoked as an intrinsic or extrinsic mechanism. Intrinsic processes operate in the ISM, often at the molecular cloud level (see, e.g., Section 3.3.4). They rely on CR containment within a galaxy. This containment can also form as part of an extrinsic feedback mechanism. The pressure support provided by CRs can help maintain the stability of the ISM. If the density of CRs becomes sufficiently high, it can disrupt hydrostatic equilibrium and give rise to a CR-driven wind [519]. The supply of CRs in a galaxy is linked to its star-formation rate. This connection sets a practical upper limit to the star-formation rate known as the CR Eddington limit, analogous to the case with radiation [519]. Recent studies have re-examined this stability limit and found that galaxies with high gas surface densities, exceeding 10^2–10^3 $M_\odot$ pc^{-2}, and large star formation rates are unlikely to approach the it. This is because the strong hadronic losses experienced by CRs interacting with the interstellar gas make them less dynamically significant [520,521]. As a consequence, galaxies in this regime become increasingly calorimetric and present higher γ-ray emission due to pion production [520]. For surface densities below $\sim 10^2$ $M_\odot$ pc^{-2}, CRs can be dynamically important. They are capable of launching winds of cool material from galactic discs, thereby curtailing star-formation through catastrophic losses [521].

Typically, quiescent, low surface density galaxies like the Milky Way and local dwarf galaxies reside within the CR-stable regime. However, many of these systems, particularly Milky Way-like galaxies, are on the cusp of instability. CRs offer significant support to the ISM in these cases [521,522]. Even slight modifications to the configuration of their ISM or the CR pressure can trigger CR-driven outflows, producing strong limits on their star-formation efficiency [521]. Studies have shown that the wind launching mechanism is relatively robust across different CR transport models [522], but the specific model adopted can affect the magnitude of the CR Eddington limit. Advection or diffusion-dominated transport generally leads to sub-Eddington galaxies [523], with CR streaming representing the most favorable scenario for galaxies to reach the Eddington limit [523].

5.2.3. Nearby Starbursts

High-energy γ-ray emission has been detected in several nearby star-forming galaxies using *Fermi*-LAT [359,487,489,524–526]. Subsequent observations with Imaging Atmospheric Cherenkov Telescopes have confirmed the persistence of this emission up to multi-TeV energies in two starburst galaxies: M82 and NGC 253 [527–529]. Future instruments like CTA, with higher sensitivities, are expected to detect other nearby starburst galaxies at similar energies [530]. High-energy γ-ray emission serves as an indicator of the presence of CRs within these galaxies. Moreover, the observed correlation between this emission and the IR luminosity of galaxies demonstrates a connection between the injection power of CRs and the level of star formation activity in a galaxy (see also Section 5.2.1). Traditionally, this correlation has been attributed to CR acceleration in core-collapse SNe and their remnants, as the rate of these events closely tracks the star-formation rate in a galaxy [96]. However, alternative possibilities, including CR acceleration in young stellar clusters and star-forming regions, have gained increasing consideration in recent years (see Section 3.1).

M82, NGC 253 and Arp 220 are worthy of dedicated discussion. Their close proximity has allowed extensive study to provide thorough insights into their internal physical conditions, including the effects of CRs. All three galaxies host outflows, which have substantial impacts on CR containment and feedback potential. These outflows are multi-phase [531–535] and are driven by the confluence of feedback winds from ongoing concentrated bursts of nuclear star-formation. M82 maintains a star formation rate of approximately 10 $M_\odot\,yr^{-1}$ [536] within a central region of diameter 0.3 kpc [537,538]. NGC 253 has a lower star-formation rate, around 5 $M_\odot\,yr^{-1}$. This is a residual burst, initiated by the collision with a gas-rich dwarf galaxy approximately 200 Myr ago [539]. Although less active than M82, approximately 40 percent of NGC 253's star formation is concentrated within the central kpc and is associated with a dense CMZ of size approximately 0.8 kpc [540]. This concentration of star formation drives an outflow, and may play a driving role in baryon recycling flows throughout the galaxy halo [541]. In contrast to the tidally triggered nuclear starbursts in M82 and NGC 253, Arp 220's activity is believed to result from a collision between two spiral galaxies a few hundred Myr ago, leading to a more intense system. The majority of the star-forming activity is concentrated within two nuclei, with rates of 65 $M_\odot\,yr^{-1}$ in an Eastern nucleus and 120 $M_\odot\,yr^{-1}$ in a Western circumnuclear disk [542]. Both nuclei exhibit fast outflows, with slightly higher velocities observed in the Western nucleus [535,543].

All three of these starbursts are good electron calorimeters. A regime of strong electron confinement and energy retention is established in their cores. Non-synchrotron losses, such as bremsstrahlung and ionization, play a significant role in establishing electron calorimetry in these galaxies, with bremsstrahlung being particularly important above a GeV [544]. The same level of calorimetry is not achieved for CR protons. None of the three galaxies are believed to be fully calorimetric to protons, although all are more so than the Milky Way.

NGC 253 has an estimated proton calorimetry fraction of a few tens of percent at 1 GeV [356,544,545][17] If current estimates are accurate, the timescale for CR protons to undergo hadronic interactions is comparable to the advection escape timescale in the galactic wind. This implies that CRs interact with the ISM in the host galaxy near its mean density, and must be far below the level needed to support the galaxy against gravity. It follows that CRs are not dynamically important in driving the NGC 253 outflow [546]. Despite this, CR feedback has been estimated to strongly impact the nuclear CMZ region of NGC 253 and potentially dominates the thermal balance of the gas in this area [547].

M82 is a better proton calorimeter compared to NGC 253 at most CR energies [356,544–546], but a large fraction of protons can still escape, particularly at higher energies [544,545,548]. CR pressure is therefore relatively low, and can sustain only small fraction (around 2 percent) of that required for hydrostatic equilibrium if CRs interact with ISM at its

mean density [546]. This suggests that CRs are also not dynamically important in M82's outflow, and CR pressure gradients are weak compared to gravity [548].

Arp 220 is considerably more abundant in CRs. It is also much denser, with the gas around its nuclear starbursts averaging $\sim 10^4$ cm^{-3} [549], compared to $\sim 10^3$ cm^{-3} in M82's core [548,550]. This high gas density creates excellent conditions for the detection of molecular ions chemically related to low-energy CR ionization. These have been used to confirm the importance of CR heating within this galaxy [551]. The high gas density also creates short CR loss times to pp interactions. This boosts proton calorimetry, and a substantial fraction of the proton flux is converted to pions. Of the three examples, Arp 220 is the closest to being a proton calorimeter, even up to CR energies of 100 GeV [356,542,544]. At 1 GeV, it may achieve in excess of 99 percent calorimetry [356]. While this suggests potential for CRs to play an important dynamical role in Arp 220, their exact importance remains uncertain due to the absence of dedicated work.

Detailed multi-wavelength studies have been conducted for each of these galaxies to investigate their non-thermal properties. These studies include one-zone models that put focus on the role of CRs in multi-wavelength emission (e.g., [446,544,552–554]). These models are often used to fit or constrain the internal physical configuration of the galaxies (e.g., [555–558]). Multi-messenger modelling has also been possible (e.g., [358,546,559,560]), and some of these galaxies have even been considered as potential neutrino source candidates for upcoming instruments such as KM3NeT and IceCube-Gen2, albeit with optimistic model parameter choices (e.g., [560] for NGC 253). More sophisticated two-zone models have also been developed [86,542,561]. They have revealed that the γ-ray and radio emission may be inconsistent with a purely starburst origin in certain cases, particularly in Arp 220. In this galaxy, a self-consistent solution may require the presence of an AGN in the western nucleus to account for excess γ-ray flux [561].

5.2.4. Dusty, and Infrared and Submillimeter Luminous Galaxies

Luminous infrared galaxies (LIRGs) are a class of galaxy characterized by their high rest-frame IR luminosities, above 10^{11} L$_\odot$. Ultra and Hyper luminous IR galaxies (ULIRGs and HyLIRGs) are particularly luminous sub-classes, above 10^{12} L$_\odot$ or 10^{13} L$_\odot$, respectively. These galaxies are believed to represent an evolutionary phase of merging spirals [562,563]. They are powered by intense starbursts, with star formation rates surpassing 100 M$_\odot$ yr^{-1} (e.g., [564]). Their IR emission mainly originates from the reprocessing by dust of strong interstellar radiation fields associated with the rapidly forming stellar population. Additional contributions from AGN are sub-dominant, typically providing no more than 10 percent of total IR galaxy luminosities [565].

The vibrant star-formation activity of LIRGs establishes them hosts of large reservoirs of CRs. This is seen in Arp 220, the closest example of a (U)LIRG, where the abundant CRs have a role in regulating its physical conditions (see Section 5.2.3). The interactions of these CRs produce γ-rays and neutrinos (e.g., [566,567]) which contribute to the extragalactic diffuse backgrounds. These backgrounds have been measured with IceCube [568–570] and *Fermi*-LAT [571]. LIRGs have recently emerged as a viable contributor to these backgrounds following a neutrino detection from the LIRG NGC 1068 [381] (see also Section 4.1). Combined multi-messenger observations of neutrinos and γ-rays suggest that some neutrino sources may be opaque to γ-rays [572,573]. If true, it would alleviate the observational constraints on source populations that can generate neutrino backgrounds without violating the observed γ-ray background [571]. Dusty LIRGs may experience suppressed γ-ray emission through pair production interactions within their intense IR radiation fields (e.g., [249]) or dense gas [574]. They may constitute an important source class capable of conforming to γ-ray constraints while still supplying significant flux to the diffuse neutrino background.

Strong IR continuum emission makes LIRGs excellent natural laboratories for the observation of CR feedback effects. In particular, gas phase species produced from CR ionization in molecular clouds can be observed in absorption against this continuum. OH^+ and H_2O^+ are relatively direct chemical tracers (see Section 3.3.2) that can be used to probe

CR ionization in galaxies [575]. These tracers have been detected in the nuclear regions of ULIRGs, revealing that strong CR irradiation is driving substantial ionization. Rates of 10^{-13} s^{-1} have been measured in some galaxies [551,576]. This exceeds the canonical value for the Milky Way by around four orders of magnitude. As CR ionization is closely related to CR heating power in ISM gas (e.g., [229]), these measurements demonstrate the likely importance of CRs in setting the thermodynamics of IR-luminous galaxies.

Dusty, bright submillimeter galaxies (SMGs) are even more compelling targets for observational studies of CR ionization and feedback. These are among the brightest and most prolific star-forming galaxies in the Universe, and are believed to form an important stage in the evolution of massive elliptical galaxies seen in the local Universe [577]. SMGs, being rich in CRs, represent a domain where our understanding of galaxy formation and evolution remains uncertain. Obtaining a clear determination of the impact of CR effects on the development of massive elliptical galaxies is therefore important. Similar to LIRGs, SMGs are very dusty [578,579]. The far-IR emission from this dust in SMGs produces a strong continuum at submillimeter wavelengths. This serves as an effective back-light for absorption lines originating from molecular ions associated with CR ionization in their ISM. The shape of the spectral energy distribution (SED) of SMGs overcomes cosmological fading. Their apparent luminosity increases with redshift, resulting in a nearly constant apparent flux density at submm wavelengths between z = 0.5–7 [580]. This so-called 'negative k-correction' is a clear observational advantage. When coupled with gravitational lensing and the excellent sensitivity of state-of-the-art facilities like ALMA, CR feedback in individual galaxies during the cosmic noon and before can be thoroughly explored.

Ground-based instruments like ALMA are crucial for high-fidelity spatial observations of CR effects throughout galaxy interiors. Although lines from favoured molecular ion species often used to trace CR ionization usually fall outside accessible frequency ranges in the rest frame, cosmological redshift can bring some of them into observable bands [581]. Indeed, OH^+ and H_2O^+ have recently been measured in cosmic noon galaxies with ALMA. CR ionization rates of $\zeta = 10^{-16}$–10^{-15} s^{-1} for SDP 17b and 10^{-16} for the Eyelash galaxy were found [581], indicative of some CR feedback activity. However, there are uncertainties in these values. For example, higher estimates, up to $\zeta = 10^{-13}$–10^{-11} s^{-1}, have been obtained for the Eyelash galaxy, but these are more model-dependent, based on the estimated galaxy SN event rate [582]. Moreover, the CR ionization rates determined by Ref. [581] may be associated with more distant, low-density, extended halo gas surrounding these compact SMGs rather than the galaxy itself.[18] Further in-depth studies are therfore required to lift some of these ambiguities and obtain a more definitive measurement of CR ionization within SMGs and their halos.

5.2.5. Primordial Galaxy Evolution

CRs have been considered as a potential cause for the quiescent behavior and complex star-formation histories observed in some high-redshift galaxies [17,223]. A specific focus has been on post-starburst galaxies (PSGs), also known as E+A galaxies, which are found at both low [584–587] and high redshifts [94,588,589]. PSGs show strong Balmer absorption lines in their SEDs, indicating the presence of young stars. However, they lack the optical emission features typically associated with ongoing star formation. Additionally, the detection of metallic absorption lines (e.g., Ca, H, and K) suggests the existence of older stellar populations within these galaxies. These observations imply that PSGs have experienced multiple episodes of star formation, with one having occurred relatively recently.

The star-formation histories of PSGs is perplexing. Their abundance of interstellar molecular gas would normally sustain star formation [584]. However, these galaxies evolved through multiple quenched epochs suggesting some kind of transient quenching mechanism arose at different points in their history. Conventional quenching mechanisms, such as those associated with AGN feedback, do not seem to play a significant role in shaping the evolution of E+A galaxies [590]. Additionally, the presence of large molecular

reservoirs, dust, and a substantial ISM make the evacuation of gas by outflows an unlikely explanation for their behavior [585–587,591].

High-redshift PSGs are challenging to observe in detail. However, lower redshift systems are more accessible and have provided certain insights into the causes of their complex star-formation histories. In particular, they have been found to have a deficiency of dense molecular gas pockets [585]. This suggests that processes capable of providing additional pressure to their molecular gas reservoirs are at play. These could prevent the fragmentation and collapse of ISM and halo gas. CRs have been proposed as a potential agent able to exert this pressure in both the ISM and CGM. They can act directly on semi-ionized magnetized gas (e.g., [232]), or they can operate indirectly by heating gas within (e.g., [230,592]) or around [593] galaxies, or by modifying inflows of gas through the CGM [17,223]. However, to establish the role of CRs conclusively, a distinctive signature of their effects within these systems is required.

Recently, several possibilities have been considered to identify a distinct 'smoking gun' signature of CR feedback in PSGs. One approach focuses on the progressive and delayed nature of this feedback. If CRs serve as the primary feedback mechanism within a galaxy, their effectiveness relies on the growth and saturation of the galactic magnetic field to levels of a few μG. This is necessary to contain of CRs and enable a sustained delivery of their feedback power [14,17]. This produces a progressive feedback effect, characterized by a delayed onset. In a population of PSGs, this delayed feedback would be identified from a proportional relationship between the level of star-forming activity during a starburst phase and the duration of a subsequent quenched phase. Additionally, an inverse correlation would be expected between the star-formation rate during the burst phase and the duration of the burst itself (see Figure 10 and Refs. [223,594]). By conducting population studies of multiple PSGs experiencing CR regulation, these trends would emerge with minimal scatter to reveal a signature of CR feedback. In contrast, more stochastic feedback mechanisms like energetic hypernova events deliver feedback abruptly and randomly, resulting in widely scattered timescales that exhibit a less pronounced inherent dependency on galaxy properties [594].

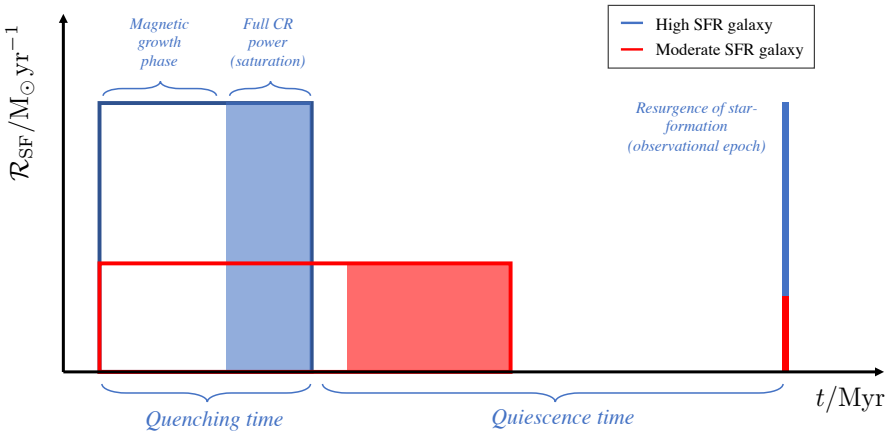

Figure 10. Illustration of the expected star-formation history of galaxies regulated by CRs. The case with a high star-formation rate shown in blue develops a saturated magnetic field relatively rapidly. Containment of CRs soon brings about the downfall of star-formation in the galaxy, before it later undergoes a resurgence. A galaxy with a lower star-formation rate, shown in red, takes longer to amplify its magnetic field, longer to generate a sufficient abundance of CRs to halt star-formation and sees weaker quenching with a quicker resurgence. Figure reproduced from Ref. [594].

5.3. Cosmic Ray Effects in Circumgalactic Media

5.3.1. Phase Structure of Circumgalactic Media and Cosmic Ray Effects

The CGM is a major component of a galaxy's ecosystem. As a conduit for all gas flows into and out of a galaxy, it can have a strong influence on a galaxy's evolution (for

reviews, see [595–597]). In particular, it regulates a galaxy's fuel supply, star formation capacity, and the hydrodynamic state of the gas that ultimately reaches a galaxy's ISM. In systems dominated by thermal pressure, the CGM consists mainly of a hot, tenuous gas phase with cool gas confined to dense filaments in local pressure equilibrium [466]. However, some galaxy-scale simulations including the effects of CRs have shown that they may dominate the pressure in the CGM surrounding certain galaxies [466,598]. This opens up the potential for CRs to participate in extrinsic feedback mechanisms which operate on the large-scale processes externally regulating the evolution of a galaxy. In cases where CR pressure dominates a galactic halo, CGM baryons primarily exist in a cold phase at approximately 10^4 K [466,599]. Observations have detected this cold gas in the CGM of galaxies of all types, extending up to around 300 kpc [600–603]. This is comparable to the full extent of the CGM (traced up to 100–200 kpc using metal-enriched gas [604]).

Some galaxies are observed to sustain massive reservoirs of cold gas in their CGM. This should be able to fuel their star formation. However some of these galaxies appear to be quenched (e.g., [605,606]). This is indicative of a feedback support mechanism operating to reduce gas in-fall, precipitation, or accretion into the host galaxy to moderate its star formation. This support may be provided by thermal pressure exerted by the hot phase of the CGM (which may be partially heated by CRs through the excitation of short-wavelength Alfvén waves [226]), and/or non-thermal pressure contributed by CRs. The presence of CRs can significantly reduce cold gas supplied to the galaxy. They can also increase the fraction of cold gas mass held in the galactic halo by preventing its precipitation back toward the galaxy [607]. These effects and their dependence on CR activity offer an opportunity to establish constraints on effective CR transport in the CGM based on parameters such as the total hydrogen column density, average star formation rate, and gas circular velocity [608].

5.3.2. Cold Gas Formation from Thermal Instabilities

The partition of matter between the hot and cold CGM phase components is set by the local thermodynamic conditions and the supply of gas. The cold phase has multiple possible origins. One possibility is its direct formation from the hot tenuous phase. In this scenario, thermal instabilities give rise to runaway cooling and cold gas condensation [532,609–613]. CRs have been shown to modify this process [607]. For example, CR pressure supports more diffuse gas at lower temperatures [464,512,614] allowing cooling without collapse [615,616] and the formation of a cool, low-density CGM component [607]. This cold gas component may form as a suspension of small cloudlets, mixed into the warmer phase. Inefficient CR transport can promote the development of larger cloudlets. These can be several orders of magnitude larger in size compared to cloudlets in a purely thermal CGM [607]. When CRs dominate the pressure of a CGM, the halo is comprised of mainly diffuse cool gas ($\sim 10^4$ K), with a large filling factor and a thermal pressure that is insufficient for virial or local pressure balance [466]. Such conditions have been shown to be more prevalent for larger halo masses and lower redshifts [617]. In these cases, the gas phase configuration and hydrodynamics differ substantially from more multi-phase CGM compositions [466]. In particular, the additional CR pressure leads to a smoother CGM on small scales, with lower temperatures [618].

5.3.3. Cold Gas Supply by Inflows and the Impacts of Preventative Feedback

In addition to its formation by thermal instabilities within the CGM, cold gas can be supplied to a galactic ecosystem by accretion from the cosmic web (see [595]; also Figure 11). At high redshifts, typically above $z \sim 2$, this happens by means of cold accretion flows [619,620] which pass through the CGM and can directly fuel efficient star formation in the host galaxy [621,622].[19] These flows can fragment as they fall through the CGM towards the host galaxy [624,625], or may be reinforced by condensation due to CGM gas cooling [626]. Recent observations have found evidence of cold accretion flows with Hydrogen recombination lines [627,628]. These lines are emitted by warm ($\gtrsim 10^4$ K) Hydrogen gas cooling as it

flows towards the host galaxy (e.g., [629,630]). CI emission has also revealed in-flowing CGM gas around galaxies at much lower temperatures of 10–100 K [625].

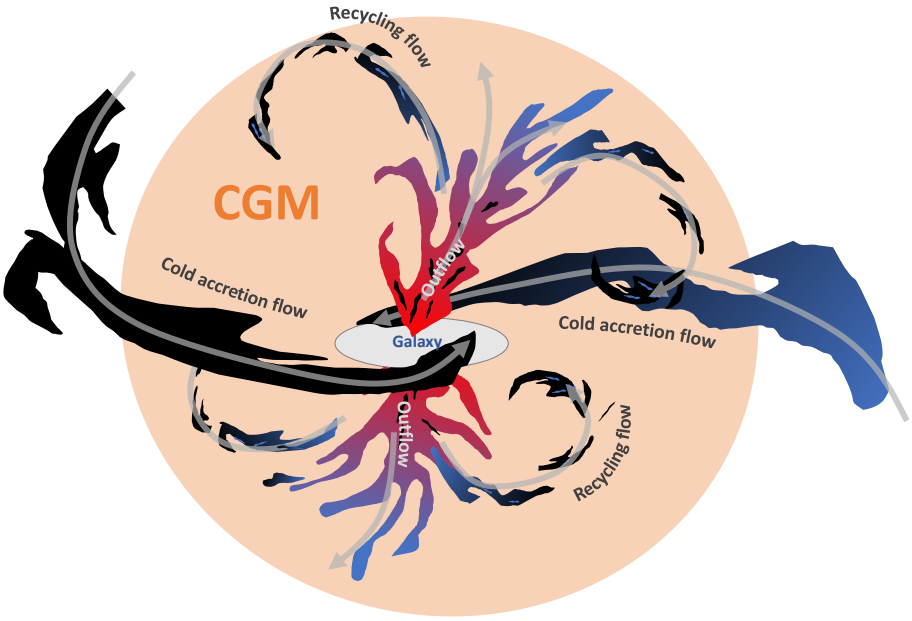

Figure 11. A schematic illustration of a secular galaxy and its circumgalactic environment. The CGM is shown in orange, with flows of gas in red (hot), blue (warm), and black (cold). Typical flow structures circulating baryons, metals, magnetic fields and CRs between the CGM and ISM of a galaxy are indicated. Outflows can be driven by the feedback activity resulting from concentrated nuclear star formation. Cold accretion flows of pristine material from the cosmic web can operate in more primordial settings above $z \sim 2$. These flows may fuel intensive starburst activity. Recycling flows, which consist of multiple phases, facilitate the transfer of gas from the ISM to the CGM, enriching the medium, promoting cooling, and inducing inflow. CRs can modify these processes by providing pressure support, by driving/modifying flows, or by heating CGM gas to raise its thermal support and stability against gravitational collapse.

Strong feedback mechanisms, such as the confluence of winds from stellar populations [631], high-energy processes associated with CRs in the host galaxy [223], or outflows (see [632]; also Section 5.3.5), can impede the ability of cold accretion flows to penetrate through the CGM. Outflows with large filling factors can introduce particularly severe disruption. These are expected to be especially widespread in CR pressure-dominated systems [466,617]. When cold accretion flows are restricted, or even stopped, a so-called *preventative* feedback scenario is established. Gas recycling in the CGM and the supply of pristine gas to the host galaxy is strongly curtailed. This preventative scenario can be regulated and enhanced by CRs, leading to considerably extended gas recycling times [633].[20] When a preventative feedback scenario has taken hold, gas may instead be supplied to build up the outer CGM. There, it can form a reservoir to fuel star formation at a later time. Stunted cosmic gas supply by preventative feedback has been considered to lead to the emergence of 'red-and-dead' massive spheroid galaxies below $z < 1$ [619]. These galaxies undergo a gradual quenching process as they deplete their remaining gas reservoir over Gyr timescales (e.g., [635]). In high redshift settings, transient preventative feedback by CRs has been proposed as a driver for more complex star formation histories [17,223] inferred for candidate $z > 7$ galaxies in recent observational studies (e.g., [94,589,636]).

5.3.4. Cold Gas Supplied from the Interstellar Medium

Cold gas within the CGM can also have its origins within the ISM of the host galaxy. It is advected into the CGM by multi-phase galactic outflow winds and fountains, which can drive gas far into the CGM. A cold phase can develop in this advected ISM gas

through various mechanisms. These include thermal instabilities [637,638], dynamical instabilities (e.g., [639]) or the entrainment of cold clumps or clouds from the ISM that are accelerated within the outflow [640]. Outflows can be driven by CR pressure, thermal gas pressure or radiation pressure (see Ref. [641] for a review). The interaction between these driving mechanisms and entrained cold clouds leads to distinct multi-phase configurations and kinematics within the outflow. For example, CR-driven flows tend to be cooler than their thermal-pressure driven counterparts, and faster than radiatively driven winds (e.g., [15]). Cold clumps within CR-driven flows are subject to significant CR pressure support. This can favour the development of larger cold clumps [607,637,638] or a lower density cold phase in the flow [234,235,638] than would be expected in a thermally driven or radiatively driven system (see [642] for a study of cloud properties in thermal and radiation-driven outflows).

Recent simulation work has set out a picture of the acceleration, survival and evolution of cold clouds in galactic outflows, as well as the effects brought about by CRs. In particular, it has been established that cold gas clouds can be accelerated by CR streaming through the CR 'bottleneck' effect in outflows [233,235,236,638] and galactic halos [234]. This is where CRs are forced to slow down when they encounter a cloud, as they cannot stream down their density gradient. CR density is enhanced on the side of the cloud facing the CR flux, exerting pressure forces and heating it. This accelerates the cloud, and can affect its structure, e.g., by stretching it [235]. Moreover, its heating impact on CR-mediated acceleration fronts broadens the cloud-halo interface, resulting in detectable changes in ionic abundances [234].

The CR bottleneck effect preferentially accelerates the side of the cloud experiencing the strongest CR pressure gradient. This is usually facing the CR source [233,638]. The resulting differential acceleration causes the fast-moving gas to detach from the bulk of the cloud to form small clouds. These are less likely to survive the acceleration process (e.g., [643]).[21] While this means cloud morphologies will be different in a CR-driven flow compared to a thermally driven system, this process implies that clumps entrained in a CR-driven wind will also experience a loss of gas mass over time. This is in contrast to clouds entrained in a hot thermally driven wind, which typically gain mass during their entrainment [638].

5.3.5. Cosmic Ray Impacts on Galactic Outflow Physics

CRs can play a key role in driving galactic outflows [15,512,646–652]. Their influence leads to modifications in the flow dynamics and physical properties [15,480,598,653,654] which can be observed in various ways, including with X-rays [655] or with Lyman-α spectra [656]. Recent numerical studies have extensively explored CR-driven winds. These have considered steady-state and time-evolving numerical models, covering a wide range of boundary parameters and physical complexity. Examples include variation of the gas conditions at the base of the flow (e.g., [654,657,658]), star formation rate in the host galaxy (e.g., [15,651,652,654]), mass input/loading rates into the flow [652,659], gravitational potential (e.g., [15,652,654,657,658]) or halo mass [660], magnetic and/or gas-to-CR pressure driving ratio (e.g., [15,652,657,659]), and flow angular momentum (e.g., [657,661,662]). The impacts of the precise CR transport physics has also seen substantial progress, with studies investigating the effects of CR advection and diffusion [512,651,653,659,661–663], diffusion and streaming [215,650,651,664],[22] impacts of driving by CR streaming [479,480,665,666], streaming suppression due to turbulent and/or wave damping [479,480,666,667], CR cooling (e.g., [667]), gas cooling with CR heating (e.g., [668]), and consideration of spectrally resolved treatments of CRs [461,479,658,669,670]. Multi-phase gas flow structure [662] and its impact on CR transport [653] and CR acceleration (e.g., [671,672]) have also been investigated. Specific parameter sets to simulate specific classes of galaxies (e.g., [659]) and model fits to individual galaxies (e.g., the M82 superwind) from γ-ray and radio emission [545,548][23] have also been provided. Additionally, simple analytic scaling relations between halo velocity, carrying capacity and mass loading have been obtained [657]. These

capture the broad variety of CR-driven and hybrid flow behaviours that are reflective of earlier scaling relations obtained empirically for mass loading factor, thermalization efficiency and flow velocity (e.g., [673–675]).

5.3.6. Cosmic Ray Effects on Circumgalactic Baryon Recycling Flows

Outflows play a direct role in the exchange of energy and baryons between a galaxy and its CGM [595,676]. They propel enriched gas into the CGM and beyond, some of which can return to the galaxy through baryonic recycling flows [677–679]. Alternatively, this gas can be completely expelled from the galactic ecosystem, contaminating the surrounding IGM with metals [680,681] and magnetic fields [682–684]. Even in cases where gas eventually recycles back to the host galaxy, it can reside in the CGM reservoir for extended periods, possibly exceeding 1 Gyr, especially in the case of very massive galaxies (e.g., [676,685,686]).[24] Despite these long timescales, simulations have demonstrated that a significant fraction, up to half [348] or more (e.g., [676,686,687]), of the baryons in the CGM within a virial radius pass through the ISM of their host galaxy at least once by $z = 0$. The influence of CR pressure can modify this recycling process significantly, leading to pronounced changes in outflow morphology (e.g., [688,689]), and a diminished [633] or even completely suppressed [690] virial shock. This results in substantial alterations to the kinematics of both warm and cool CGM gas [691,692]. CR-driven outflows tend to exhibit cooler temperatures and smoother density structures [232,598,614], extending far into the CGM [510,512,633,647,648,688,689,692–695]. It is this extended reach which gives them particularly influence over the regulation of CGM recycling flows.

The effect of CRs on CGM recycling can be especially consequential in massive halos (above $10^{11}\,M_{\odot}$) and at low redshifts ($z \leq 1-2$) [633]. CR effects have also been examined in relation to regulating the baryonic content of dwarf galaxies [465], where CR diffusion has been found to yield relatively cold, dense winds. In the absence of CRs, the high thermal pressure of gas typically traps galactic outflows near the disk of their host galaxy [633]. This forces the development of low-altitude recycling flows and practically mimics a scenario where an outflow is not present at all [595]. The presence of CRs leads to the formation of a halo with lower thermal pressure, facilitating outflow escape (the CR pressure does not resist outflow expansion due to diffusion). The continuous flow acceleration provided by CR pressure propels material deep into the CGM, spanning Mpc scales [617]. This reduced confinement of material has been demonstrated to diminish flow recycling in some simulations (e.g., [633]) with significant long-term consequences for the evolution of the host galaxy. Higher CR fluxes counter this effect by transferring more energy to the gas, driving stronger outflows [522] with radically altered morphologies. In strongly CR-dominated halos, outflows become nearly volume-filing and are predominantly comprised of cool gas ($T \sim 10^5$ K) [466,617]. This leads to considerable modification of the dynamical structure of the CGM [633]. In multi-phase flows, the CR pressure support within cold clouds reduces their density and alters their kinematics [607]. The associated change in their buoyancy could have considerable consequences for the enrichment and star formation history of galaxies in CR-dominated ecosystems.

5.3.7. Cosmic Ray Micro-Physics on Circumgalactic and Galactic Scales

Many of the large-scale effects of CRs in the CGM are greatly influenced by the underlying models used to describe CR propagation and interactions on very small scales, called the *micro-physics*. These models are subject to substantial uncertainty and are poorly constrained. This can lead to large variations in predicted galaxy properties, which are even more severe in the CGM [464,618]. Even relatively small differences in CR transport treatments or numerical approaches [696,697] can produce tremendous variation in simulated galaxies and their CGM [464,664], and circumgalactic flows (e.g., [649]). Discrepancies also arise when comparing CR propagation models with observed CR scaling relations in the solar-terrestrial environment, such as spectral slopes and the Boron-to-Carbon (B/C)

ratio. It is therefore clear that the reliability of most current treatments of CR transport micro-physics is limited (in particular, see [482,698]).

Observational data can provide some constraints on the CR transport models. However, suitable data for the transport of relatively low-energy GeV CRs is limited. These CRs typically scatter over gyro-radii of $r_{gy} \approx 0.22\,(E_p/1\,\mathrm{GeV})\,(B/1\,\mu\mathrm{G})^{-1}$ au in the magnetic fields associated with galactic ecosystems. This gyro-radius serves as a reference length-scale, indicating where CR transport becomes diffusive (i.e., where the gyro-radius becomes comparable to the local coherence length of magnetic turbulence). Practically, it defines the scale where CR micro-physics must be resolved in order to make reliable macroscopic predictions about their transport. Achieving such gyro-scale resolutions in galaxy simulations or observations is extremely challenging. This poses a significant obstacle to the reliable construction and testing of CR transport models derived self-consistently from micro-scale CR processes. The resulting theoretical and observational uncertainties are substantial, and only weak constraints are possible. Even when adopting constraints from Milky Way observations such as diffusion coefficients adjusted to match γ-ray observations [466,651], variations in micro-physical modeling have still demonstrated vast differences in macro-physical predictions (e.g., [651]).

In recent years, significant effort has been devoted to thoroughly exploring the impacts of different model prescriptions and uncertainties on galaxy-scale predictions of CR effects. Work has been conducted to critically examine the impacts of a wide range of standard approximations and physical treatments, including spectrally resolved CRs [461,669,670,699,700], anisotropic diffusion in CR-driven wind models [510,512,660], moderately super-Alfvénic streaming [480,512][25], anisotropic streaming [466], CR transport with self-confinement or extrinsic turbulence [29,702,703], constant diffusivity, explicitly evolved CR diffusivities, and varying turbulent cascade assumptions [703]. Although specific model configurations and parameter choices have been identified where all observational constraints can be reproduced (in particular, see [703]), these studies suggest that no single approach can be universally adopted for a complete treatment of CR transport while properly capturing all relevant micro-physical effects.

Despite this, progress has still been possible. Much of this has focused on connecting micro-scale CR transport to intermediate-scale effective fluid theories (e.g., [704–707]). These efforts are providing more robust ways of treating effective CR transport as a function of local plasma properties [19,29]. Moreover, galaxy simulation work has started to reach pc-scale resolution (e.g., [617]). This can capture environmental variations through interstellar and circumgalactic media which affect CR transport. It can also reach the deflection length-scales of GeV CRs for observationally favoured values of the CR scattering rate [703] so CR trajectories can be followed over the structural scales of their medium. While a full model of au-scale CR propagation is not yet within reach, current capabilities are now sufficient to construct reliable effective CR transport prescriptions as a function of local physical conditions. Theoretical studies are now beginning to propose simplified relations that are physically robust on galaxy or CGM scales and computationally efficient to adopt [708]. These efforts open up the potential for tangible advancements in the development of self-consistent effective transport models on galactic scales.

6. Summary and Conclusions

In this review, we have provided a cross-section of recent advancements in our understanding of CR processes within galactic environments. By adopting a multi-scale perspective, we have explored the significance of CRs in galaxies, with a particular focus on their origins, containment, feedback impacts and observable signatures. To conclude, we have identified several areas where significant challenges exist that will be important to overcome if we are to significantly advance our understanding of CR feedback effects. We also highlight upcoming observational opportunities and emerging theoretical advancements that show promise to support progress in addressing these challenges in the near term. These opportunities and advancements bear the capability to elevate our understand-

ing of CR processes in galaxies beyond its current level of maturity, and will likely guide future research directions in the coming years.

6.1. Pressing Issues

As we seek to consolidate our understanding of the role of CRs in galaxy formation and evolution, certain areas stand-out as focal points requiring particular attention. These represent emerging priorities within the field, where advancements would considerably aid progress in the construction and testing of the next generation of models. Addressing these priorities will serve as important milestones in our path forward:

- Development of robust connections between multi-wavelength/multi-messenger observables and models of CR propagation and interaction, to support efficient testing of models with the wealth of upcoming new data.
- Establish ways to address the significant numerical challenges involved with studying the effects of local plasma variations on CR instability growth rates, CR-MHD wave scattering and interaction rates, MHD wave damping, and micro-physical CR transport prescriptions.
- Development of a self-consistent CR transport theory, including self-confinement effects, that aligns with observations.
- Enhancement of CR+MHD numerical simulations to incorporate physically robust CR interaction and transport physics on galactic scales, that correctly account for physics at micro-scales.
- Creation of a comprehensive suite of reliable CR transport theories applicable to galaxies across a wide range of scales and conditions, particularly in the vicinity of CR sources.
- Construction of efficient models of CR interactions and propagation within multi-phase media, including 'bottleneck' effects around dense clouds, suitable for integration into MHD simulations.
- Advancement of our understanding of wind-driving effects of CRs, including their interaction with MHD waves undergoing damping, within multi-phase fluid flows, and self-consistent coupling with existing treatments of radiation hydrodynamics.
- Establish a comprehensive understanding of the thermal and dynamical impacts of CR heating and pressure support in the CGM, including their effects on inflows and outflows.

6.2. Upcoming Opportunities

The advancing capabilities of ground-based γ-ray telescope arrays will soon allow new science to be conducted at the highest of photon energies with unprecedented angular resolution and sensitivity. The principal development in this domain is CTA, which is expected to facilitate substantial scientific advancements (see [709]). Potential up-coming Southern observatories using the water Cherenkov detector technique, such as SWGO, will provide complementary capabilities such as a first unbiased survey more sensitive to PeVatrons in the Southern hemisphere [209,710]. Up-coming developments in the MeV band are also noteworthy. The Compton Spectrometer and Imager (COSI) [711,712] will be of particular importance in the coming decade, as it will open-up the possibility to conduct pioneering studies of γ-ray polarization, as well as presenting significant improvements in sensitivity, spectral resolution, angular resolution, and sky coverage. COSI will particularly serve as a crucial tool for testing models of CR acceleration in nearby environments. It establishes a more complete picture of CR feedback in galaxies, by offering excellent continuum sensitivity that bridges the gap between the thermal and non-thermal regimes.

The next generation of high-energy instruments will also open-up the multi-messenger domain, principally through advancements in neutrino observations. The development of new facilities scheduled to be fully operational in the next decade, including KM3NeT [713], Baikal-GVD [714], IceCube-Gen2 [195], and P-ONE [196], will soon make the exploration of galaxies with multi-messengers a reality. In addition to this, recently established new facilities form part of an armada of observatories operating across the electromagnetic spectrum. Chief among these are ALMA and *JWST*. These are already allowing us to study

external galaxies in unprecedented detail, and have opened-up new ways to pin-down the effects of CRs throughout the hierarchy of structures of galaxy media.

Theoretical and numerical developments form another avenue where significant progress is being made, paving the way for new scientific capability. Some especially noteworthy advancements are the emergence of simplified treatments of CR physics that are physically robust on galaxy or CGM scales and computationally efficient to adopt (e.g., [708]), and numerical tools that tackle CR transport physics and observational signatures simultaneously (e.g., [715]). There has also been considerable advancement of suites of simulations that are adopting more sophisticated physical recipes (for a recent review, see [716]), and moving beyond standard CR+MHD treatments. This emerging broader framework encompasses a wider range of physical effects relevant to CRs in galaxies. For instance, spectrally resolved CRs (e.g., [461,669,670,699,700]), alternative mechanisms for CR self-confinement and heating of thermal gas (such as pressure anisotropy instability) [717],[26] and numerical simulations of MHD-dust-CR interactions, where the charged dust and CR gyro-radii on au scales are fully resolved [718].

With these ongoing theoretical advancements and the upcoming observational opportunities, we will soon be well-placed to confidently investigate the role of CRs in galaxies as active agents involved in shaping their evolution. This will allow us to refine our treatment of CR feedback dynamics in our understanding of galaxy evolution, bridging the gap from microscopic to macroscopic scales.

Author Contributions: E.R.O., K.W. and Y.I. wrote the draft of the paper. H.-Y.K.Y. and A.M.W.M. improved the manuscript by contributing text and providing insightful comments. All authors have read and agreed to the published version of the manuscript.

Funding: E.R.O. is an overseas researcher under the Postdoctoral Fellowship of Japan Society for the Promotion of Science (JSPS), supported by JSPS KAKENHI Grant Number JP22F22327. E.R.O. also acknowledges support from the Munich Institute for Astro-, Particle and BioPhysics (MIAPbP), where where some of this work was conducted and where insightful discussions at the "Star-Forming Clumps and Clustered Starbursts across Cosmic Time" program informed the early stages of this work. MIAPbP is funded by the Deutsche Forschungsgemeinschaft (DFG, German Research Foundation) under Germany's Excellence Strategy–EXC-2094–390783311. K.W. was supported in part by a UK STFC Consolidated Grant awarded to UCL MSSL and by the UCL Cosmoparticle Initiative. Y.I. is supported by JSPS KAKENHI Grant Number JP18H05458, JP19K14772, and JP22K18277. This work was supported by World Premier International Research Center Initiative (WPI), MEXT, Japan. H.-Y.K.Y. is supported by the National Science and Technology Council (NSTC) of Taiwan (109-2112-M-007-037-MY3) and the Yushan Scholar Program of the Ministry of Education (MoE) of Taiwan (ROC). A.M.W.M. is supported by the DFG—Project Number 452934793.

Data Availability Statement: No new data were created or analyzed in this study. Data sharing is not applicable to this article.

Acknowledgments: The authors thank Kentaro Nagamine (Osaka University), Shinsuke Takasao (Osaka University), Marcel Strzys (Institute for Cosmic Ray Research, University of Tokyo), Tomonari Michiyama (Shunan University), Sheng-Jun Lin (Academia Sinica Institute for Astronomy and Astrophysics), Ignacio Ferreras (Instituto de Astrofísica de Canarias) and Anatoli Fedynitch (Academia Sinica Institute of Physics) for discussions that helped to inform parts of this work, and two anonymous referees for their constructive comments on this article. Figures 2 and 3 are reproduced from Ref. [273], "The secret agent of galaxy evolution" (Figures 5 and 8), E. R. Owen, *Astronomy & Geophysics*, Volume 64, Issue 1, February 2023, Pages 1.29–1.35, under Rights and New Business Development—RAS Journals: permissions. Figure 3 is reproduced from Figure 7 of Ref. [305], "Probing the sea of galactic cosmic rays with *Fermi*-LAT", *Physical Review D* 101, 083018 (2020), https://doi.org/10.1103/PhysRevD.101.083018, under the Creative Commons Attribution 4.0 International license. Figures 8 and 9 (left panel) are reproduced in accordance with NASA Media Usage Guidelines. Figure 9 (right panel) was adapted from Lopez-Rodriguez et al. [516] (their Figure 1, left panel), under the terms of the CC BY 4.0 license. Figure 10 was reproduced from Ref. [594], under the terms of the CC BY 4.0 license.

Conflicts of Interest: The authors declare no conflicts of interest.

Abbreviations

The following abbreviations are used in this manuscript:

AGN	Active galactic nucleus
ALMA	Atacama Large Millimeter/Submillimeter Array
Baikal-GVD	Baikal–Gigaton Volume Detector
CC	Core-collapse
CGM	Circumgalactic medium
CMZ	Central molecular zone
CMB	Cosmic microwave background
COSI	Compton Spectrometer and Imager
CR	Cosmic ray
CSM	Circumstellar medium
CTA	Cherenkov Telescope Array
EBL	Extragalactic background light
FIR	Far infrared
GC	Galactic center
HAWC	High Altitude Water Cherenkov Observatory
HAWC+	High-Angular Wideband Camera Plus
HIM	Hot ionized medium
HMXB	High-mass X-ray binary
HVC	High velocity cloud
HyLIRG	Hyperluminous infrared galaxy
IceCube	IceCube Neutrino Observatory
IGM	Intergalactic medium
IMF	Initial mass function
IR	Infrared
ISRF	Interstellar radiation field
JCMT	James Clerk Maxwell Telescope
JWST	*James Webb* Space Telescope
KM3NeT	The Cubic Kilometre Neutrino Telescope
LAT	Large Area Telescope (on the *Fermi* Gamma-ray Space Telescope)
LHC	Large Hadron Collider
LHAASO	Large High Altitude Air Shower Observatory
LIRG	Luminous infrared galaxy
LMXB	Low-mass X-ray binary
MC	Monte Carlo
MHD	Magnetohydrodynamic
NIRSpec	Near Infra-Red Spectrograph
NRSI	Non-resonant streaming instability
PAH	Polycyclic aromatic hydrocarbon
P-ONE	Pacific Ocean Neutrino Experiment
PSG	Post-starburst galaxy
SED	Spectral energy distribution
SKA	Square Kilometer Array
SMG	Submillimeter galaxy
SMBH	Supermassive black hole
SN	Supernova
SNR	Supernova remnant
SOFIA	Stratospheric Observatory For Infrared Astronomy
SWGO	Southern Wide-Field Gamma-Ray Observatory
UFO	Ultra-fast outflow
ULIRG	Ultraluminous infrared galaxy
UV	Ultra-violet
VHE	Very high energy
VLT	Very large telescope
WIM	Warm interstellar medium
WR	Wolf–Rayet
XRB	X-ray binary

Notes

1 This is different from a non-resonant instability (see Section 2.1.3; also called Bell's instability).
2 CR energy gains and losses are balanced, as they cancel owing to equal-intensity waves propagating in opposite directions [29]
3 It has also been shown that the opposite effect is possible, if dust streams super-Alfénically. In this case, CR propagation is suppressed, particularly on scales which are gyro-resonant with the dust [32].
4 Hadronic CRs are assumed in this discussion. Modified forms of the NRSI are relevant when it is driven by leptonic CRs [33].
5 It has been proposed that such production of muon anti-muon pairs can be part of a purely leptonic mechanism to produce TeV-scale neutrinos in astrophysical environments [77].
6 Prior to the Sedov-Taylor phase, a very small amount of particle escape may also arise during the ejecta-dominated phase (e.g., [118]), when the SNR shock experiences very minor deceleration [119].
7 This can also accelerate particles by a second-order Fermi mechanism (see, e.g., [151]).
8 O is the main progenitor CR of Be and B in typical spallation reaction chains, so the total production rate becomes proportional to the amount of O released into the ISM by SNe enrichment, and the amount of O as a source of Be and B production by spallation [168].
9 This is with the exception of secondary CRs injected by hadronic primaries, which may be non-negligible (e.g., see [192] which shows that the leptonic CR abdunance of galaxies could be a significant or dominant component of the leptonic CR flux in starburst galaxies).
10 We note that, at the time of writing, a recent pre-print for the First LHAASO Catalog indicates the number of detections at energies above 100 TeV may now have increased to 43 sources with a significance of 4σ [199].
11 However, an old SNR as an accelerator has been proposed as one possible scenario [208].
12 This instability develops when a perturbation to the magnetic field causes the field lines to bend. Gravity then pulls gas into the valleys of the magnetic field, which sinks and deepens the valleys.
13 More comprehensive approaches are possible by using sophisticated chemical codes to obtain a robust determination of CR ionization (e.g., `UCLCHEM` [268] or `Astrochem` [269]) and can relax steady-state approximations. Beyond direct studies of CRs themselves, other applications require a reliable determination of local CR ionization rate. For example, in the age determinations of molecular cloud cores [270].
14 Constraints on their hadronic and leptonic components have been estimated from the isotropic γ-ray background [471], and the maximum synchrotron flux remaining after subtraction of the Galaxy's contribution to the anisotropic radio background [472,473].
15 The far-IR radio correlation appears to be valid up to $z \sim 2$–3 [492]. It may not hold at higher redshifts due to increased inverse Compton losses experienced by CR electrons interacting with the CMB. Conversely, the far-IR γ-ray relation should not theoretically see strong variation with redshift, however instrumental constraints and extragalactic background light (EBL) attenuation make all but the nearest starbursts detectable in γ-rays (see Section 5.2.3).
16 'Conspiracies' typically include efficient cooling of CR electrons in starbursts, and a combination of low effective ulta-violet (UV) dust opacity in lower surface density galaxies. Contributions from secondary CR electrons can also be invoked to counter decreased radio emission from bremsstrahlung, ionization, and inverse Compton cooling in starbursts [500]. However, these models can still pose a problem where CR electron density is directly proportional to the star formation rate of a galaxy, because of the increased radio synchrotron emission associated with the secondary electrons. These issues may instead be resolved by invoking models combining CR escape, cooling and secondary production [500].
17 Higher values are obtained if the possible advective impacts of outflows on CR containment are excluded (e.g., [546]).
18 This is because CH^+ generally arises in similar conditions regions of high OH^+ and H_2O^+ abundances in clouds, and it has been proposed that CH^+ absorption lines from SMGs originate primarily in halo gas [583].
19 Recent studies have found tentative indications that gas inflows may persist around some high-mass galaxies in the nearby Universe [623].
20 Similar effects have been reported in other contexts. For example, even modest CR pressures can suppress cooling flows in galaxy clusters [634].
21 Magnetic draping (see [644]) can can partially mitigate cloud mass loss [645], and the inclusion of radiative cooling has been shown to enhance the resilience of clouds against CR effects, such as heating [235].
22 Note, however that Ref. [215] reported CR transport itself cannot reach a steady state and is not well described by either the CR streaming paradigm, the CR diffusion paradigm, or a combination of both.
23 Constraints on the the underlying wind physics have found that the role of CRs in the case of the M82 superwind is relatively limited [548].
24 Shorter median recycling timescales around 100s Myr have been reported by some studies (e.g., [686]).
25 For a review of Alfvén wave damping in MHD turbulence for CR streaming in galactic winds, see Ref. [701].
26 This development may be especially important on meso-scales, particularly near sites of CR injection [717].

References

1. Shimizu, I.; Todoroki, K.; Yajima, H.; Nagamine, K. Osaka feedback model: Isolated disc galaxy simulations. *Mon. Not. R. Astron. Soc.* **2019**, *484*, 2632–2655.
2. Oku, Y.; Tomida, K.; Nagamine, K.; Shimizu, I.; Cen, R. Osaka Feedback Model. II. Modeling Supernova Feedback Based on High-resolution Simulations. *Astrophys. J. Suppl.* **2022**, *262*, 9. [CrossRef]
3. Ostriker, E.C.; Kim, C.G. Pressure-regulated, Feedback-modulated Star Formation in Disk Galaxies. *Astrophys. J.* **2022**, *936*, 137. [CrossRef]
4. Orr, M.E.; Fielding, D.B.; Hayward, C.C.; Burkhart, B. Bursting Bubbles: Feedback from Clustered Supernovae and the Trade-off Between Turbulence and Outflows. *Astrophys. J.* **2022**, *932*, 88. [CrossRef]
5. Rosado, M.; Ambrocio-Cruz, P.; Le Coarer, E.; Marcelin, M. Kinematics of the galactic supernova remnants RCW 86, MSH 15-56 and MSH 11-61A. *Astropart. Phys.* **1996**, *315*, 243–252.
6. Sánchez-Cruces, M.; Rosado, M.; Fuentes-Carrera, I.; Ambrocio-Cruz, P. Kinematics of the Galactic Supernova Remnant G109.1-1.0 (CTB 109). *Mon. Not. R. Astron. Soc.* **2018**, *473*, 1705–1717. [CrossRef]
7. Sánchez-Cruces, M.; Sardaneta, M.M.; Fuentes-Carrera, I.; Rosado, M.; Cárdenas-Martínez, N.; Lara-López, M.A. A kinematical study of the dwarf irregular galaxy NGC 1569 and its supernova remnants. *Mon. Not. R. Astron. Soc.* **2022**, *513*, 1755–1773. [CrossRef]
8. Hopkins, P.F.; Grudić, M.Y.; Wetzel, A.; Kereš, D.; Faucher-Giguère, C.A.; Ma, X.; Murray, N.; Butcher, N. Radiative stellar feedback in galaxy formation: Methods and physics. *Mon. Not. R. Astron. Soc.* **2020**, *491*, 3702–3729. [CrossRef]
9. Qiu, Y.; Bogdanović, T.; Li, Y.; Park, K.; Wise, J.H. The Interplay of Kinetic and Radiative Feedback in Galaxy Clusters. *Astrophys. J.* **2019**, *877*, 47. [CrossRef]
10. Chen, H. The Role of Quasar Radiative Feedback on Galaxy Formation during Cosmic Reionization. *Astrophys. J.* **2020**, *893*, 165. [CrossRef]
11. Yajima, H.; Nagamine, K.; Zhu, Q.; Khochfar, S.; Dalla Vecchia, C. Growth of First Galaxies: Impacts of Star Formation and Stellar Feedback. *Astrophys. J.* **2017**, *846*, 30. [CrossRef]
12. Kornecki, P.; Pellizza, L.J.; del Palacio, S.; Müller, A.L.; Albacete-Colombo, J.F.; Romero, G.E. γ-ray/infrared luminosity correlation of star-forming galaxies. *Astropart. Phys.* **2020**, *641*, A147. [CrossRef]
13. Kornecki, P.; Peretti, E.; del Palacio, S.; Benaglia, P.; Pellizza, L.J. Exploring the physics behind the non-thermal emission from star-forming galaxies detected in γ rays. *Astropart. Phys.* **2022**, *657*, A49. [CrossRef]
14. Owen, E.R.; Jacobsen, I.B.; Wu, K.; Surajbali, P. Interactions between ultra-high-energy particles and protogalactic environments. *Mon. Not. R. Astron. Soc.* **2018**, *481*, 666–687. [CrossRef]
15. Yu, B.P.B.; Owen, E.R.; Wu, K.; Ferreras, I. A hydrodynamical study of outflows in starburst galaxies with different driving mechanisms. *Mon. Not. R. Astron. Soc.* **2020**, *492*, 3179–3193. [CrossRef]
16. Krumholz, M.R.; Crocker, R.M.; Offner, S.S.R. The cosmic ray ionization and γ-ray budgets of star-forming galaxies. *Mon. Not. R. Astron. Soc.* **2023**, *520*, 5126–5143. [CrossRef]
17. Owen, E.R.; Jin, X.; Wu, K.; Chan, S. Hadronic interactions of energetic charged particles in protogalactic outflow environments and implications for the early evolution of galaxies. *Mon. Not. R. Astron. Soc.* **2019**, *484*, 1645–1671. [CrossRef]
18. Ruszkowski, M.; Pfrommer, C. Cosmic ray feedback in galaxies and galaxy clusters—A pedagogical introduction and a topical review of the acceleration, transport, observables, and dynamical impact of cosmic rays. *arXiv* **2023**, arXiv:2306.03141. [CrossRef]
19. Thomas, T.; Pfrommer, C. Cosmic-ray hydrodynamics: Alfvén-wave regulated transport of cosmic rays. *Mon. Not. R. Astron. Soc.* **2019**, *485*, 2977–3008. [CrossRef]
20. Amato, E.; Blasi, P. Cosmic ray transport in the Galaxy: A review. *Adv. Space Res.* **2018**, *62*, 2731–2749. [CrossRef]
21. Strong, A.W.; Moskalenko, I.V. Propagation of Cosmic-Ray Nucleons in the Galaxy. *Astrophys. J.* **1998**, *509*, 212–228. [CrossRef]
22. Maurin, D.; Donato, F.; Taillet, R.; Salati, P. Cosmic Rays below Z = 30 in a Diffusion Model: New Constraints on Propagation Parameters. *Astrophys. J.* **2001**, *555*, 585–596. [CrossRef]
23. Evoli, C.; Gaggero, D.; Grasso, D.; Maccione, L. Cosmic ray nuclei, antiprotons and gamma rays in the galaxy: A new diffusion model. *J. Cosmol. Astropart. Phys.* **2008**, *2008*, 018. [CrossRef]
24. Kissmann, R. PICARD: A novel code for the Galactic Cosmic Ray propagation problem. *Astropart. Phys.* **2014**, *55*, 37–50. [CrossRef]
25. Skilling, J. Cosmic ray streaming—III. Self-consistent solutions. *Mon. Not. R. Astron. Soc.* **1975**, *173*, 255–269. [CrossRef]
26. Aloisio, R.; Blasi, P.; Serpico, P.D. Nonlinear cosmic ray Galactic transport in the light of AMS-02 and Voyager data. *Astropart. Phys.* **2015**, *583*, A95. [CrossRef]
27. Wentzel, D.G. Cosmic-ray propagation in the Galaxy: Collective effects. *Annu. Rev. Astron. Astrophys.* **1974**, *12*, 71–96. [CrossRef]
28. Cesarsky, C.J. Cosmic-ray confinement in the galaxy. *Annu. Rev. Astron. Astrophys.* **1980**, *18*, 289–319. [CrossRef]
29. Zweibel, E.G. The basis for cosmic ray feedback: Written on the wind. *Phys. Plasmas* **2017**, *24*, 055402. [CrossRef]
30. Plotnikov, I.; Ostriker, E.C.; Bai, X.N. Influence of Ion-Neutral Damping on the Cosmic-Ray Streaming Instability: Magnetohydrodynamic Particle-in-cell Simulations. *Astrophys. J.* **2021**, *914*, 3. [CrossRef]
31. Marret, A.; Ciardi, A.; Smets, R.; Fuchs, J.; Nicolas, L. Enhancement of the Nonresonant Streaming Instability by Particle Collisions. *Phys. Rev. Lett.* **2022**, *128*, 115101. [CrossRef] [PubMed]

32. Squire, J.; Hopkins, P.F.; Quataert, E.; Kempski, P. The impact of astrophysical dust grains on the confinement of cosmic rays. *Mon. Not. R. Astron. Soc.* **2021**, *502*, 2630–2644. [CrossRef]
33. Gupta, S.; Caprioli, D.; Haggerty, C.C. Lepton-driven Nonresonant Streaming Instability. *Astrophys. J.* **2021**, *923*, 208. [CrossRef]
34. Zweibel, E.G.; Everett, J.E. Environments for Magnetic Field Amplification by Cosmic Rays. *Astrophys. J.* **2010**, *709*, 1412–1419. [CrossRef]
35. Pelletier, G.; Lemoine, M.; Marcowith, A. Turbulence and particle acceleration in collisionless supernovae remnant shocks. I. Anisotropic spectra solutions. *Astropart. Phys.* **2006**, *453*, 181–191. [CrossRef]
36. Amato, E.; Blasi, P. A kinetic approach to cosmic-ray-induced streaming instability at supernova shocks. *Mon. Not. R. Astron. Soc.* **2009**, *392*, 1591–1600. [CrossRef]
37. Amato, E. The streaming instability: A review. *Mem. Soc. Astron. Ital.* **2011**, *82*, 806.
38. Reville, B.; Kirk, J.G.; Duffy, P.; O'Sullivan, S. Environmental Limits on the Nonresonant Cosmic-Ray Current-Driven Instability. *Int. J. Mod. Phys. D* **2008**, *17*, 1795–1801. [CrossRef]
39. Marret, A.; Ciardi, A.; Smets, R.; Fuchs, J. On the growth of the thermally modified non-resonant streaming instability. *Mon. Not. R. Astron. Soc.* **2021**, *500*, 2302–2315. [CrossRef]
40. Blasi, P. The origin of galactic cosmic rays. *Astron. Astrophys. Rev.* **2013**, *21*, 70. [CrossRef]
41. Amato, E. The origin of galactic cosmic rays. *Int. J. Mod. Phys. D* **2014**, *23*, 1430013. [CrossRef]
42. Bell, A.R. Turbulent amplification of magnetic field and diffusive shock acceleration of cosmic rays. *Mon. Not. R. Astron. Soc.* **2004**, *353*, 550–558. [CrossRef]
43. Vink, J. Supernova remnants: The X-ray perspective. *Astron. Astrophys. Rev.* **2012**, *20*, 49. [CrossRef]
44. Bykov, A.M.; Ellison, D.C.; Renaud, M. Magnetic Fields in Cosmic Particle Acceleration Sources. *Space Sci. Rev.* **2012**, *166*, 71–95. [CrossRef]
45. Riquelme, M.A.; Spitkovsky, A. Nonlinear Study of Bell's Cosmic Ray Current-Driven Instability. *Astrophys. J.* **2009**, *694*, 626–642. [CrossRef]
46. Schroer, B.; Pezzi, O.; Caprioli, D.; Haggerty, C.; Blasi, P. Dynamical Effects of Cosmic Rays on the Medium Surrounding Their Sources. *Astrophys. J. Lett.* **2021**, *914*, L13. [CrossRef]
47. Schroer, B.; Pezzi, O.; Caprioli, D.; Haggerty, C.C.; Blasi, P. Cosmic-ray generated bubbles around their sources. *Mon. Not. R. Astron. Soc.* **2022**, *512*, 233–244. [CrossRef]
48. Commerçon, B.; Marcowith, A.; Dubois, Y. Cosmic-ray propagation in the bi-stable interstellar medium. I. Conditions for cosmic-ray trapping. *Astropart. Phys.* **2019**, *622*, A143. [CrossRef]
49. Simpson, C.M.; Pakmor, R.; Pfrommer, C.; Glover, S.C.O.; Smith, R. How cosmic rays mediate the evolution of the interstellar medium. *Mon. Not. R. Astron. Soc.* **2023**, *520*, 4621–4645. [CrossRef]
50. Almeida, S.P.; Rushbrooke, J.G.; Scharenguivel, J.H.; Behrens, M.; Blobel, V.; Borecka, I.; Dehne, H.C.; Dfaz, J.; Knies, G.; Schmitt, A.; et al. pp Interactions at 10 GeV/ *c*. *Phys. Rev.* **1968**, *174*, 1638. [CrossRef]
51. Skorodko, T.; Bashkanov, M.; Bogoslawsky, D.; Calen, H.; Cappellaro, F.; Clement, H.; Demiroers, L.; Doroshkevich, E.; Duniec, D.; Ekström, C.; et al. Excitation of the Roper resonance in single- and double-pion production in nucleon-nucleon collisions. *Eur. Phys. J. A* **2008**, *35*, 317. [CrossRef]
52. Blattnig, S.R.; Swaminathan, S.R.; Kruger, A.T.; Ngom, M.; Norbury, J.W. Parametrizations of inclusive cross sections for pion production in proton-proton collisions. *Phys. Rev. D* **2000**, *62*, 094030. [CrossRef]
53. Patrignani, C. Review of Particle Physics. *Chin. Phys.* **2016**, *C40*, 100001. [CrossRef]
54. Amenomori, M.; Bi, X.J.; Chen, D.; Chen, T.L.; Chen, W.Y.; Cui, S.W.; Danzengluobu.; Ding, L.K.; Feng, C.F.; Feng, Z.; et al. Test of the hadronic interaction models SIBYLL2.3, EPOS-LHC and QGSJETII—04 with Tibet EAS core data. *Eur. Phys. J. Web Conf.* **2019**, *208*, 08013. [CrossRef]
55. Bähr, M.; Gieseke, S.; Gigg, M.A.; Grellscheid, D.; Hamilton, K.; Latunde-Dada, O.; Plätzer, S.; Richardson, P.; Seymour, M.H.; Sherstnev, A.; et al. Herwig++ physics and manual. *Eur. Phys. J. C* **2008**, *58*, 639–707. [CrossRef]
56. Gleisberg, T.; Höche, S.; Krauss, F.; Schönherr, M.; Schumann, S.; Siegert, F.; Winter, J. Event generation with SHERPA 1.1. *J. High Energy Phys.* **2009**, *2009*, 7. [CrossRef]
57. Allison, J.; Amako, K.; Apostolakis, J.; Araujo, H.; Dubois, P.A.; Asai, M.; Barrand, G.; Capra, R.; Chauvie, S.; Chytracek, R.; et al. Geant4 developments and applications. *IEEE Trans. Nucl. Sci.* **2006**, *53*, 270–278. [CrossRef]
58. Allison, J.; Amako, K.; Apostolakis, J.; Arce, P.; Asai, M.; Aso, T.; Bagli, E.; Bagulya, A.; Banerjee, S.; Barrand, G.; et al. Recent developments in GEANT4. *Nucl. Instrum. Methods Phys. Res. A* **2016**, *835*, 186–225. [CrossRef]
59. Agostinelli, S.; Allison, J.; Amako, K.; Apostolakis, J.; Araujo, H.; Arce, P.; Asai, M.; Axen, D.; Banerjee, S.; Barrand, G.; et al. G EANT4—A simulation toolkit. *Nucl. Instrum. Methods Phys. Res. A* **2003**, *506*, 250–303. [CrossRef]
60. Sjöstrand, T.; Mrenna, S.; Skands, P. A brief introduction to PYTHIA 8.1. *Comput. Phys. Commun.* **2008**, *178*, 852–867. [CrossRef]
61. Sjöstrand, T.; Mrenna, S.; Skands, P. PYTHIA 6.4 physics and manual. *J. High Energy Phys.* **2006**, *2006*, 026. [CrossRef]
62. Bierlich, C.; Chakraborty, S.; Desai, N.; Gellersen, L.; Helenius, I.; Ilten, P.; Lönnblad, L.; Mrenna, S.; Prestel, S.; Preuss, C.T.; et al. A comprehensive guide to the physics and usage of PYTHIA 8.3. *arXiv* **2022**, arXiv:2203.11601. [CrossRef]
63. Engel, R.; Ranft, J.; Roesler, S. Hard diffraction in hadron-hadron interactions and in photoproduction. *Phys. Rev. D* **1995**, *52*, 1459–1468. [CrossRef]

64. Bopp, F.W.; Ranft, J.; Engel, R.; Roesler, S. Antiparticle to particle production ratios in hadron-hadron and d-Au collisions in the DPMJET-III Monte Carlo model. *Phys. Rev. C* **2008**, *77*, 014904. [CrossRef]
65. Werner, K.; Liu, F.M.; Pierog, T. Parton ladder splitting and the rapidity dependence of transverse momentum spectra in deuteron-gold collisions at the BNL Relativistic Heavy Ion Collider. *Phys. Rev. C* **2006**, *74*, 044902. [CrossRef]
66. Ahn, E.J.; Engel, R.; Gaisser, T.K.; Lipari, P.; Stanev, T. Cosmic ray interaction event generator SIBYLL 2.1. *Phys. Rev. D* **2009**, *80*, 094003. [CrossRef]
67. Fletcher, R.S.; Gaisser, T.K.; Lipari, P.; Stanev, T. sibyll: An event generator for simulation of high energy cosmic ray cascades. *Phys. Rev. D* **1994**, *50*, 5710–5731. [CrossRef]
68. Engel, J.; Gaisser, T.K.; Lipari, P.; Stanev, T. Nucleus-nucleus collisions and interpretation of cosmic-ray cascades. *Phys. Rev. D* **1992**, *46*, 5013–5025. [CrossRef]
69. Fedynitch, A.; Riehn, F.; Engel, R.; Gaisser, T.K.; Stanev, T. Hadronic interaction model uc(sibyll) 2.3 c and inclusive lepton fluxes. *Phys. Rev. D* **2019**, *100*, 103018. [CrossRef]
70. Ostapchenko, S. QGSJET-II: Towards reliable description of very high energy hadronic interactions. *Nucl. Phys. Proc. Suppl.* **2006**, *151*, 143–146. [CrossRef]
71. Ostapchenko, S. Status of QGSJET. In *Collicers to Cosmic Rays*; American Institute of Physics Conference Series; Tripathi, M., Breedon, R.E., Eds.; AIP Publishing LLC: Melville, NY, USA, 2007; Volume 928, pp. 118–125. [CrossRef]
72. Kafexhiu, E.; Aharonian, F.; Taylor, A.M.; Vila, G.S. Parametrization of gamma-ray production cross sections for p p interactions in a broad proton energy range from the kinematic threshold to PeV energies. *Phys. Rev. D* **2014**, *90*, 123014. [CrossRef]
73. Kelner, S.R.; Aharonian, F.A.; Bugayov, V.V. Energy spectra of gamma rays, electrons, and neutrinos produced at proton-proton interactions in the very high energy regime. *Phys. Rev. D* **2006**, *74*, 034018. [CrossRef]
74. Kamae, T.; Karlsson, N.; Mizuno, T.; Abe, T.; Koi, T. Parameterization of γ, $e^{+/-}$, and Neutrino Spectra Produced by p-p Interaction in Astronomical Environments. *Astrophys. J.* **2006**, *647*, 692–708. [CrossRef]
75. Kachelrieß, M.; Moskalenko, I.V.; Ostapchenko, S. AAfrag: Interpolation routines for Monte Carlo results on secondary production in proton-proton, proton-nucleus and nucleus-nucleus interactions. *Comput. Phys. Commun.* **2019**, *245*, 106846. [CrossRef] [PubMed]
76. Koldobskiy, S.; Kachelrieß, M.; Lskavyan, A.; Neronov, A.; Ostapchenko, S.; Semikoz, D.V. Energy spectra of secondaries in proton-proton interactions. *Phys. Rev. D* **2021**, *104*, 123027. [CrossRef]
77. Hooper, D.; Plant, K. A Leptonic Model for Neutrino Emission From Active Galactic Nuclei. *arXiv* **2023**, arXiv:2305.06375. [CrossRef]
78. Mücke, A.; Rachen, J.P.; Engel, R.; Protheroe, R.J.; Stanev, T. Photohadronic Processes in Astrophysical Environments. *Pub. Astron. Soc. Aust.* **1999**, *16*, 160. [CrossRef]
79. Berezinsky, V.S.; Gazizov, A.Z. Production of high-energy cosmic neutrinos in $p\gamma$ and $n\gamma$ scattering. I. Neutrino yields for power-law spectra of protons and neutrons. *Phys. Rev. D* **1993**, *47*, 4206. [CrossRef]
80. Nakamura, K. Review of Particle Physics. *J. Phys. G Nucl. Part. Phys.* **2010**, *37*, 075021. [CrossRef]
81. Hümmer, S.; Rüger, M.; Spanier, F.; Winter, W. Simplified Models for Photohadronic Interactions in Cosmic Accelerators. *Astrophys. J.* **2010**, *721*, 630–652. [CrossRef]
82. Dermer, C.D.; Menon, G. *High Energy Radiation from Black Holes: Gamma Rays, Cosmic Rays, and Neutrinos*; Princeton University Press: Princeton, NJ, USA, 2009.
83. Mücke, A.; Engel, R.; Rachen, J.P.; Protheroe, R.J.; Stanev, T. Monte Carlo simulations of photohadronic processes in astrophysics. *Comput. Phys. Commun.* **2000**, *124*, 290–314. [CrossRef]
84. Kelner, S.R.; Aharonian, F.A. Energy spectra of gamma rays, electrons, and neutrinos produced at interactions of relativistic protons with low energy radiation. *Phys. Rev. D* **2008**, *78*, 034013. [CrossRef]
85. Draine, B.T. *Physics of the Interstellar and Intergalactic Medium*; Princeton University Press: Princeton, NJ, USA, 2011.
86. Yoast-Hull, T.M.; Murray, N. Breaking the radio—Gamma-ray connection in Arp 220. *Mon. Not. R. Astron. Soc.* **2019**, *484*, 3665–3680. [CrossRef]
87. Wilson, C.D.; Rangwala, N.; Glenn, J.; Maloney, P.R.; Spinoglio, L.; Pereira-Santaella, M. Extreme Dust Disks in Arp 220 as Revealed by ALMA. *Astrophys. J. Lett.* **2014**, *789*, L36. [CrossRef]
88. Scoville, N.; Murchikova, L.; Walter, F.; Vlahakis, C.; Koda, J.; Vanden Bout, P.; Barnes, J.; Hernquist, L.; Sheth, K.; Yun, M.; et al. ALMA Resolves the Nuclear Disks of Arp 220. *Astrophys. J.* **2017**, *836*, 66. [CrossRef]
89. Rowan-Robinson, M. Hyperluminous infrared galaxies. *Mon. Not. R. Astron. Soc.* **2000**, *316*, 885–900. [CrossRef]
90. Chakraborty, N.; Fields, B.D. Inverse-Compton Contribution to the Star-forming Extragalactic Gamma-Ray Background. *Astrophys. J.* **2013**, *773*, 104. [CrossRef]
91. Schober, J.; Schleicher, D.R.G.; Klessen, R.S. X-ray emission from star-forming galaxies - signatures of cosmic rays and magnetic fields. *Mon. Not. R. Astron. Soc.* **2015**, *446*, 2–17. [CrossRef]
92. Wilman, R.J.; Fabian, A.C.; Cutri, R.M.; Crawford, C.S.; Brandt, W.N. Limits on the X-ray emission from several hyperluminous IRAS galaxies. *Mon. Not. R. Astron. Soc.* **1998**, *300*, L7–L10. [CrossRef]
93. Danielson, A.L.R.; Swinbank, A.M.; Smail, I.; Cox, P.; Edge, A.C.; Weiss, A.; Harris, A.I.; Baker, A.J.; De Breuck, C.; Geach, J.E.; et al. The properties of the interstellar medium within a star-forming galaxy at z = 2.3. *Mon. Not. R. Astron. Soc.* **2011**, *410*, 1687–1702. [CrossRef]

94. Hashimoto, T.; Laporte, N.; Mawatari, K.; Ellis, R.S.; Inoue, A.K.; Zackrisson, E.; Roberts-Borsani, G.; Zheng, W.; Tamura, Y.; Bauer, F.E.; et al. The onset of star formation 250 million years after the Big Bang. *Nature* **2018**, *557*, 392–395. [CrossRef] [PubMed]
95. Bohlin, R.C.; Savage, B.D.; Drake, J.F. A survey of interstellar H I from Lalpha absorption measurements. II. *Astrophys. J.* **1978**, *224*, 132–142. [CrossRef]
96. Bykov, A.M.; Ellison, D.C.; Marcowith, A.; Osipov, S.M. Cosmic Ray Production in Supernovae. *Space Sci. Rev.* **2018**, *214*, 41. [CrossRef]
97. Berezinskii, V.S.; Bulanov, S.V.; Ginzburg, V.L.; Dogel, V.A.; Ptuskin, V.S. *Astrophysics of Cosmic Rays*; North-Holland: Amsterdam, The Netherlands, 1984.
98. Lingenfelter, R.E. Superbubble origin of cosmic rays. In Proceedings of the Centenary Symposium 2012: Discovery of Cosmic Rays, Denver, CO, USA, 26–28 June 2012; American Institute of Physics Conference Series; Ormes, J.F., Ed.; AIP Publishing LLC: Melville, NY, USA, 2013; Volume 1516, pp. 162–166. [CrossRef]
99. Cristofari, P. The Hunt for Pevatrons: The Case of Supernova Remnants. *Universe* **2021**, *7*, 324. [CrossRef]
100. Li, W.; Chornock, R.; Leaman, J.; Filippenko, A.V.; Poznanski, D.; Wang, X.; Ganeshalingam, M.; Mannucci, F. Nearby supernova rates from the Lick Observatory Supernova Search—III. The rate-size relation, and the rates as a function of galaxy Hubble type and colour. *Mon. Not. R. Astron. Soc.* **2011**, *412*, 1473–1507. [CrossRef]
101. Lingenfelter, R.E. Cosmic rays from supernova remnants and superbubbles. *Adv. Space Res.* **2018**, *62*, 2750–2763. [CrossRef]
102. Marcowith, A.; Dwarkadas, V.V.; Renaud, M.; Tatischeff, V.; Giacinti, G. Core-collapse supernovae as cosmic ray sources. *Mon. Not. R. Astron. Soc.* **2018**, *479*, 4470–4485. [CrossRef]
103. Murase, K.; Franckowiak, A.; Maeda, K.; Margutti, R.; Beacom, J.F. High-energy Emission from Interacting Supernovae: New Constraints on Cosmic-Ray Acceleration in Dense Circumstellar Environments. *Astrophys. J.* **2019**, *874*, 80. [CrossRef]
104. Hillas, A.M. The Origin of Ultra-High-Energy Cosmic Rays. *Annu. Rev. Astron. Astrophys.* **1984**, *22*, 425–444. [CrossRef]
105. Achterberg, A. Modification of scattering waves and its importance for shock acceleration. *Astropart. Phys.* **1983**, *119*, 274–278.
106. Bell, A.R.; Schure, K.M.; Reville, B.; Giacinti, G. Cosmic-ray acceleration and escape from supernova remnants. *Mon. Not. R. Astron. Soc.* **2013**, *431*, 415–429. [CrossRef]
107. Schure, K.M.; Bell, A.R. Cosmic ray acceleration in young supernova remnants. *Mon. Not. R. Astron. Soc.* **2013**, *435*, 1174–1185. [CrossRef]
108. Schure, K.M.; Bell, A.R. From cosmic ray source to the Galactic pool. *Mon. Not. R. Astron. Soc.* **2014**, *437*, 2802–2805. [CrossRef]
109. Casanova, S. On the Search for the Galactic PeVatrons by Means of Gamma-Ray Astronomy. *Universe* **2022**, *8*, 505. [CrossRef]
110. Petropoulou, M.; Coenders, S.; Vasilopoulos, G.; Kamble, A.; Sironi, L. Point-source and diffuse high-energy neutrino emission from Type IIn supernovae. *Mon. Not. R. Astron. Soc.* **2017**, *470*, 1881–1893. [CrossRef]
111. Waxman, E.; Loeb, A. TeV Neutrinos and GeV Photons from Shock Breakout in Supernovae. *Phys. Rev. Lett.* **2001**, *87*, 071101. [CrossRef]
112. Chevalier, R.A.; Fransson, C. Shock Breakout Emission from a Type Ib/c Supernova: XRT 080109/SN 2008D. *Astrophys. J. Lett.* **2008**, *683*, L135. [CrossRef]
113. Ensman, L.; Burrows, A. Shock Breakout in SN 1987A. *Astrophys. J.* **1992**, *393*, 742. [CrossRef]
114. Chevalier, R.A.; Klein, R.I. Nonequilibrium processes in the evolution of type II supernovae. *Astrophys. J.* **1979**, *234*, 597–608. [CrossRef]
115. Giacinti, G.; Bell, A.R. Collisionless shocks and TeV neutrinos before Supernova shock breakout from an optically thick wind. *Mon. Not. R. Astron. Soc.* **2015**, *449*, 3693–3699. [CrossRef]
116. Bell, A.R. The acceleration of cosmic rays in shock fronts—II. *Mon. Not. R. Astron. Soc.* **1978**, *182*, 443–455. [CrossRef]
117. Bell, A.R. The acceleration of cosmic rays in shock fronts—I. *Mon. Not. R. Astron. Soc.* **1978**, *182*, 147–156. [CrossRef]
118. Celli, S.; Morlino, G.; Gabici, S.; Aharonian, F.A. Exploring particle escape in supernova remnants through gamma rays. *Mon. Not. R. Astron. Soc.* **2019**, *490*, 4317–4333. [CrossRef]
119. Truelove, J.K.; McKee, C.F. Evolution of Nonradiative Supernova Remnants. *Astrophys. J. Suppl.* **1999**, *120*, 299–326. [CrossRef]
120. Drury, L.O. Escaping the accelerator: How, when and in what numbers do cosmic rays get out of supernova remnants? *Mon. Not. R. Astron. Soc.* **2011**, *415*, 1807–1814. [CrossRef]
121. Peron, G.; Aharonian, F.; Casanova, S.; Zanin, R.; Romoli, C. On the Gamma-Ray Emission of W44 and Its Surroundings. *Astrophys. J. Lett.* **2020**, *896*, L23. [CrossRef]
122. Feijen, K.; Einecke, S.; Rowell, G.; Braiding, C.; Burton, M.G.; Wong, G.F. Modelling the gamma-ray morphology of HESSJ1804-216 from two supernova remnants in a hadronic scenario. *Mon. Not. R. Astron. Soc.* **2022**, *511*, 5915–5926. [CrossRef]
123. Abdalla, H. et al. [H. E. S. S. Collaboration] Upper limits on very-high-energy gamma-ray emission from core-collapse supernovae observed with H.E.S.S. *Astropart. Phys.* **2019**, *626*, A57. [CrossRef]
124. Li, Y.; Xin, Y.; Liu, S.; He, Y. Advanced γ-Ray Emission Studies of G15.4+0.1 with Fermi-LAT: Evidence of Escaping Cosmic Rays Interacting with Surrounding Molecular Clouds. *Astrophys. J.* **2023**, *945*, 21. [CrossRef]
125. Aruga, M.; Sano, H.; Fukui, Y.; Reynoso, E.M.; Rowell, G.; Tachihara, K. Molecular and Atomic Clouds Associated with the Gamma-Ray Supernova Remnant Puppis A. *Astrophys. J.* **2022**, *938*, 94. [CrossRef]
126. Zhang, Y.; Liu, R.Y.; Li, H.; Shao, S.; Yan, H.; Wang, X.Y. Measuring the Mass of Missing Baryons in the Halo of Andromeda Galaxy with Gamma-Ray Observations. *Astrophys. J.* **2021**, *911*, 58. [CrossRef]

127. Zhong, W.J.; Zhang, X.; Chen, Y.; Zhang, Q.Q. A study of GeV gamma-ray emission towards supernova remnant G51.26+0.11 and its molecular environment. *Mon. Not. R. Astron. Soc.* **2023**, *521*, 1931–1940. [CrossRef]
128. Yeung, P.K.H.; Bamba, A.; Sano, H. Multiwavelength studies of G298.6-0.0: An old GeV supernova remnant interacting with molecular clouds. *Publ. Astron. Soc. Jpn.* **2023**, *75*, 384–396. [CrossRef]
129. Supan, L.; Fischetto, G.; Castelletti, G. Supernova remnant G46.8-0.3: A new case of interaction with molecular material. *Astropart. Phys.* **2022**, *664*, A89. [CrossRef]
130. Reynolds, S.P. Supernova remnants at high energy. *Annu. Rev. Astron. Astrophys.* **2008**, *46*, 89–126. [CrossRef]
131. Murase, K.; Thompson, T.A.; Ofek, E.O. Probing cosmic ray ion acceleration with radio-submm and gamma-ray emission from interaction-powered supernovae. *Mon. Not. R. Astron. Soc.* **2014**, *440*, 2528–2543. [CrossRef]
132. Helder, E.A.; Vink, J.; Bykov, A.M.; Ohira, Y.; Raymond, J.C.; Terrier, R. Observational Signatures of Particle Acceleration in Supernova Remnants. *Space Sci. Rev.* **2012**, *173*, 369–431. [CrossRef]
133. Bykov, A.M.; Marcowith, A.; Amato, E.; Kalyashova, M.E.; Kruijssen, J.M.D.; Waxman, E. High-Energy Particles and Radiation in Star-Forming Regions. *Space Sci. Rev.* **2020**, *216*, 42. [CrossRef]
134. Tatischeff, V.; Gabici, S. Particle Acceleration by Supernova Shocks and Spallogenic Nucleosynthesis of Light Elements. *Annu. Rev. Nucl. Part. Sci.* **2018**, *68*, 377–404. [CrossRef]
135. Abeysekara, A.U.; Albert, A.; Alfaro, R.; Alvarez, C.; Camacho, J.R.A.; Arteaga-Velázquez, J.C.; Arunbabu, K.P.; Rojas, D.A.; Solares, H.A.A.; Baghmanyan, V.; et al. HAWC observations of the acceleration of very-high-energy cosmic rays in the Cygnus Cocoon. *Nat. Astron.* **2021**, *5*, 465–471. [CrossRef]
136. Cao, Z.; Aharonian, F.A.; An, Q.; Axikegu; Bai, L.X.; Bai, Y.X.; Bao, Y.W.; Bastieri, D.; Bi, X.J.; Bi, Y.J.; et al. Ultrahigh-energy photons up to 1.4 petaelectronvolts from 12 γ-ray Galactic sources. *Nature* **2021**, *594*, 33–36. [CrossRef] [PubMed]
137. Ackermann, M.; Ajello, M.; Allafort, A.; Baldini, L.; Ballet, J.; Barbiellini, G.; Bastieri, D.; Belfiore, A.; Bellazzini, R.; Berenji, B.; et al. A Cocoon of Freshly Accelerated Cosmic Rays Detected by Fermi in the Cygnus Superbubble. *Science* **2011**, *334*, 1103. [CrossRef] [PubMed]
138. Bartoli, B.; Bernardini, P.; Bi, X.J.; Branchini, P.; Budano, A.; Camarri, P.; Cao, Z.; Cardarelli, R.; Catalanotti, S.; Chen, S.Z.; et al. Identification of the TeV Gamma-Ray Source ARGO J2031+4157 with the Cygnus Cocoon. *Astrophys. J.* **2014**, *790*, 152. [CrossRef]
139. Dzhappuev, D.D.; Afashokov, Y.Z.; Dzaparova, I.M.; Dzhatdoev, T.A.; Gorbacheva, E.A.; Karpikov, I.S.; Khadzhiev, M.M.; Klimenko, N.F.; Kudzhaev, A.U.; Kurenya, A.N.; et al. Observation of Photons above 300 TeV Associated with a High-energy Neutrino from the Cygnus Region. *Astrophys. J. Lett.* **2021**, *916*, L22. [CrossRef]
140. Yang, R.Z.; Wang, Y. The diffuse gamma-ray emission toward the Galactic mini starburst W43. *Astropart. Phys.* **2020**, *640*, A60. [CrossRef]
141. Aharonian, F.; Ashkar, H.; Backes, M.; Barbosa Martins, V.; Becherini, Y.; Berge, D.; Bi, B.; Böttcher, M.; de Bony de Lavergne, M.; Bradascio, F.; et al. A deep spectromorphological study of the γ-ray emission surrounding the young massive stellar cluster Westerlund 1. *Astropart. Phys.* **2022**, *666*, A124. [CrossRef]
142. Härer, L.K.; Reville, B.; Hinton, J.; Mohrmann, L.; Vieu, T. Understanding the TeV γ-ray emission surrounding the young massive star cluster Westerlund 1. *Astropart. Phys.* **2023**, *671*, A4. [CrossRef]
143. Mestre, E.; de Oña Wilhelmi, E.; Torres, D.F.; Holch, T.L.; Schwanke, U.; Aharonian, F.; Parkinson, P.S.; Yang, R.; Zanin, R. Probing the hadronic nature of the gamma-ray emission associated with Westerlund 2. *Mon. Not. R. Astron. Soc.* **2021**, *505*, 2731–2740. [CrossRef]
144. Ge, T.T.; Sun, X.N.; Yang, R.Z.; Liang, Y.F.; Liang, E.W. Diffuse γ-ray emission around the massive star forming region of Carina Nebula Complex. *Mon. Not. R. Astron. Soc.* **2022**, *517*, 5121–5128. [CrossRef]
145. Baghmanyan, V.; Peron, G.; Casanova, S.; Aharonian, F.; Zanin, R. Evidence of Cosmic-Ray Excess from Local Giant Molecular Clouds. *Astrophys. J. Lett.* **2020**, *901*, L4. [CrossRef]
146. Cesarsky, C.J.; Montmerle, T. Gamma-Rays from Active Regions in the Galaxy—The Possible Contribution of Stellar Winds. *Space Sci. Rev.* **1983**, *36*, 173–193. [CrossRef]
147. Voelk, H.J.; Forman, M. Cosmic rays and gamma-rays from OB stars. *Astrophys. J.* **1982**, *253*, 188–198. [CrossRef]
148. Mac Low, M.M.; McCray, R. Superbubbles in Disk Galaxies. *Astrophys. J.* **1988**, *324*, 776. [CrossRef]
149. Reimer, A.; Pohl, M.; Reimer, O. Nonthermal High-Energy Emission from Colliding Winds of Massive Stars. *Astrophys. J.* **2006**, *644*, 1118–1144. [CrossRef]
150. Vieu, T.; Reville, B.; Aharonian, F. Can superbubbles accelerate ultrahigh energy protons? *Mon. Not. R. Astron. Soc.* **2022**, *515*, 2256–2265. [CrossRef]
151. Bykov, A.M.; Toptygin, I.N. A Model of Particle Acceleration to High Energies by Multiple Supernova Explosions in OB Associations. *Astron. Lett.* **2001**, *27*, 625–633. [CrossRef]
152. Bykov, A.M.; Fleishman, G.D. On non-thermal particle generation in superbubbles. *Mon. Not. R. Astron. Soc.* **1992**, *255*, 269–275. [CrossRef]
153. Bykov, A.M. Nonthermal particles and photons in starburst regions and superbubbles. *Astron. Astrophys. Rev.* **2014**, *22*, 77. [CrossRef]
154. Parizot, E.; Marcowith, A.; van der Swaluw, E.; Bykov, A.M.; Tatischeff, V. Superbubbles and energetic particles in the Galaxy. I. Collective effects of particle acceleration. *Astropart. Phys.* **2004**, *424*, 747–760. [CrossRef]

155. Higdon, J.C.; Lingenfelter, R.E. OB Associations, Supernova-generated Superbubbles, and the Source of Cosmic Rays. *Astrophys. J.* **2005**, *628*, 738–749. [CrossRef]
156. Wang, K.; Zhang, H.M.; Liu, R.Y.; Wang, X.Y. Detection of Diffuse γ-Ray Emission toward a Massive Star-forming Region Hosting Wolf-Rayet Stars. *Astrophys. J.* **2022**, *935*, 129. [CrossRef]
157. Kamijima, S.F.; Ohira, Y. Escape of cosmic rays from perpendicular shocks in the circumstellar magnetic field. *Phys. Rev. D* **2022**, *106*, 123025. [CrossRef]
158. Gupta, S.; Nath, B.B.; Sharma, P.; Eichler, D. Realistic modelling of wind and supernovae shocks in star clusters: Addressing ^{22}Ne/^{20}Ne and other problems in Galactic cosmic rays. *Mon. Not. R. Astron. Soc.* **2020**, *493*, 3159–3177. [CrossRef]
159. Gupta, S.; Nath, B.B.; Sharma, P.; Eichler, D. Lack of thermal energy in superbubbles: Hint of cosmic rays? *Mon. Not. R. Astron. Soc.* **2018**, *473*, 1537–1553. [CrossRef]
160. Morlino, G.; Blasi, P.; Peretti, E.; Cristofari, P. Particle acceleration in winds of star clusters. *Mon. Not. R. Astron. Soc.* **2021**, *504*, 6096–6105. [CrossRef]
161. Gabici, S. Star clusters as cosmic ray accelerators. *arXiv* **2023**, arXiv:2301.06505. [CrossRef]
162. Murphy, R.P.; Sasaki, M.; Binns, W.R.; Brandt, T.J.; Hams, T.; Israel, M.H.; Labrador, A.W.; Link, J.T.; Mewaldt, R.A.; Mitchell, J.W.; et al. Galactic Cosmic Ray Origins and OB Associations: Evidence from SuperTIGER Observations of Elements $_{26}$Fe through $_{40}$Zr. *Astrophys. J.* **2016**, *831*, 148. [CrossRef]
163. Tatischeff, V.; Raymond, J.C.; Duprat, J.; Gabici, S.; Recchia, S. The origin of Galactic cosmic rays as revealed by their composition. *Mon. Not. R. Astron. Soc.* **2021**, *508*, 1321–1345. [CrossRef]
164. Rauch, B.F.; Link, J.T.; Lodders, K.; Israel, M.H.; Barbier, L.M.; Binns, W.R.; Christian, E.R.; Cummings, J.R.; de Nolfo, G.A.; Geier, S.; et al. Cosmic Ray origin in OB Associations and Preferential Acceleration of Refractory Elements: Evidence from Abundances of Elements $_{26}$Fe through $_{34}$Se. *Astrophys. J.* **2009**, *697*, 2083–2088. [CrossRef]
165. Wiedenbeck, M.E.; Binns, W.R.; Cummings, A.C.; Davis, A.J.; de Nolfo, G.A.; Israel, M.H.; Leske, R.A.; Mewaldt, R.A.; Stone, E.C.; von Rosenvinge, T.T. An Overview of the Origin of Galactic Cosmic Rays as Inferred from Observations of Heavy Ion Composition and Spectra. *Space Sci. Rev.* **2007**, *130*, 415–429. [CrossRef]
166. Meyer, J.P.; Drury, L.O.; Ellison, D.C. Galactic Cosmic Rays from Supernova Remnants. I. A Cosmic-Ray Composition Controlled by Volatility and Mass-to-Charge Ratio. *Astrophys. J.* **1997**, *487*, 182–196. [CrossRef]
167. Ellison, D.C.; Drury, L.O.; Meyer, J.P. Galactic Cosmic Rays from Supernova Remnants. II. Shock Acceleration of Gas and Dust. *Astrophys. J.* **1997**, *487*, 197–217. [CrossRef]
168. Parizot, E. Superbubbles and the Galactic evolution of Li, Be and B. *Astropart. Phys.* **2000**, *362*, 786–798. [CrossRef]
169. Meneguzzi, M.; Audouze, J.; Reeves, H. The production of the elements Li, Be, B by galactic cosmic rays in space and its relation with stellar observations. *Astropart. Phys.* **1971**, *15*, 337.
170. Reeves, H.; Fowler, W.A.; Hoyle, F. Galactic Cosmic Ray Origin of Li, Be and B in Stars. *Nature* **1970**, *226*, 727–729. [CrossRef]
171. Kulikov, G.; Khristiansen, G. On the size spectrum of extensive air showers. *Sov. Phys. JETP* **1959**, *35*, 441–444.
172. Parizot, E. Cosmic Ray Origin: Lessons from Ultra-High-Energy Cosmic Rays and the Galactic/Extragalactic Transition. *Nucl. Phys. B Proc. Suppl.* **2014**, *256*, 197–212. [CrossRef]
173. Antoni, T.; Apel, W.D.; Badea, A.F.; Bekk, K.; Bercuci, A.; Blümer, J.; Bozdog, H.; Brancus, I.M.; Chilingarian, A.; Daumiller, K.; et al. KASCADE measurements of energy spectra for elemental groups of cosmic rays: Results and open problems. *Astroparticle Physics* **2005**, *24*, 1–25. [CrossRef]
174. Adriani, O.; Barbarino, G.C.; Bazilevskaya, G.A.; Bellotti, R.; Boezio, M.; Bogomolov, E.A.; Bonechi, L.; Bongi, M.; Bonvicini, V.; Borisov, S.; et al. PAMELA Measurements of Cosmic-Ray Proton and Helium Spectra. *Science* **2011**, *332*, 69. [CrossRef]
175. Aguilar, M.; Aisa, D.; Alpat, B.; Alvino, A.; Ambrosi, G.; Andeen, K.; Arruda, L.; Attig, N.; Azzarello, P.; Bachlechner, A.; et al. Precision Measurement of the Proton Flux in Primary Cosmic Rays from Rigidity 1 GV to 1.8 TV with the Alpha Magnetic Spectrometer on the International Space Station. *Phys. Rev. Lett.* **2015**, *114*, 171103. [CrossRef]
176. Aguilar, M.; Aisa, D.; Alpat, B.; Alvino, A.; Ambrosi, G.; Andeen, K.; Arruda, L.; Attig, N.; Azzarello, P.; Bachlechner, A.; et al. Precision Measurement of the Helium Flux in Primary Cosmic Rays of Rigidities 1.9 GV to 3 TV with the Alpha Magnetic Spectrometer on the International Space Station. *Phys. Rev. Lett.* **2015**, *115*, 211101. [CrossRef] [PubMed]
177. Bartoli, B.; Bernardini, P.; Bi, X.J.; Cao, Z.; Catalanotti, S.; Chen, S.Z.; Chen, T.L.; Cui, S.W.; Dai, B.Z.; D'Amone, A.; et al. Knee of the cosmic hydrogen and helium spectrum below 1 PeV measured by ARGO-YBJ and a Cherenkov telescope of LHAASO. *Phys. Rev. D* **2015**, *92*, 092005. [CrossRef]
178. Cao, Z. et al. [Lhaaso Collaboration]. Peta-electron volt gamma-ray emission from the Crab Nebula. *Science* **2021**, *373*, 425–430. [CrossRef]
179. Liu, R.Y.; Wang, X.Y. PeV Emission of the Crab Nebula: Constraints on the Proton Content in Pulsar Wind and Implications. *Astrophys. J.* **2021**, *922*, 221. [CrossRef]
180. Peng, Q.Y.; Bao, B.W.; Lu, F.W.; Zhang, L. Multiband Emission up to PeV Energy from the Crab Nebula in a Spatially Dependent Lepto-hadronic Model. *Astrophys. J.* **2022**, *926*, 7. [CrossRef]
181. Baade, W.; Zwicky, F. Cosmic Rays from Super-novae. *Proc. Natl. Acad. Sci. USA* **1934**, *20*, 259–263. [CrossRef] [PubMed]
182. Abramowski, A. et al. [HESS Collaboration]. Acceleration of petaelectronvolt protons in the Galactic Centre. *Nature* **2016**, *531*, 476–479. [CrossRef]

183. Bednarek, W.; Protheroe, R.J. Contribution of nuclei accelerated by gamma-ray pulsars to cosmic rays in the Galaxy. *Astropart. Phys.* **2002**, *16*, 397–409. [CrossRef]
184. Escobar, G.J.; Pellizza, L.J.; Romero, G.E. Highly collimated microquasar jets as efficient cosmic-ray sources. *Astropart. Phys.* **2022**, *665*, A145. [CrossRef]
185. Yang, R.Z.; Aharonian, F.; de Oña Wilhelmi, E. Massive star clusters as the an alternative source population of galactic cosmic rays. *Rend. Lincei. Sci. Fis. Nat.* **2019**, *30*, 159–164. [CrossRef]
186. Abramowski, A.; Acero, F.; Aharonian, F.; Akhperjanian, A.G.; Anton, G.; Balzer, A.; Barnacka, A.; Barres de Almeida, U.; Becherini, Y.; Becker, J.; et al. Discovery of extended VHE γ-ray emission from the vicinity of the young massive stellar cluster Westerlund 1. *Astropart. Phys.* **2012**, *537*, A114. [CrossRef]
187. Abramowski, A. et al. [H. E. S. S. Collaboration]. The exceptionally powerful TeV γ-ray emitters in the Large Magellanic Cloud. *Science* **2015**, *347*, 406–412. [CrossRef]
188. Yang, R.z.; de Oña Wilhelmi, E.; Aharonian, F. Diffuse γ-ray emission in the vicinity of young star cluster Westerlund 2. *Astropart. Phys.* **2018**, *611*, A77. [CrossRef]
189. Vieu, T.; Reville, B. Massive star cluster origin for the galactic cosmic ray population at very-high energies. *Mon. Not. R. Astron. Soc.* **2023**, *519*, 136–147. [CrossRef]
190. Cristofari, P.; Blasi, P.; Amato, E. The low rate of Galactic pevatrons. *Astropart. Phys.* **2020**, *123*, 102492. [CrossRef]
191. Zirakashvili, V.N.; Ptuskin, V.S. Diffusive Shock Acceleration with Magnetic Amplification by Nonresonant Streaming Instability in Supernova Remnants. *Astrophys. J.* **2008**, *678*, 939–949. [CrossRef]
192. Lacki, B.C.; Beck, R. The equipartition magnetic field formula in starburst galaxies: Accounting for pionic secondaries and strong energy losses. *Mon. Not. R. Astron. Soc.* **2013**, *430*, 3171–3186. [CrossRef]
193. Halzen, F.; Kappes, A.; Ó Murchadha, A. Prospects for identifying the sources of the Galactic cosmic rays with IceCube. *Phys. Rev. D* **2008**, *78*, 063004. [CrossRef]
194. Avrorin, A.D. et al. [Baikal-GVD Collaboration]. Baikal-GVD: Status and prospects. *arXiv* **2018**, arXiv:1808.10353. [CrossRef]
195. Aartsen, M.G.; Abbasi, R.; Ackermann, M.; Adams, J.; Aguilar, J.A.; Ahlers, M.; Ahrens, M.; Alispach, C.; Allison, P.; Amin, N.M.; et al. IceCube-Gen2: The window to the extreme Universe. *J. Phys. Nucl. Phys.* **2021**, *48*, 060501. [CrossRef]
196. Agostini, M.; Böhmer, M.; Bosma, J.; Clark, K.; Danninger, M.; Fruck, C.; Gernhäuser, R.; Gärtner, A.; Grant, D.; Henningsen, F.; et al. The Pacific Ocean Neutrino Experiment. *Nat. Astron.* **2020**, *4*, 913–915. [CrossRef]
197. Ye, Z.P.; Hu, F.; Tian, W.; Chang, Q.C.; Chang, Y.L.; Cheng, Z.S.; Gao, J.; Ge, T.; Gong, G.H.; Guo, J.; et al. Proposal for a neutrino telescope in South China Sea. *arXiv* **2022**, arXiv:2207.04519. [CrossRef]
198. Amenomori, M.; Bao, Y.W.; Bi, X.J.; Chen, D.; Chen, T.L.; Chen, W.Y.; Chen, X.; Chen, Y.; Cirennima; Cui, S.W.; et al. First Detection of sub-PeV Diffuse Gamma Rays from the Galactic Disk: Evidence for Ubiquitous Galactic Cosmic Rays beyond PeV Energies. *Phys. Rev. Lett.* **2021**, *126*, 141101. [CrossRef] [PubMed]
199. Cao, Z.; Aharonian, F.; An, Q.; Axikegu; Bai, Y.X.; Bao, Y.W.; Bastieri, D.; Bi, X.J.; Bi, Y.J.; Cai, J.T.; et al. The First LHAASO Catalog of Gamma-Ray Sources. *arXiv* **2023**, arXiv:2305.17030. [CrossRef]
200. Abeysekara, A.U.; Albert, A.; Alfaro, R.; Angeles Camacho, J.R.; Arteaga-Velázquez, J.C.; Arunbabu, K.P.; Avila Rojas, D.; Ayala Solares, H.A.; Baghmanyan, V.; Belmont-Moreno, E.; et al. Multiple Galactic Sources with Emission above 56 TeV Detected by HAWC. *Phys. Rev. Lett.* **2020**, *124*, 021102. [CrossRef] [PubMed]
201. Blumenthal, G.R.; Gould, R.J. Bremsstrahlung, Synchrotron Radiation, and Compton Scattering of High-Energy Electrons Traversing Dilute Gases. *Rev. Mod. Phys.* **1970**, *42*, 237–271. [CrossRef]
202. Breuhaus, M.; Hahn, J.; Romoli, C.; Reville, B.; Giacinti, G.; Tuffs, R.; Hinton, J.A. Ultra-high Energy Inverse Compton Emission from Galactic Electron Accelerators. *Astrophys. J. Lett.* **2021**, *908*, L49. [CrossRef]
203. Amenomori, M. et al. [Tibet ASγ Collaboration] Potential PeVatron supernova remnant G106.3+2.7 seen in the highest-energy gamma rays. *Nat. Astron.* **2021**, *5*, 460–464. [CrossRef]
204. Abe, H. et al. [MAGIC Collaboration] MAGIC observations provide compelling evidence of hadronic multi-TeV emission from the putative PeVatron SNR G106.3+2.7. *Astropart. Phys.* **2023**, *671*, A12. [CrossRef]
205. de la Fuente, E.; Toledano-Juarez, I.; Kawata, K.; Trinidad, M.A.; Tafoya, D.; Sano, H.; Tokuda, K.; Nishimura, A.; Onishi, T.; Sako, T.; et al. Detection of a new molecular cloud in the LHAASO J2108+5157 region supporting a hadronic PeVatron scenario. *Publ. Astron. Soc. Jpn.* **2023**, *75*, 546–566. [CrossRef]
206. de la Fuente, E.; Toledano-Juárez, I.; Kawata, K.; Trinidad, M.A.; Yamagishi, M.; Takekawa, S.; Tafoya, D.; Ohnishi, M.; Nishimura, A.; Kato, S.; et al. Evidence for a gamma-ray molecular target in the enigmatic PeVatron candidate LHAASO J2108+5157. *arXiv* **2023**, arXiv:2306.11921. [CrossRef]
207. Abe, S.; Aguasca-Cabot, A.; Agudo, I.; Alvarez Crespo, N.; Antonelli, L.A.; Aramo, C.; Arbet-Engels, A.; Artero, M.; Asano, K.; Aubert, P.; et al. Multiwavelength study of the galactic PeVatron candidate LHAASO J2108+5157. *Astropart. Phys.* **2023**, *673*, A75. [CrossRef]
208. De Sarkar, A. Supernova connection of unidentified ultra-high-energy gamma-ray source LHAASO J2108+5157. *Mon. Not. R. Astron. Soc.* **2023**, *521*, L5–L10. [CrossRef]
209. Albert, A.; Alfaro, R.; Ashkar, H.; Alvarez, C.; Álvarez, J.; Arteaga-Velázquez, J.C.; Ayala Solares, H.A.; Arceo, R.; Bellido, J.A.; BenZvi, S.; et al. Science Case for a Wide Field-of-View Very-High-Energy Gamma-Ray Observatory in the Southern Hemisphere. *arXiv* **2019**, arXiv:1902.08429. [CrossRef]

210. Atoyan, A.M.; Aharonian, F.A. On the mechanisms of gamma radiation in the Crab Nebula. *Mon. Not. R. Astron. Soc.* **1996**, *278*, 525–541. [CrossRef]
211. Sudoh, T.; Beacom, J.F. Where are Milky Way's hadronic PeVatrons? *Phys. Rev. D* **2023**, *107*, 043002. [CrossRef]
212. Scannapieco, E.; Madau, P.; Woosley, S.; Heger, A.; Ferrara, A. The Detectability of Pair-Production Supernovae at z $\lesssim$ 6. *Astrophys. J.* **2005**, *633*, 1031–1041. [CrossRef]
213. Cristofari, P.; Renaud, M.; Marcowith, A.; Dwarkadas, V.V.; Tatischeff, V. Time-dependent high-energy gamma-ray signal from accelerated particles in core-collapse supernovae: The case of SN 1993J. *Mon. Not. R. Astron. Soc.* **2020**, *494*, 2760–2765. [CrossRef]
214. Cristofari, P.; Marcowith, A.; Renaud, M.; Dwarkadas, V.V.; Tatischeff, V.; Giacinti, G.; Peretti, E.; Sol, H. The first days of Type II-P core collapse supernovae in the gamma-ray range. *Mon. Not. R. Astron. Soc.* **2022**, *511*, 3321–3329. [CrossRef]
215. Thomas, T.; Pfrommer, C.; Pakmor, R. Cosmic-ray-driven galactic winds: Transport modes of cosmic rays and Alfvén-wave dark regions. *Mon. Not. R. Astron. Soc.* **2023**, *521*, 3023–3042. [CrossRef]
216. Armillotta, L.; Ostriker, E.C.; Jiang, Y.F. Cosmic-Ray Transport in Simulations of Star-forming Galactic Disks. *Astrophys. J.* **2021**, *922*, 11. [CrossRef]
217. Xu, S.; Lazarian, A. Cosmic Ray Streaming in the Turbulent Interstellar Medium. *Astrophys. J.* **2022**, *927*, 94. [CrossRef]
218. Cesarsky, C.J.; Volk, H.J. Cosmic Ray Penetration into Molecular Clouds. *Astropart. Phys.* **1978**, *70*, 367.
219. Kulsrud, R.; Pearce, W.P. The Effect of Wave-Particle Interactions on the Propagation of Cosmic Rays. *Astrophys. J.* **1969**, *156*, 445. [CrossRef]
220. Zweibel, E.G.; Shull, J.M. Confinement of cosmic rays in molecular clouds. *Astrophys. J.* **1982**, *259*, 859–868. [CrossRef]
221. Yang, R.Z.; Li, G.X.; Wilhelmi, E.d.O.; Cui, Y.D.; Liu, B.; Aharonian, F. Effective shielding of $\lesssim$10 GeV cosmic rays from dense molecular clumps. *Nat. Astron.* **2023**, *7*, 351 . [CrossRef]
222. Hill, A.S.; Mac Low, M.M.; Gatto, A.; Ibáñez-Mejía, J.C. Effect of the Heating Rate on the Stability of the Three-phase Interstellar Medium. *Astrophys. J.* **2018**, *862*, 55. [CrossRef]
223. Owen, E.R.; Wu, K.; Jin, X.; Surajbali, P.; Kataoka, N. Starburst and post-starburst high-redshift protogalaxies. The feedback impact of high energy cosmic rays. *Astropart. Phys.* **2019**, *626*, A85. [CrossRef]
224. Walker, M.A. Heating of the Warm Ionized Medium by Low-energy Cosmic Rays. *Astrophys. J.* **2016**, *818*, 23. [CrossRef]
225. Minter, A.H.; Spangler, S.R. Heating of the Interstellar Diffuse Ionized Gas via the Dissipation of Turbulence. *Astrophys. J.* **1997**, *485*, 182–194. [CrossRef]
226. Wiener, J.; Zweibel, E.G.; Oh, S.P. Cosmic Ray Heating of the Warm Ionized Medium. *Astrophys. J.* **2013**, *767*, 87. [CrossRef]
227. Wentzel, D.G. Acceleration and Heating of Interstellar Gas by Cosmic Rays. *Astrophys. J.* **1971**, *163*, 503. [CrossRef]
228. Rathjen, T.E.; Naab, T.; Girichidis, P.; Walch, S.; Wünsch, R.; Dinnbier, F.; Seifried, D.; Klessen, R.S.; Glover, S.C.O. SILCC VI—Multiphase ISM structure, stellar clustering, and outflows with supernovae, stellar winds, ionizing radiation, and cosmic rays. *Mon. Not. R. Astron. Soc.* **2021**, *504*, 1039–1061. [CrossRef]
229. Owen, E.R.; On, A.Y.L.; Lai, S.P.; Wu, K. Observational Signatures of Cosmic-Ray Interactions in Molecular Clouds. *Astrophys. J.* **2021**, *913*, 52. [CrossRef]
230. Papadopoulos, P.P.; Thi, W.F.; Miniati, F.; Viti, S. Extreme cosmic ray dominated regions: A new paradigm for high star formation density events in the Universe. *Mon. Not. R. Astron. Soc.* **2011**, *414*, 1705–1714. [CrossRef]
231. Semenov, V.A.; Kravtsov, A.V.; Caprioli, D. Cosmic-Ray Diffusion Suppression in Star-forming Regions Inhibits Clump Formation in Gas-rich Galaxies. *Astrophys. J.* **2021**, *910*, 126. [CrossRef]
232. Farcy, M.; Rosdahl, J.; Dubois, Y.; Blaizot, J.; Martin-Alvarez, S. Radiation-magnetohydrodynamics simulations of cosmic ray feedback in disc galaxies. *Mon. Not. R. Astron. Soc.* **2022**, *513*, 5000–5019. [CrossRef]
233. Bustard, C.; Zweibel, E.G. Cosmic-Ray Transport, Energy Loss, and Influence in the Multiphase Interstellar Medium. *Astrophys. J.* **2021**, *913*, 106. [CrossRef]
234. Wiener, J.; Oh, S.P.; Zweibel, E.G. Interaction of cosmic rays with cold clouds in galactic haloes. *Mon. Not. R. Astron. Soc.* **2017**, *467*, 646–660. [CrossRef]
235. Wiener, J.; Zweibel, E.G.; Ruszkowski, M. Cosmic ray acceleration of cool clouds in the circumgalactic medium. *Mon. Not. R. Astron. Soc.* **2019**, *489*, 205–223. [CrossRef]
236. Brüggen, M.; Scannapieco, E. The Launching of Cold Clouds by Galaxy Outflows. IV. Cosmic-Ray-driven Acceleration. *Astrophys. J.* **2020**, *905*, 19. [CrossRef]
237. Heintz, E.; Bustard, C.; Zweibel, E.G. The Role of the Parker Instability in Structuring the Interstellar Medium. *Astrophys. J.* **2020**, *891*, 157. [CrossRef]
238. Heintz, E.; Zweibel, E.G. The Parker Instability with Cosmic-Ray Streaming. *Astrophys. J.* **2018**, *860*, 97. [CrossRef]
239. Protheroe, R.J.; Ott, J.; Ekers, R.D.; Jones, D.I.; Crocker, R.M. Interpretation of radio continuum and molecular line observations of Sgr B2: Free-free and synchrotron emission, and implications for cosmic rays. *Mon. Not. R. Astron. Soc.* **2008**, *390*, 683–692. [CrossRef]
240. Dogiel, V.A.; Chernyshov, D.O.; Kiselev, A.M.; Nobukawa, M.; Cheng, K.S.; Hui, C.Y.; Ko, C.M.; Nobukawa, K.K.; Tsuru, T.G. Spectrum of Relativistic and Subrelativistic Cosmic Rays in the 100 pc Central Region. *Astrophys. J.* **2015**, *809*, 48. [CrossRef]
241. Ivlev, A.V.; Dogiel, V.A.; Chernyshov, D.O.; Caselli, P.; Ko, C.M.; Cheng, K.S. Penetration of Cosmic Rays into Dense Molecular Clouds: Role of Diffuse Envelopes. *Astrophys. J.* **2018**, *855*, 23. [CrossRef]
242. Everett, J.E.; Zweibel, E.G. The Interaction of Cosmic Rays with Diffuse Clouds. *Astrophys. J.* **2011**, *739*, 60. [CrossRef]

243. Skilling, J.; Strong, A.W. Cosmic ray exclusion from dense molecular clouds. *Astropart. Phys.* **1976**, *53*, 253–258.
244. Silsbee, K.; Ivlev, A.V. Exclusion of Cosmic Rays from Molecular Clouds by Self-generated Electric Fields. *Astrophys. J. Lett.* **2020**, *902*, L25. [CrossRef]
245. Ko, C.M. A note on the hydrodynamical description of cosmic ray propagation. *Astropart. Phys.* **1992**, *259*, 377–381.
246. Padoan, P.; Scalo, J. Confinement-driven Spatial Variations in the Cosmic-Ray Flux. *Astrophys. J. Lett.* **2005**, *624*, L97–L100. [CrossRef]
247. Chandran, B.D.G. Confinement and Isotropization of Galactic Cosmic Rays by Molecular-Cloud Magnetic Mirrors When Turbulent Scattering Is Weak. *Astrophys. J.* **2000**, *529*, 513–535. [CrossRef]
248. Desch, S.J.; Connolly, H.C.J.; Srinivasan, G. An Interstellar Origin for the Beryllium 10 in Calcium-rich, Aluminum-rich Inclusions. *Astrophys. J.* **2004**, *602*, 528–542. [CrossRef]
249. Owen, E.R.; Lee, K.G.; Kong, A.K.H. Characterizing the signatures of star-forming galaxies in the extragalactic γ-ray background. *Mon. Not. R. Astron. Soc.* **2021**, *506*, 52–72. [CrossRef]
250. Silsbee, K.; Ivlev, A.V.; Padovani, M.; Caselli, P. Magnetic Mirroring and Focusing of Cosmic Rays. *Astrophys. J.* **2018**, *863*, 188. [CrossRef]
251. Albertsson, T.; Kauffmann, J.; Menten, K.M. Atlas of Cosmic-Ray-induced Astrochemistry. *Astrophys. J.* **2018**, *868*, 40. [CrossRef]
252. Li, G.X.; Burkert, A. Quantifying the interplay between gravity and magnetic field in molecular clouds—A possible multiscale energy equipartition in NGC 6334. *Mon. Not. R. Astron. Soc.* **2018**, *474*, 2167–2172. [CrossRef]
253. Padovani, M.; Ivlev, A.V.; Galli, D.; Caselli, P. Cosmic-ray ionisation in circumstellar discs. *Astropart. Phys.* **2018**, *614*, A111. [CrossRef]
254. Phan, V.H.M.; Morlino, G.; Gabici, S. What causes the ionization rates observed in diffuse molecular clouds? The role of cosmic ray protons and electrons. *Mon. Not. R. Astron. Soc.* **2018**, *480*, 5167–5174. [CrossRef]
255. Morlino, G.; Gabici, S. Cosmic ray penetration in diffuse clouds. *Mon. Not. R. Astron. Soc.* **2015**, *451*, L100–L104. [CrossRef]
256. Dogiel, V.A.; Chernyshov, D.O.; Ivlev, A.V.; Malyshev, D.; Strong, A.W.; Cheng, K.S. Gamma-Ray Emission from Molecular Clouds Generated by Penetrating Cosmic Rays. *Astrophys. J.* **2018**, *868*, 114. [CrossRef]
257. Padovani, M.; Galli, D.; Glassgold, A.E. Cosmic-ray ionization of molecular clouds. *Astropart. Phys.* **2009**, *501*, 619–631. [CrossRef]
258. Gabici, S. Low-energy cosmic rays: Regulators of the dense interstellar medium. *Astron. Astrophys. Rev.* **2022**, *30*, 4. [CrossRef]
259. Oka, T.; Geballe, T.R.; Goto, M.; Usuda, T.; Benjamin.; McCall, J.; Indriolo, N. The Central 300 pc of the Galaxy Probed by Infrared Spectra of H3+ and CO. I. Predominance of Warm and Diffuse Gas and High H2 Ionization Rate. *Astrophys. J.* **2019**, *883*, 54. [CrossRef]
260. Indriolo, N. Absorption-line Observations of H_3^+ and CO in Sight Lines Toward the Vela and W28 Supernova Remnants. *Astrophys. J.* **2023**, *950*, 64. [CrossRef]
261. Le Petit, F.; Ruaud, M.; Bron, E.; Godard, B.; Roueff, E.; Languignon, D.; Le Bourlot, J. Physical conditions in the central molecular zone inferred by H_3^+. *Astropart. Phys.* **2016**, *585*, A105. [CrossRef]
262. Sabatini, G.; Bovino, S.; Redaelli, E. First ALMA maps of cosmic ray ionisation rate in high-mass star-forming regions. *arXiv* **2023**, arXiv:2304.00329. [CrossRef]
263. Schilke, P.; Neufeld, D.A.; Müller, H.S.P.; Comito, C.; Bergin, E.A.; Lis, D.C.; Gerin, M.; Black, J.H.; Wolfire, M.; Indriolo, N.; et al. Ubiquitous argonium (ArH^+) in the diffuse interstellar medium: A molecular tracer of almost purely atomic gas. *Astropart. Phys.* **2014**, *566*, A29. [CrossRef]
264. Jacob, A.M.; Menten, K.M.; Wyrowski, F.; Winkel, B.; Neufeld, D.A. Extending the view of ArH^+ chemistry in diffuse clouds. *Astropart. Phys.* **2020**, *643*, A91. [CrossRef]
265. Bialy, S.; Neufeld, D.; Wolfire, M.; Sternberg, A.; Burkhart, B. Chemical Abundances in a Turbulent Medium-H_2, OH^+, H_2O^+, ArH^+. *Astrophys. J.* **2019**, *885*, 109. [CrossRef]
266. Jacob, A.M.; Neufeld, D.A.; Schilke, P.; Wiesemeyer, H.; Kim, W.J.; Bialy, S.; Busch, M.; Elia, D.; Falgarone, E.; Gerin, M.; et al. HyGAL: Characterizing the Galactic Interstellar Medium with Observations of Hydrides and Other Small Molecules. I. Survey Description and a First Look Toward W3(OH), W3 IRS5. and NGC 7538 IRS1. *Astrophys. J.* **2022**, *930*, 141. [CrossRef]
267. Indriolo, N.; McCall, B.J. Investigating the Cosmic-Ray Ionization Rate in the Galactic Diffuse Interstellar Medium through Observations of H^+_3. *Astrophys. J.* **2012**, *745*, 91. [CrossRef]
268. Holdship, J.; Viti, S.; Jiménez-Serra, I.; Makrymallis, A.; Priestley, F. UCLCHEM: A Gas-grain Chemical Code for Clouds, Cores, and C-Shocks. *Astron. J.* **2017**, *154*, 38. [CrossRef]
269. Maret, S.; Bergin, E.A. Astrochem: Abundances of Chemical Species in the Interstellar Medium. Astrophysics Source Code Library, record ascl:1507.010. 2015.
270. Lin, S.J.; Pagani, L.; Lai, S.P.; Lefèvre, C.; Lique, F. Physical and chemical modeling of the starless core L 1512. *Astropart. Phys.* **2020**, *635*, A188. [CrossRef]
271. Indriolo, N.; Blake, G.A.; Goto, M.; Usuda, T.; Oka, T.; Geballe, T.R.; Fields, B.D.; McCall, B.J. Investigating the Cosmic-ray Ionization Rate Near the Supernova Remnant IC 443 through H^+_3 Observations. *Astrophys. J.* **2010**, *724*, 1357–1365. [CrossRef]
272. Ceccarelli, C.; Hily-Blant, P.; Montmerle, T.; Dubus, G.; Gallant, Y.; Fiasson, A. Supernova-enhanced Cosmic-Ray Ionization and Induced Chemistry in a Molecular Cloud of W51C. *Astrophys. J. Lett.* **2011**, *740*, L4. [CrossRef]
273. Owen, E. The secret agent of galaxy evolution. *Astron. Geophys.* **2023**, *64*, 1.29–1.35. [CrossRef]

274. Caselli, P.; Walmsley, C.M.; Terzieva, R.; Herbst, E. The Ionization Fraction in Dense Cloud Cores. *Astrophys. J.* **1998**, *499*, 234–249. [CrossRef]
275. Morales Ortiz, J.L.; Ceccarelli, C.; Lis, D.C.; Olmi, L.; Plume, R.; Schilke, P. Ionization toward the high-mass star-forming region NGC 6334 I. *Astropart. Phys.* **2014**, *563*, A127. [CrossRef]
276. Hezareh, T.; Houde, M.; McCoey, C.; Vastel, C.; Peng, R. Simultaneous Determination of the Cosmic Ray Ionization Rate and Fractional Ionization in DR 21(OH). *Astrophys. J.* **2008**, *684*, 1221–1227. [CrossRef]
277. van der Tak, F.F.S.; van Dishoeck, E.F. Limits on the cosmic-ray ionization rate toward massive young stars. *Astropart. Phys.* **2000**, *358*, L79–L82. [CrossRef]
278. de Boisanger, C.; Helmich, F.P.; van Dishoeck, E.F. The ionization fraction in dense clouds. *Astropart. Phys.* **1996**, *310*, 315–327. [CrossRef]
279. Redaelli, E.; Sipilä, O.; Padovani, M.; Caselli, P.; Galli, D.; Ivlev, A.V. The cosmic-ray ionisation rate in the pre-stellar core L1544. *Astropart. Phys.* **2021**, *656*, A109. [CrossRef]
280. Porras, A.J.; Federman, S.R.; Welty, D.E.; Ritchey, A.M. OH^+ in Diffuse Molecular Clouds. *Astrophys. J. Lett.* **2014**, *781*, L8. [CrossRef]
281. Indriolo, N.; Geballe, T.R.; Oka, T.; McCall, B.J. H^+_3 in Diffuse Interstellar Clouds: A Tracer for the Cosmic-Ray Ionization Rate. *Astrophys. J.* **2007**, *671*, 1736–1747. [CrossRef]
282. Indriolo, N.; Neufeld, D.A.; Gerin, M.; Schilke, P.; Benz, A.O.; Winkel, B.; Menten, K.M.; Chambers, E.T.; Black, J.H.; Bruderer, S.; et al. Herschel Survey of Galactic OH^+, H_2O^+, and H_3O^+: Probing the Molecular Hydrogen Fraction and Cosmic-Ray Ionization Rate. *Astrophys. J.* **2015**, *800*, 40. [CrossRef]
283. Bacalla, X.L.; Linnartz, H.; Cox, N.L.J.; Cami, J.; Roueff, E.; Smoker, J.V.; Farhang, A.; Bouwman, J.; Zhao, D. The EDIBLES survey. IV. Cosmic ray ionization rates in diffuse clouds from near-ultraviolet observations of interstellar OH^+. *Astropart. Phys.* **2019**, *622*, A31. [CrossRef]
284. Padovani, M.; Galli, D. Synchrotron emission in molecular cloud cores: The SKA view. *Astropart. Phys.* **2018**, *620*, L4. [CrossRef]
285. Padovani, M.; Bialy, S.; Galli, D.; Ivlev, A.V.; Grassi, T.; Scarlett, L.H.; Rehill, U.S.; Zammit, M.C.; Fursa, D.V.; Bray, I. Cosmic rays in molecular clouds probed by H_2 rovibrational lines. Perspectives for the James Webb Space Telescope. *Astropart. Phys.* **2022**, *658*, A189. [CrossRef]
286. Tatischeff, V.; Decourchelle, A.; Maurin, G. Nonthermal X-rays from low-energy cosmic rays: Application to the 6.4 keV line emission from the Arches cluster region. *Astropart. Phys.* **2012**, *546*, A88. [CrossRef]
287. Okon, H.; Imai, M.; Tanaka, T.; Uchida, H.; Tsuru, T.G. Probing cosmic rays with Fe Kα line structures generated by multiple ionization process. *Publ. Astron. Soc. Jpn.* **2020**, *72*, L7. [CrossRef]
288. Bialy, S. Cold clouds as cosmic-ray detectors. *Commun. Phys.* **2020**, *3*, 32. [CrossRef]
289. Bialy, S.; Belli, S.; Padovani, M. Constraining the cosmic-ray ionization rate and spectrum with NIR spectroscopy of dense clouds. A testbed for JWST. *Astropart. Phys.* **2022**, *658*, L13. [CrossRef]
290. Gaches, B.A.L.; Bialy, S.; Bisbas, T.G.; Padovani, M.; Seifried, D.; Walch, S. Cosmic-ray-induced H_2 line emission. Astrochemical modeling and implications for JWST observations. *Astropart. Phys.* **2022**, *664*, A150. [CrossRef]
291. Casanova, S.; Aharonian, F.A.; Fukui, Y.; Gabici, S.; Jones, D.I.; Kawamura, A.; Onishi, T.; Rowell, G.; Sano, H.; Torii, K.; et al. Molecular Clouds as Cosmic-Ray Barometers. *Publ. Astron. Soc. Jpn.* **2010**, *62*, 769. [CrossRef]
292. Cavasinni, V.; Grasso, D.; Maccione, L. TeV neutrinos from supernova remnants embedded in giant molecular clouds. *Astroparticle Physics* **2006**, *26*, 41–49. [CrossRef]
293. Banik, P.; Bhadra, A. An interacting molecular cloud scenario for production of gamma-rays and neutrinos from MAGIC J1835-069, and MAGIC J1837-073. *Eur. Phys. J. C* **2021**, *81*, 478. [CrossRef]
294. Sarmah, P.; Chakraborty, S.; Joshi, J.C. Probing LHAASO galactic PeVatrons through gamma-ray and neutrino correspondence. *Mon. Not. R. Astron. Soc.* **2023**, *521*, 1144–1151. [CrossRef]
295. Abbasi, R.; Ackermann, M.; Adams, J.; Aggarwal, N.; Aguilar, J.A.; Ahlers, M.; Alameddine, J.M.; Alves, A.A.; Amin, N.M.; Andeen, K.; et al. Searches for Neutrinos from Large High Altitude Air Shower Observatory Ultra-high-energy γ-Ray Sources Using the IceCube Neutrino Observatory. *Astrophys. J. Lett.* **2023**, *945*, L8. [CrossRef]
296. Voisin, F.J.; Rowell, G.P.; Burton, M.G.; Fukui, Y.; Sano, H.; Aharonian, F.; Maxted, N.; Braiding, C.; Blackwell, R.; Lau, J. Connecting the ISM to TeV PWNe and PWN candidates. *Pub. Astron. Soc. Aust.* **2019**, *36*, e014. [CrossRef]
297. Aharonian, F. et al. [H. E. S. S. Collaboration] HESS J1809−193: A halo of escaped electrons around a pulsar wind nebula? *arXiv* **2023**, arXiv:2302.13663. [CrossRef]
298. Crutcher, R.M. Magnetic Fields in Molecular Clouds. *Annu. Rev. Astron. Astrophys.* **2012**, *50*, 29–63. [CrossRef]
299. Rodríguez, L.F.; Zapata, L.A. Star Formation in the Massive "Starless" Infrared Dark Cloud G0.253+0.016. *Astrophys. J. Lett.* **2013**, *767*, L13. [CrossRef]
300. Jones, D.I. Prospects for Detection of Synchrotron Emission from Secondary Electrons and Positrons in Starless Cores: Application to G0.216+0.016. *Astrophys. J. Lett.* **2014**, *792*, L14. [CrossRef]
301. Zhang, J.; Hopkins, A.; Barnes, P.J.; Cagnes, M.; Yonekura, Y.; Fukui, Y. The Radio-FIR Correlation in the Milky Way. *Pub. Astron. Soc. Aust.* **2010**, *27*, 340–346. [CrossRef]
302. Filho, M.E.; Tabatabaei, F.S.; Sánchez Almeida, J.; Muñoz-Tuñón, C.; Elmegreen, B.G. Global correlations between the radio continuum, infrared, and CO emissions in dwarf galaxies. *Mon. Not. R. Astron. Soc.* **2019**, *484*, 543–561. [CrossRef]

303. Strong, A.W.; Dickinson, C.; Murphy, E.J. Synchrotron radiation from molecular clouds. *arXiv* **2014**, arXiv:1412.4500. [CrossRef]
304. Gabici, S.; Aharonian, F.A.; Casanova, S. Broad-band non-thermal emission from molecular clouds illuminated by cosmic rays from nearby supernova remnants. *Mon. Not. R. Astron. Soc.* **2009**, *396*, 1629–1639. [CrossRef]
305. Aharonian, F.; Peron, G.; Yang, R.; Casanova, S.; Zanin, R. Probing the sea of galactic cosmic rays with Fermi-LAT. *Phys. Rev. D* **2020**, *101*, 083018. [CrossRef]
306. Aharonian, F.A. Gamma Rays From Molecular Clouds. *Space Sci. Rev.* **2001**, *99*, 187–196. [CrossRef]
307. Abrahams, R.D.; Teachey, A.; Paglione, T.A.D. Calibrating Column Density Tracers with Gamma-Ray Observations of the ρ Ophiuchi Molecular Cloud. *Astrophys. J.* **2017**, *834*, 91. [CrossRef]
308. Peron, G.; Aharonian, F. Probing the galactic cosmic-ray density with current and future γ-ray instruments. *Astropart. Phys.* **2022**, *659*, A57. [CrossRef]
309. Neufeld, D.A.; Wolfire, M.G. The Cosmic-Ray Ionization Rate in the Galactic Disk, as Determined from Observations of Molecular Ions. *Astrophys. J.* **2017**, *845*, 163. [CrossRef]
310. Phan, V.H.M.; Recchia, S.; Mertsch, P.; Gabici, S. Stochasticity of cosmic rays from supernova remnants and the ionization rates in molecular clouds. *Phys. Rev. D* **2023**, *107*, 123006. [CrossRef]
311. Phan, V.H.M.; Schulze, F.; Mertsch, P.; Recchia, S.; Gabici, S. Stochastic Fluctuations of Low-Energy Cosmic Rays and the Interpretation of Voyager Data. *Phys. Rev. Lett.* **2021**, *127*, 141101. [CrossRef] [PubMed]
312. Huang, X.; Yuan, Q.; Fan, Y.Z. A GeV-TeV particle component and the barrier of cosmic-ray sea in the Central Molecular Zone. *Nat. Commun.* **2021**, *12*, 6169. [CrossRef]
313. Chernyshov, D.O.; Egorov, A.E.; Dogiel, V.A.; Ivlev, A.V. On a Possible Origin of the Gamma-ray Excess around the Galactic Center. *Symmetry* **2021**, *13*, 1432. [CrossRef]
314. Acero, F.; Ackermann, M.; Ajello, M.; Albert, A.; Baldini, L.; Ballet, J.; Barbiellini, G.; Bastieri, D.; Bellazzini, R.; Bissaldi, E.; et al. Development of the Model of Galactic Interstellar Emission for Standard Point-source Analysis of Fermi Large Area Telescope Data. *Astrophys. J. Suppl.* **2016**, *223*, 26. [CrossRef]
315. Guo, Y.Q.; Yuan, Q. Understanding the spectral hardenings and radial distribution of Galactic cosmic rays and Fermi diffuse γ rays with spatially-dependent propagation. *Phys. Rev. D* **2018**, *97*, 063008. [CrossRef]
316. Peron, G.; Aharonian, F.; Casanova, S.; Yang, R.; Zanin, R. Probing the Cosmic-Ray Density in the Inner Galaxy. *Astrophys. J. Lett.* **2021**, *907*, L11. [CrossRef]
317. Rogers, F.; Zhang, S.; Perez, K.; Clavel, M.; Taylor, A. New Constraints on Cosmic Particle Populations at the Galactic Center Using X-ray Observations of the Molecular Cloud Sagittarius B2. *Astrophys. J.* **2022**, *934*, 19. [CrossRef]
318. Yusef-Zadeh, F.; Law, C.; Wardle, M.; Wang, Q.D.; Fruscione, A.; Lang, C.C.; Cotera, A. Detection of X-ray Emission from the Arches Cluster near the Galactic Center. *Astrophys. J.* **2002**, *570*, 665–670. [CrossRef]
319. Wang, Q.D.; Dong, H.; Lang, C. The interplay between star formation and the nuclear environment of our Galaxy: Deep X-ray observations of the Galactic centre Arches and Quintuplet clusters. *Mon. Not. R. Astron. Soc.* **2006**, *371*, 38–54. [CrossRef]
320. Kuznetsova, E.; Krivonos, R.; Clavel, M.; Lutovinov, A.; Chernyshov, D.; Hong, J.; Mori, K.; Ponti, G.; Tomsick, J.; Zhang, S. Investigating the origin of the faint non-thermal emission of the Arches cluster using the 2015-2016 NuSTAR and XMM-Newton X-ray observations. *Mon. Not. R. Astron. Soc.* **2019**, *484*, 1627–1636. [CrossRef]
321. Clavel, M.; Soldi, S.; Terrier, R.; Tatischeff, V.; Maurin, G.; Ponti, G.; Goldwurm, A.; Decourchelle, A. Variation of the X-ray non-thermal emission in the Arches cloud. *Mon. Not. R. Astron. Soc.* **2014**, *443*, L129–L133. [CrossRef]
322. Krivonos, R.A.; Tomsick, J.A.; Bauer, F.E.; Baganoff, F.K.; Barriere, N.M.; Bodaghee, A.; Boggs, S.E.; Christensen, F.E.; Craig, W.W.; Grefenstette, B.W.; et al. First Hard X-ray Detection of the Non-thermal Emission around the Arches Cluster: Morphology and Spectral Studies with NuSTAR. *Astrophys. J.* **2014**, *781*, 107. [CrossRef]
323. Chernyshov, D.O.; Ko, C.M.; Krivonos, R.A.; Dogiel, V.A.; Cheng, K.S. Time Variability of Equivalent Width of 6.4 keV Line from the Arches Complex: Reflected X-rays or Charged Particles? *Astrophys. J.* **2018**, *863*, 85. [CrossRef]
324. Nobukawa, K.K.; Saji, S.; Hirayama, A.; Nobukawa, M.; Yamauchi, S.; Matsumoto, H.; Koyama, K. Measurement of Low-Energy Cosmic Rays via the Neutral Iron Line. *J. Phys. Conf. Ser.* **2019**, *1181*, 012040. [CrossRef]
325. Bergin, E.A.; Tafalla, M. Cold Dark Clouds: The Initial Conditions for Star Formation. *Annu. Rev. Astron. Astrophys.* **2007**, *45*, 339–396. [CrossRef]
326. Rodríguez, L.F.R. Molecular Clouds: Fragmentation, Modeling and Observations. In Proceedings of the The Cool Universe: Observing Cosmic Dawn, Valparaiso, Chile, 4–8 October 2004; Astronomical Society of the Pacific Conference Series; Lidman, C., Alloin, D., Eds.; Astronomical Society of the Pacific: San Francisco, CA, USA, 2005; Volume 344, p. 146.
327. Myers, P.C. Star Forming Molecular Clouds. In *Molecular Clouds and Star Formation*; Chi, Y., You, J., Eds., World Scientific Publishing Co Pte Ltd.: Singapore, 1995; p. 47.
328. Spitzer, L.J.; Tomasko, M.G. Heating of H i Regions by Energetic Particles. *Astrophys. J.* **1968**, *152*, 971. [CrossRef]
329. Goldsmith, P.F. Molecular Depletion and Thermal Balance in Dark Cloud Cores. *Astrophys. J.* **2001**, *557*, 736–746. [CrossRef]
330. Consolandi, C. Precision Measurement of the Proton Flux in Primary Cosmic Rays from 1 GV to 1.8 TV with the Alpha Magnetic Spectrometer on the International Space Station. *arXiv* **2016**, arXiv:1612.08562. [CrossRef]
331. Crutcher, R.M.; Wandelt, B.; Heiles, C.; Falgarone, E.; Troland, T.H. Magnetic Fields in Interstellar Clouds from Zeeman Observations: Inference of Total Field Strengths by Bayesian Analysis. *Astrophys. J.* **2010**, *725*, 466–479. [CrossRef]

332. Elmegreen, B.G. Magnetic diffusion and ionization fractions in dense molecular clouds: The role of charged grains. *Astrophys. J.* **1979**, *232*, 729–739. [CrossRef]
333. Bisbas, T.G.; van Dishoeck, E.F.; Papadopoulos, P.P.; Szűcs, L.; Bialy, S.; Zhang, Z.Y. Cosmic-ray Induced Destruction of CO in Star-forming Galaxies. *Astrophys. J.* **2017**, *839*, 90. [CrossRef]
334. Gaches, B.A.L.; Offner, S.S.R. Exploration of Cosmic-ray Acceleration in Protostellar Accretion Shocks and a Model for Ionization Rates in Embedded Protoclusters. *Astrophys. J.* **2018**, *861*, 87. [CrossRef]
335. Gong, M.; Ostriker, E.C.; Wolfire, M.G. A Simple and Accurate Network for Hydrogen and Carbon Chemistry in the Interstellar Medium. *Astrophys. J.* **2017**, *843*, 38. [CrossRef]
336. Pazianotto, M.T.; Pilling, S.; Quesada Molina, J.M.; Federico, C.A. Energy Deposition by Cosmic Rays in the Molecular Cloud Using GEANT4 Code and Voyager I Data. *Astrophys. J.* **2021**, *911*, 129. [CrossRef]
337. Pazianotto, M.T.; Pilling, S. Computational simulation of the bombardment of molecular clump by realistic cosmic ray field employing GEANT4 code. *Mon. Not. R. Astron. Soc.* **2023**, *518*, 1735–1743. [CrossRef]
338. Pilling, S.; Pazianotto, M.T.; de Souza, L.A.; Maciel do Nascimento, L. Realistic energy deposition and temperature heating in molecular clouds due to cosmic rays: A computation simulation with the GEANT4 code employing light particles and medium-mass and heavy ions. *Mon. Not. R. Astron. Soc.* **2022**, *509*, 6169–6178. [CrossRef]
339. Aharonian, F.A. Vary High and Ultra High Energy Gamma-Rays from Giant Molecular Clouds. *Astrophys. Space Sci.* **1991**, *180*, 305–320. [CrossRef]
340. Fujita, Y.; Nobukawa, K.K.; Sano, H. Intrusion of MeV-TeV Cosmic Rays into Molecular Clouds Studied by Ionization, the Neutral Iron Line, and Gamma Rays. *Astrophys. J.* **2021**, *908*, 136. [CrossRef]
341. Nobukawa, K.K.; Nobukawa, M.; Koyama, K.; Yamauchi, S.; Uchiyama, H.; Okon, H.; Tanaka, T.; Uchida, H.; Tsuru, T.G. Evidence for a Neutral Iron Line Generated by MeV Protons from Supernova Remnants Interacting with Molecular Clouds. *Astrophys. J.* **2018**, *854*, 87. [CrossRef]
342. Maxted, N.I.; Braiding, C.; Wong, G.F.; Rowell, G.P.; Burton, M.G.; Filipović, M.D.; Voisin, F.; Urošević, D.; Vukotić, B.; Pavlović, M.Z.; et al. Searching for an interstellar medium association for HESS J1534 - 571. *Mon. Not. R. Astron. Soc.* **2018**, *480*, 134–148. [CrossRef]
343. Okon, H.; Uchida, H.; Tanaka, T.; Matsumura, H.; Tsuru, T.G. The origin of recombining plasma and the detection of the Fe-K line in the supernova remnant W 28. *Publ. Astron. Soc. Jpn.* **2018**, *70*, 35. [CrossRef]
344. Saji, S.; Matsumoto, H.; Nobukawa, M.; Nobukawa, K.K.; Uchiyama, H.; Yamauchi, S.; Koyama, K. Discovery of 6.4 keV line and soft X-ray emissions from G323.7-1.0 with Suzaku. *Publ. Astron. Soc. Jpn.* **2018**, *70*, 23. [CrossRef]
345. Makino, K.; Fujita, Y.; Nobukawa, K.K.; Matsumoto, H.; Ohira, Y. Interaction between molecular clouds and MeV-TeV cosmic-ray protons escaped from supernova remnants. *Publ. Astron. Soc. Jpn.* **2019**, *71*, 78. [CrossRef]
346. Nobukawa, K.K.; Hirayama, A.; Shimaguchi, A.; Fujita, Y.; Nobukawa, M.; Yamauchi, S. Neutral iron line in the supernova remnant IC 443 and implications for MeV cosmic rays. *Publ. Astron. Soc. Jpn.* **2019**, *71*, 115. [CrossRef]
347. Shimaguchi, A.; Nobukawa, K.K.; Yamauchi, S.; Nobukawa, M.; Fujita, Y. Suzaku observations of Fe K-shell lines in the supernova remnant W 51 C and hard X-ray sources in the proximity. *Publ. Astron. Soc. Jpn.* **2022**, *74*, 656–663. [CrossRef]
348. Mitchell, A.M.W.; Rowell, G.P.; Celli, S.; Einecke, S. Using interstellar clouds to search for Galactic PeVatrons: Gamma-ray signatures from supernova remnants. *Mon. Not. R. Astron. Soc.* **2021**, *503*, 3522–3539. [CrossRef]
349. Hewitt, J.W.; Yusef-Zadeh, F.; Wardle, M. Correlation of Supernova Remnant Masers and Gamma-Ray Sources. *Astrophys. J. Lett.* **2009**, *706*, L270–L274. [CrossRef]
350. Voisin, F.; Rowell, G.; Burton, M.G.; Walsh, A.; Fukui, Y.; Aharonian, F. ISM gas studies towards the TeV PWN HESS J1825-137 and northern region. *Mon. Not. R. Astron. Soc.* **2016**, *458*, 2813–2835. [CrossRef]
351. Abdalla, H. et al. [H. E. S. S. Collaboration] The H.E.S.S. Galactic plane survey. *Astropart. Phys.* **2018**, *612*, A1. [CrossRef]
352. Sano, H.; Yoshiike, S.; Yamane, Y.; Hayashi, K.; Enokiya, R.; Tokuda, K.; Tachihara, K.; Rowell, G.; Filipović, M.D.; Fukui, Y. ALMA CO Observations of the Mixed-morphology Supernova Remnant W49B: Efficient Production of Recombining Plasma and Hadronic Gamma Rays via Shock-Cloud Interactions. *Astrophys. J.* **2021**, *919*, 123. [CrossRef]
353. Jacobs, H.; Mertsch, P.; Phan, V.H.M. Self-confinement of low-energy cosmic rays around supernova remnants. *J. Cosmol. Astropart. Phys.* **2022**, *2022*, 024. [CrossRef]
354. Fujii, M.S.; Portegies Zwart, S. The Formation and Dynamical Evolution of Young Star Clusters. *Astrophys. J.* **2016**, *817*, 4. [CrossRef]
355. Li, M.; Ostriker, J.P.; Cen, R.; Bryan, G.L.; Naab, T. Supernova Feedback and the Hot Gas Filling Fraction of the Interstellar Medium. *Astrophys. J.* **2015**, *814*, 4. [CrossRef]
356. Krumholz, M.R.; Crocker, R.M.; Xu, S.; Lazarian, A.; Rosevear, M.T.; Bedwell-Wilson, J. Cosmic ray transport in starburst galaxies. *Mon. Not. R. Astron. Soc.* **2020**, *493*, 2817–2833. [CrossRef]
357. Peng, F.K.; Xi, S.Q.; Wang, X.Y.; Zhi, Q.J.; Li, D. Comparative study of gamma-ray emission from molecular clouds and star-forming galaxies. *Astropart. Phys.* **2019**, *621*, A70. [CrossRef]
358. Eichmann, B.; Becker Tjus, J. The Radio-Gamma Correlation in Starburst Galaxies . *Astrophys. J.* **2016**, *821*, 87. [CrossRef]
359. Ajello, M.; Di Mauro, M.; Paliya, V.S.; Garrappa, S. The γ-Ray Emission of Star-forming Galaxies . *Astrophys. J.* **2020**, *894*, 88. [CrossRef]

360. Kauffmann, G.; Heckman, T.M.; Tremonti, C.; Brinchmann, J.; Charlot, S.; White, S.D.M.; Ridgway, S.E.; Brinkmann, J.; Fukugita, M.; Hall, P.B.; et al. The host galaxies of active galactic nuclei. *Mon. Not. R. Astron. Soc.* **2003**, *346*, 1055–1077. [CrossRef]
361. Schawinski, K.; Urry, C.M.; Virani, S.; Coppi, P.; Bamford, S.P.; Treister, E.; Lintott, C.J.; Sarzi, M.; Keel, W.C.; Kaviraj, S.; et al. Galaxy Zoo: The Fundamentally Different Co-Evolution of Supermassive Black Holes and Their Early- and Late-Type Host Galaxies. *Astrophys. J.* **2010**, *711*, 284–302. [CrossRef]
362. Wilson, A.S.; Ulvestad, J.S. A Radiative Bow Shock Wave (?) Driven by Nuclear Ejecta in a Seyfert Galaxy. *Astrophys. J.* **1987**, *319*, 105. [CrossRef]
363. Michiyama, T.; Inoue, Y.; Doi, A.; Khangulyan, D. ALMA Detection of Parsec-scale Blobs at the Head of a Kiloparsec-scale Jet in the Nearby Seyfert Galaxy NGC 1068. *Astrophys. J. Lett.* **2022**, *936*, L1. [CrossRef]
364. Tombesi, F.; Cappi, M.; Reeves, J.N.; Palumbo, G.G.C.; Yaqoob, T.; Braito, V.; Dadina, M. Evidence for ultra-fast outflows in radio-quiet AGNs. I. Detection and statistical incidence of Fe K-shell absorption lines. *Astropart. Phys.* **2010**, *521*, A57. [CrossRef]
365. Tombesi, F.; Cappi, M.; Reeves, J.N.; Braito, V. Evidence for ultrafast outflows in radio-quiet AGNs - III. Location and energetics. *Mon. Not. R. Astron. Soc.* **2012**, *422*, L1–L5. [CrossRef]
366. Gofford, J.; Reeves, J.N.; McLaughlin, D.E.; Braito, V.; Turner, T.J.; Tombesi, F.; Cappi, M. The Suzaku view of highly ionized outflows in AGN - II. Location, energetics and scalings with bolometric luminosity. *Mon. Not. R. Astron. Soc.* **2015**, *451*, 4169–4182. [CrossRef]
367. Wang, X.; Loeb, A. Probing the gaseous halo of galaxies through non-thermal emission from AGN-driven outflows. *Mon. Not. R. Astron. Soc.* **2015**, *453*, 837–848. [CrossRef]
368. Lamastra, A.; Fiore, F.; Guetta, D.; Antonelli, L.A.; Colafrancesco, S.; Menci, N.; Puccetti, S.; Stamerra, A.; Zappacosta, L. Galactic outflow driven by the active nucleus and the origin of the gamma-ray emission in NGC 1068. *Astropart. Phys.* **2016**, *596*, A68. [CrossRef]
369. Liu, R.Y.; Murase, K.; Inoue, S.; Ge, C.; Wang, X.Y. Can Winds Driven by Active Galactic Nuclei Account for the Extragalactic Gamma-Ray and Neutrino Backgrounds? *Astrophys. J.* **2018**, *858*, 9. [CrossRef]
370. Inoue, S.; Cerruti, M.; Murase, K.; Liu, R.Y. High-energy neutrinos and gamma rays from winds and tori in active galactic nuclei. *arXiv* **2022**, arXiv:2207.02097. [CrossRef]
371. Peretti, E.; Lamastra, A.; Saturni, F.G.; Ahlers, M.; Blasi, P.; Morlino, G.; Cristofari, P. Diffusive shock acceleration at EeV and associated multimessenger flux from ultra-fast outflows driven by Active Galactic Nuclei. *arXiv* **2023**, arXiv:2301.13689. [CrossRef]
372. Kahler, S.W. Solar flares and coronal mass ejections. *Annu. Rev. Astron. Astrophys.* **1992**, *30*, 113–141. [CrossRef]
373. Cliver, E.W.; Schrijver, C.J.; Shibata, K.; Usoskin, I.G. Extreme solar events. *Living Rev. Sol. Phys.* **2022**, *19*, 2. [CrossRef]
374. Kazanas, D.; Ellison, D.C. The Central Engine of Quasars and Active Galactic Nuclei: Hadronic Interactions of Shock-accelerated Relativistic Protons. *Astrophys. J.* **1986**, *304*, 178. [CrossRef]
375. Zdziarski, A.A. On the Origin of the Infrared and X-ray Continua of Active Galactic Nuclei. *Astrophys. J.* **1986**, *305*, 45. [CrossRef]
376. Sikora, M.; Kirk, J.G.; Begelman, M.C.; Schneider, P. Electron Injection by Relativistic Protons in Active Galactic Nuclei. *Astrophys. J. Lett.* **1987**, *320*, L81. [CrossRef]
377. Begelman, M.C.; Rudak, B.; Sikora, M. Consequences of Relativistic Proton Injection in Active Galactic Nuclei. *Astrophys. J.* **1990**, *362*, 38. [CrossRef]
378. Stecker, F.W.; Done, C.; Salamon, M.H.; Sommers, P. Erratum: "High-energy neutrinos from active galactic nuclei" [Phys. Rev. Lett. 66. 2697 (1991)]. *Phys. Rev. Lett.* **1992**, *69*, 2738. [CrossRef]
379. Inoue, Y.; Khangulyan, D.; Inoue, S.; Doi, A. On High-energy Particles in Accretion Disk Coronae of Supermassive Black Holes: Implications for MeV Gamma-rays and High-energy Neutrinos from AGN Cores. *Astrophys. J.* **2019**, *880*, 40. [CrossRef]
380. Kimura, S.S.; Murase, K.; Toma, K. Neutrino and Cosmic-Ray Emission and Cumulative Background from Radiatively Inefficient Accretion Flows in Low-luminosity Active Galactic Nuclei. *Astrophys. J.* **2015**, *806*, 159. [CrossRef]
381. Abbasi, R. et al. [IceCube Collaboration]. Evidence for neutrino emission from the nearby active galaxy NGC 1068. *Science* **2022**, *378*, 538–543. [CrossRef] [PubMed]
382. Lenain, J.P.; Ricci, C.; Türler, M.; Dorner, D.; Walter, R. Seyfert 2 galaxies in the GeV band: Jets and starburst. *Astropart. Phys.* **2010**, *524*, A72. [CrossRef]
383. Ajello, M.; Atwood, W.B.; Baldini, L.; Ballet, J.; Barbiellini, G.; Bastieri, D.; Bellazzini, R.; Bissaldi, E.; Blandford, R.D.; Bloom, E.D.; et al. 3FHL: The Third Catalog of Hard Fermi-LAT Sources. *Astrophys. J. Suppl.* **2017**, *232*, 18. [CrossRef]
384. Abdollahi, S. et al. [The Fermi-LAT Collaboration]. Fermi Large Area Telescope Fourth Source Catalog. *arXiv* **2019**, arXiv:1902.10045.
385. Aartsen, M.G. et al. [IceCube Collaboration]. Time-integrated Neutrino Source Searches with 10 years of IceCube Data. *arXiv* **2019**, arXiv:1910.08488.
386. Inoue, Y.; Khangulyan, D.; Doi, A. On the Origin of High-energy Neutrinos from NGC 1068: The Role of Nonthermal Coronal Activity. *Astrophys. J. Lett.* **2020**, *891*, L33. [CrossRef]
387. Murase, K.; Kimura, S.S.; Mészáros, P. Hidden Cores of Active Galactic Nuclei as the Origin of Medium-Energy Neutrinos: Critical Tests with the MeV Gamma-Ray Connection. *Phys. Rev. Lett.* **2020**, *125*, 011101. [CrossRef]
388. Eichmann, B.; Oikonomou, F.; Salvatore, S.; Dettmar, R.J.; Tjus, J.B. Solving the Multimessenger Puzzle of the AGN-starburst Composite Galaxy NGC 1068. *Astrophys. J.* **2022**, *939*, 43. [CrossRef]

389. Michel, F.C. Cosmic-ray acceleration by pulsars. *Adv. Space Res.* **1984**, *4*, 387–391. [CrossRef]
390. Heyl, J.S.; Gill, R.; Hernquist, L. Cosmic rays from pulsars and magnetars. *Mon. Not. R. Astron. Soc.* **2010**, *406*, L25–L29. [CrossRef]
391. Fang, K.; Kotera, K.; Murase, K.; Olinto, A.V. Testing the newborn pulsar origin of ultrahigh energy cosmic rays with EeV neutrinos. *Phys. Rev. D* **2014**, *90*, 103005. [CrossRef]
392. Piro, A.L.; Kollmeier, J.A. Ultrahigh-energy Cosmic Rays from the "En Caul" Birth of Magnetars. *Astrophys. J.* **2016**, *826*, 97. [CrossRef]
393. Bowden, C.C.G.; Bradbury, S.M.; Chadwick, P.M.; Dickinson, J.E.; Dipper, N.A.; Edwards, P.J.; Lincoln, E.W.; McComb, T.J.L.; Orford, K.J.; Rayner, S.M.; et al. 350 GeV gamma rays from AE Aqr. *Astropart. Phys.* **1992**, *1*, 47–59. [CrossRef]
394. Li, J.; Torres, D.F.; Rea, N.; de Oña Wilhelmi, E.; Papitto, A.; Hou, X.; Mauche, C.W. Search for Gamma-Ray Emission from AE Aquarii with Seven Years of Fermi-LAT Observations. *Astrophys. J.* **2016**, *832*, 35. [CrossRef]
395. Meintjes, P.J.; Madzime, S.T.; Kaplan, Q.; van Heerden, H.J. Spun-Up Rotation-Powered Magnetized White Dwarfs in Close Binaries as Possible Gamma-ray Sources: Signatures of Pulsed Modulation from AE Aquarii and AR Scorpii in Fermi-LAT Data. *Galaxies* **2023**, *11*, 14. [CrossRef]
396. Cooper, A.J.; Gaggero, D.; Markoff, S.; Zhang, S. High-energy cosmic ray production in X-ray binary jets. *Mon. Not. R. Astron. Soc.* **2020**, *493*, 3212–3222. [CrossRef]
397. Linares, M.; Kachelrieß, M. Cosmic ray positrons from compact binary millisecond pulsars. *J. Cosmol. Astropart. Phys.* **2021**, *2021*, 030. [CrossRef]
398. Harding, A.K. The Emission Physics of Millisecond Pulsars. In *Astrophysics and Space Science Library*; Bhattacharyya, S., Papitto, A., Bhattacharya, D., Eds.; Springer: London, UK, 2022; Volume 465, pp. 57–85. [CrossRef]
399. Fabrika, S. The jets and supercritical accretion disk in SS433. *Astrophys. Space Phys. Res.* **2004**, *12*, 1–152. [CrossRef]
400. Cherepashchuk, A.M.; Belinski, A.A.; Dodin, A.V.; Postnov, K.A. Discovery of orbital eccentricity and evidence for orbital period increase of SS433. *Mon. Not. R. Astron. Soc.* **2021**, *507*, L19–L23. [CrossRef]
401. Hillwig, T.C.; Gies, D.R.; Huang, W.; McSwain, M.V.; Stark, M.A.; van der Meer, A.; Kaper, L. Identification of the Mass Donor Star's Spectrum in SS 433. *Astrophys. J.* **2004**, *615*, 422–431. [CrossRef]
402. Han, Q.; Li, X.D. On the Formation of SS433. *Astrophys. J.* **2020**, *896*, 34. [CrossRef]
403. Roberts, D.H.; Wardle, J.F.C.; Lipnick, S.L.; Selesnick, P.L.; Slutsky, S. Structure and Magnetic Fields in the Precessing Jet System SS 433. I. Multifrequency Imaging from 1998. *Astrophys. J.* **2008**, *676*, 584–593. [CrossRef]
404. Bowler, M.G.; Keppens, R. W 50 and SS 433. *Astropart. Phys.* **2018**, *617*, A29. [CrossRef]
405. Abeysekara, A.U.; Albert, A.; Alfaro, R.; Alvarez, C.; Álvarez, J.D.; Arceo, R.; Arteaga-Velázquez, J.C.; Avila Rojas, D.; Ayala Solares, H.A.; Belmont-Moreno, E.; et al. Very-high-energy particle acceleration powered by the jets of the microquasar SS 433. *Nature* **2018**, *562*, 82–85. [CrossRef]
406. Watson, M.G.; Willingale, R.; Grindlay, J.E.; Seward, F.D. The X-ray lobes of SS 433. *Astrophys. J.* **1983**, *273*, 688–696. [CrossRef]
407. Yamauchi, S.; Kawai, N.; Aoki, T. A Non-Thermal X-ray Spectrum from the Supernova Remnant W 50. *Publ. Astron. Soc. Jpn.* **1994**, *46*, L109–L113.
408. Brinkmann, W.; Aschenbach, B.; Kawai, N. ROSAT observations of the W 50/SS 433 system. *Astropart. Phys.* **1996**, *312*, 306–316.
409. Safi-Harb, S.; Ögelman, H. ROSAT and ASCA Observations of W50 Associated with the Peculiar Source SS 433. *Astrophys. J.* **1997**, *483*, 868–881. [CrossRef]
410. Safi-Harb, S.; Petre, R. Rossi X-ray Timing Explorer Observations of the Eastern Lobe of W50 Associated with SS 433. *Astrophys. J.* **1999**, *512*, 784–792. [CrossRef]
411. Kayama, K.; Tanaka, T.; Uchida, H.; Tsuru, T.G.; Sudoh, T.; Inoue, Y.; Khangulyan, D.; Tsuji, N.; Yamamoto, H. Spatially resolved study of the SS 433/W 50 west region with Chandra: X-ray structure and spectral variation of non-thermal emission. *Publ. Astron. Soc. Jpn.* **2022**, *74*, 1143–1156. [CrossRef]
412. Sudoh, T.; Inoue, Y.; Khangulyan, D. Multiwavelength Emission from Galactic Jets: The Case of the Microquasar SS433. *Astrophys. J.* **2020**, *889*, 146. [CrossRef]
413. Kimura, S.S.; Murase, K.; Mészáros, P. Deciphering the Origin of the GeV-TeV Gamma-Ray Emission from SS 433. *Astrophys. J.* **2020**, *904*, 188. [CrossRef]
414. Pakull, M.W.; Soria, R.; Motch, C. A 300-parsec-long jet-inflated bubble around a powerful microquasar in the galaxy NGC 7793. *Nature* **2010**, *466*, 209–212. [CrossRef]
415. Cseh, D.; Corbel, S.; Kaaret, P.; Lang, C.; Grisé, F.; Paragi, Z.; Tzioumis, A.; Tudose, V.; Feng, H. Black Hole Powered Nebulae and a Case Study of the Ultraluminous X-ray Source IC 342 X-1. *Astrophys. J.* **2012**, *749*, 17. [CrossRef]
416. Inoue, Y.; Lee, S.H.; Tanaka, Y.T.; Kobayashi, S.B. High energy gamma rays from nebulae associated with extragalactic microquasars and ultra-luminous X-ray sources. *Astropart. Phys.* **2017**, *90*, 14–19. [CrossRef]
417. Mason, K.O.; Cordova, F.A.; White, N.E. Simultaneous X-ray and Infrared Observations of Cygnus X-3. *Astrophys. J.* **1986**, *309*, 700. [CrossRef]
418. Stark, M.J.; Saia, M. Doppler Modulation of X-ray Lines in Cygnus X-3. *Astrophys. J. Lett.* **2003**, *587*, L101–L104. [CrossRef]
419. van Kerkwijk, M.H.; Geballe, T.R.; King, D.L.; van der Klis, M.; van Paradijs, J. The Wolf-Rayet counterpart of Cygnus X-3. *Astropart. Phys.* **1996**, *314*, 521–540. [CrossRef]

420. Lommen, D.; Yungelson, L.; van den Heuvel, E.; Nelemans, G.; Portegies Zwart, S. Cygnus X-3 and the problem of the missing Wolf-Rayet X-ray binaries. *Astropart. Phys.* **2005**, *443*, 231–241. [CrossRef]
421. Egron, E.; Pellizzoni, A.; Righini, S.; Giroletti, M.; Koljonen, K.; Pottschmidt, K.; Trushkin, S.; Lobina, J.; Pilia, M.; Wilms, J.; et al. Investigating the Mini and Giant Radio Flare Episodes of Cygnus X-3. *Astrophys. J.* **2021**, *906*, 10. [CrossRef]
422. Koljonen, K.I.I.; McCollough, M.L.; Hannikainen, D.C.; Droulans, R. 2006 May-July major radio flare episodes in Cygnus X-3: Spectrotiming analysis of the X-ray data. *Mon. Not. R. Astron. Soc.* **2013**, *429*, 1173–1188. [CrossRef]
423. Mioduszewski, A.J.; Rupen, M.P.; Hjellming, R.M.; Pooley, G.G.; Waltman, E.B. A One-sided Highly Relativistic Jet from Cygnus X-3. *Astrophys. J.* **2001**, *553*, 766–775. [CrossRef]
424. Tudose, V.; Miller-Jones, J.C.A.; Fender, R.P.; Paragi, Z.; Sakari, C.; Szostek, A.; Garrett, M.A.; Dhawan, V.; Rushton, A.; Spencer, R.E.; et al. Probing the behaviour of the X-ray binary Cygnus X-3 with very long baseline radio interferometry. *Mon. Not. R. Astron. Soc.* **2010**, *401*, 890–900. [CrossRef]
425. Abdo, A. et al. [Fermi LAT Collaboration]. Modulated High-Energy Gamma-Ray Emission from the Microquasar Cygnus X-3. *Science* **2009**, *326*, 1512. [CrossRef]
426. Tavani, M.; Bulgarelli, A.; Piano, G.; Sabatini, S.; Striani, E.; Evangelista, Y.; Trois, A.; Pooley, G.; Trushkin, S.; Nizhelskij, N.A.; et al. Extreme particle acceleration in the microquasar CygnusX-3. *Nature* **2009**, *462*, 620–623. [CrossRef]
427. Dubus, G.; Cerutti, B.; Henri, G. The relativistic jet of Cygnus X-3 in gamma-rays. *Mon. Not. R. Astron. Soc.* **2010**, *404*, L55–L59. [CrossRef]
428. Susa, H.; Hasegawa, K.; Tominaga, N. The Mass Spectrum of the First Stars. *Astrophys. J.* **2014**, *792*, 32. [CrossRef]
429. Chantavat, T.; Chongchitnan, S.; Silk, J. The most massive Population III stars. *Mon. Not. R. Astron. Soc.* **2023**, *522*, 3256–3262. [CrossRef]
430. Haemmerlé, L.; Woods, T.E.; Klessen, R.S.; Heger, A.; Whalen, D.J. The evolution of supermassive Population III stars. *Mon. Not. R. Astron. Soc.* **2018**, *474*, 2757–2773. [CrossRef]
431. Moriya, T.J.; Wong, K.C.; Koyama, Y.; Tanaka, M.; Oguri, M.; Hilbert, S.; Nomoto, K. Searches for Population III pair-instability supernovae: Predictions for ULTIMATE-Subaru and WFIRST. *Publ. Astron. Soc. Jpn.* **2019**, *71*, 59. [CrossRef]
432. Sotomayor Checa, P.; Romero, G.E. Model for Population III microquasars. *Astropart. Phys.* **2019**, *629*, A76. [CrossRef]
433. Verbunt, F.; Zwaan, C. Magnetic braking in low-mass X-ray binaries. *Astropart. Phys.* **1981**, *100*, L7–L9.
434. Eggleton, P.P. Aproximations to the radii of Roche lobes. *Astrophys. J.* **1983**, *268*, 368–369. [CrossRef]
435. Bhattacharya, D.; van den Heuvel, E.P.J. Formation and evolution of binary and millisecond radio pulsars. *Phys. Rep.* **1991**, *203*, 1–124. [CrossRef]
436. Postnov, K.A.; Yungelson, L.R. The Evolution of Compact Binary Star Systems. *Living Rev. Relativ.* **2014**, *17*, 3. [CrossRef] [PubMed]
437. Romero, G.E.; Vila, G.S. The proton low-mass microquasar: High-energy emission. *Astropart. Phys.* **2008**, *485*, 623–631. [CrossRef]
438. Smponias, T. Synthetic Neutrino Imaging of a Microquasar. *Galaxies* **2021**, *9*, 80. [CrossRef]
439. Mücke, A.; Protheroe, R.J. A proton synchrotron blazar model for flaring in Markarian 501. *Astropart. Phys.* **2001**, *15*, 121–136. [CrossRef]
440. Reynoso, M.M.; Medina, M.C.; Romero, G.E. A lepto-hadronic model for high-energy emission from FR I radiogalaxies. *Astropart. Phys.* **2011**, *531*, A30. [CrossRef]
441. Carulli, A.M.; Reynoso, M.M.; Romero, G.E. Neutrino production in Population III microquasars. *Astropart. Phys.* **2021**, *128*, 102557. [CrossRef]
442. Tibaldo, L.; Gaggero, D.; Martin, P. Gamma Rays as Probes of Cosmic-Ray Propagation and Interactions in Galaxies. *Universe* **2021**, *7*, 141. [CrossRef]
443. Tsuboi, M.; Handa, T.; Ukita, N. Dense Molecular Clouds in the Galactic Center Region. I. Observations and Data. *Astrophys. J. Suppl.* **1999**, *120*, 1–39. [CrossRef]
444. Molinari, S.; Bally, J.; Noriega-Crespo, A.; Compiègne, M.; Bernard, J.P.; Paradis, D.; Martin, P.; Testi, L.; Barlow, M.; Moore, T.; et al. A 100 pc Elliptical and Twisted Ring of Cold and Dense Molecular Clouds Revealed by Herschel Around the Galactic Center. *Astrophys. J. Lett.* **2011**, *735*, L33. [CrossRef]
445. Yusef-Zadeh, F.; Hewitt, J.W.; Wardle, M.; Tatischeff, V.; Roberts, D.A.; Cotton, W.; Uchiyama, H.; Nobukawa, M.; Tsuru, T.G.; Heinke, C.; et al. Interacting Cosmic Rays with Molecular Clouds: A Bremsstrahlung Origin of Diffuse High-energy Emission from the Inner 2°×1° of the Galactic Center. *Astrophys. J.* **2013**, *762*, 33. [CrossRef]
446. Yoast-Hull, T.M.; Gallagher, J.S., III; Zweibel, E.G. The Cosmic-Ray Population of the Galactic Central Molecular Zone. *Astrophys. J.* **2014**, *790*, 86. [CrossRef]
447. Crocker, R.M.; Jones, D.I.; Melia, F.; Ott, J.; Protheroe, R.J. A lower limit of 50 microgauss for the magnetic field near the Galactic Centre. *Nature* **2010**, *463*, 65–67. [CrossRef]
448. Calore, F.; Di Mauro, M.; Donato, F.; Hessels, J.W.T.; Weniger, C. Radio Detection Prospects for a Bulge Population of Millisecond Pulsars as Suggested by Fermi-LAT Observations of the Inner Galaxy. *Astrophys. J.* **2016**, *827*, 143. [CrossRef]
449. Ackermann, M.; Albert, A.; Atwood, W.B.; Baldini, L.; Ballet, J.; Barbiellini, G.; Bastieri, D.; Bellazzini, R.; Bissaldi, E.; Blandford, R.D.; et al. The Spectrum and Morphology of the Fermi Bubbles. *Astrophys. J.* **2014**, *793*, 64. [CrossRef]
450. Yang, H.Y.; Ruszkowski, M.; Zweibel, E. Unveiling the Origin of the Fermi Bubbles. *Galaxies* **2018**, *6*, 29. [CrossRef]
451. Yang, H.Y.K.; Ruszkowski, M.; Zweibel, E. Unveiling the Origin of the Fermi/eRosita Bubbles. *PoS* **2023**, *ECRS*, 023. [CrossRef]

452. Crocker, R.M. Non-thermal insights on mass and energy flows through the Galactic Centre and into the Fermi bubbles. *Mon. Not. R. Astron. Soc.* **2012**, *423*, 3512–3539. [CrossRef]
453. Razzaque, S.; Yang, L. Hadronic Models of the Fermi Bubbles: Future Perspectives. *Galaxies* **2018**, *6*, 47. [CrossRef]
454. Yang, H.Y.K.; Ruszkowski, M.; Ricker, P.M.; Zweibel, E.; Lee, D. The Fermi Bubbles: Supersonic Active Galactic Nucleus Jets with Anisotropic Cosmic-Ray Diffusion. *Astrophys. J.* **2012**, *761*, 185. [CrossRef]
455. Su, M.; Slatyer, T.R.; Finkbeiner, D.P. Giant Gamma-ray Bubbles from Fermi-LAT: Active Galactic Nucleus Activity or Bipolar Galactic Wind? *Astrophys. J.* **2010**, *724*, 1044–1082. [CrossRef]
456. Zubovas, K.; King, A.R.; Nayakshin, S. The Milky Way's Fermi bubbles: Echoes of the last quasar outburst? *Mon. Not. R. Astron. Soc.* **2011**, *415*, L21–L25. [CrossRef]
457. Tourmente, O.; Rodgers-Lee, D.; Taylor, A.M. A galactic breeze origin for the Fermi bubbles emission. *Mon. Not. R. Astron. Soc.* **2023**, *518*, 6083–6091. [CrossRef]
458. Taylor, A.M.; Giacinti, G. Cosmic rays in a galactic breeze. *Phys. Rev. D* **2017**, *95*, 023001. [CrossRef]
459. Guo, F.; Mathews, W.G. The Fermi Bubbles. I. Possible Evidence for Recent AGN Jet Activity in the Galaxy. *Astrophys. J.* **2012**, *756*, 181. [CrossRef]
460. Yang, H.Y.K.; Ruszkowski, M.; Zweibel, E. The Fermi bubbles: Gamma-ray, microwave and polarization signatures of leptonic AGN jets. *Mon. Not. R. Astron. Soc.* **2013**, *436*, 2734–2746. [CrossRef]
461. Yang, H.Y.K.; Ruszkowski, M. The Spatially Uniform Spectrum of the Fermi Bubbles: The Leptonic Active Galactic Nucleus Jet Scenario. *Astrophys. J.* **2017**, *850*, 2. [CrossRef]
462. Yang, H.Y.K.; Ruszkowski, M.; Zweibel, E.G. Fermi and eROSITA bubbles as relics of the past activity of the Galaxy's central black hole. *Nat. Astron.* **2022**, *6*, 584–591. [CrossRef]
463. Mulcahy, D.D.; Horneffer, A.; Beck, R.; Krause, M.; Schmidt, P.; Basu, A.; Chyży, K.T.; Dettmar, R.J.; Haverkorn, M.; Heald, G.; et al. Investigation of the cosmic ray population and magnetic field strength in the halo of NGC 891. *Astropart. Phys.* **2018**, *615*, A98. [CrossRef]
464. Butsky, I.S.; Quinn, T.R. The Role of Cosmic-ray Transport in Shaping the Simulated Circumgalactic Medium. *Astrophys. J.* **2018**, *868*, 108. [CrossRef]
465. Dashyan, G.; Dubois, Y. Cosmic ray feedback from supernovae in dwarf galaxies. *Astropart. Phys.* **2020**, *638*, A123. [CrossRef]
466. Ji, S.; Chan, T.K.; Hummels, C.B.; Hopkins, P.F.; Stern, J.; Kereš, D.; Quataert, E.; Faucher-Giguère, C.A.; Murray, N. Properties of the circumgalactic medium in cosmic ray-dominated galaxy haloes. *Mon. Not. R. Astron. Soc.* **2020**, *496*, 4221–4238. [CrossRef]
467. Recchia, S.; Gabici, S.; Aharonian, F.A.; Niro, V. Giant Cosmic-Ray Halos around M31 and the Milky Way. *Astrophys. J.* **2021**, *914*, 135. [CrossRef]
468. Pshirkov, M.S.; Vasiliev, V.V.; Postnov, K.A. Evidence of Fermi bubbles around M31. *Mon. Not. R. Astron. Soc.* **2016**, *459*, L76–L80. [CrossRef]
469. Roy, M.; Nath, B.B. Gamma-rays from the circumgalactic medium of M31. *Mon. Not. R. Astron. Soc.* **2022**, *514*, 1412–1421. [CrossRef]
470. Tibaldo, L.; Digel, S.W.; Casandjian, J.M.; Franckowiak, A.; Grenier, I.A.; Jóhannesson, G.; Marshall, D.J.; Moskalenko, I.V.; Negro, M.; Orlando, E.; et al. Fermi-LAT Observations of High- and Intermediate-velocity Clouds: Tracing Cosmic Rays in the Halo of the Milky Way. *Astrophys. J.* **2015**, *807*, 161. [CrossRef] [PubMed]
471. Subrahmanyan, R.; Cowsik, R. Is there an Unaccounted for Excess in the Extragalactic Cosmic Radio Background? *Astrophys. J.* **2013**, *776*, 42. [CrossRef]
472. Jana, R.; Roy, M.; Nath, B.B. Gamma-Ray and Radio Background Constraints on Cosmic Rays in Milky Way Circumgalactic Medium. *Astrophys. J. Lett.* **2020**, *903*, L9. [CrossRef]
473. Fixsen, D.J.; Kogut, A.; Levin, S.; Limon, M.; Lubin, P.; Mirel, P.; Seiffert, M.; Singal, J.; Wollack, E.; Villela, T.; et al. ARCADE 2 Measurement of the Absolute Sky Brightness at 3–90 GHz. *Astrophys. J.* **2011**, *734*, 5. [CrossRef]
474. Joubaud, T.; Grenier, I.A.; Casandjian, J.M.; Tolksdorf, T.; Schlickeiser, R. The cosmic-ray content of the Orion-Eridanus superbubble. *Astropart. Phys.* **2020**, *635*, A96. [CrossRef]
475. Feldmann, R.; Hooper, D.; Gnedin, N.Y. Circum-galactic Gas and the Isotropic Gamma-Ray Background. *Astrophys. J.* **2013**, *763*, 21. [CrossRef]
476. Blasi, P.; Amato, E. Escape of Cosmic Rays from the Galaxy and Effects on the Circumgalactic Medium. *Phys. Rev. Lett.* **2019**, *122*, 051101. [CrossRef]
477. Taylor, A.M.; Gabici, S.; Aharonian, F. Galactic halo origin of the neutrinos detected by IceCube. *Phys. Rev. D* **2014**, *89*, 103003. [CrossRef]
478. Kalashev, O.; Martynenko, N.; Troitsky, S. On the contribution of cosmic-ray interactions in the circumgalactic gas to the observed high-energy neutrino flux. *J. Cosmol. Astropart. Phys.* **2023**, *2023*, 053. [CrossRef]
479. Recchia, S.; Blasi, P.; Morlino, G. Cosmic ray driven Galactic winds. *Mon. Not. R. Astron. Soc.* **2016**, *462*, 4227–4239. [CrossRef]
480. Holguin, F.; Ruszkowski, M.; Lazarian, A.; Farber, R.; Yang, H.Y.K. Role of cosmic-ray streaming and turbulent damping in driving galactic winds. *Mon. Not. R. Astron. Soc.* **2019**, *490*, 1271–1282. [CrossRef]
481. Dogiel, V.A.; Ivlev, A.V.; Chernyshov, D.O.; Ko, C.M. Formation of the Cosmic-Ray Halo: Galactic Spectrum of Primary Cosmic Rays. *Astrophys. J.* **2020**, *903*, 135. [CrossRef]

482. Kempski, P.; Quataert, E. Reconciling cosmic ray transport theory with phenomenological models motivated by Milky-Way data. *Mon. Not. R. Astron. Soc.* **2022**, *514*, 657–674. [CrossRef]
483. Evoli, C.; Blasi, P.; Morlino, G.; Aloisio, R. Origin of the Cosmic Ray Galactic Halo Driven by Advected Turbulence and Self-Generated Waves. *Phys. Rev. Lett.* **2018**, *121*, 021102. [CrossRef]
484. Schober, J.; Schleicher, D.R.G.; Klessen, R.S. Magnetic field amplification in young galaxies. *Astropart. Phys.* **2013**, *560*, A87. [CrossRef]
485. Bernet, M.L.; Miniati, F.; Lilly, S.J.; Kronberg, P.P.; Dessauges-Zavadsky, M. Strong magnetic fields in normal galaxies at high redshift. *Nature* **2008**, *454*, 302–304. [CrossRef]
486. Hammond, A.M.; Robishaw, T.; Gaensler, B.M. A New Catalog of Faraday Rotation Measures and Redshifts for Extragalactic Radio Sources. *arXiv* **2012**, arXiv:1209.1438. [CrossRef]
487. Peng, F.K.; Wang, X.Y.; Liu, R.Y.; Tang, Q.W.; Wang, J.F. First Detection of GeV Emission from an Ultraluminous Infrared Galaxy: Arp 220 as Seen with the Fermi Large Area Telescope. *Astrophys. J. Lett.* **2016**, *821*, L20. [CrossRef]
488. Read, S.C.; Smith, D.J.B.; Gürkan, G.; Hardcastle, M.J.; Williams, W.L.; Best, P.N.; Brinks, E.; Calistro-Rivera, G.; ChyŻy, K.T.; Duncan, K.; et al. The Far-Infrared Radio Correlation at low radio frequency with LOFAR/H-ATLAS. *Mon. Not. R. Astron. Soc.* **2018**, *480*, 5625–5644. [CrossRef]
489. Ackermann, M.; Ajello, M.; Allafort, A.; Baldini, L.; Ballet, J.; Bastieri, D.; Bechtol, K.; Bellazzini, R.; Berenji, B.; Bloom, E.D.; et al. GeV Observations of Star-forming Galaxies with the Fermi Large Area Telescope. *Astrophys. J.* **2012**, *755*, 164. [CrossRef]
490. Sargent, M.T.; Schinnerer, E.; Murphy, E.; Carilli, C.L.; Helou, G.; Aussel, H.; Le Floc'h, E.; Frayer, D.T.; Ilbert, O.; Oesch, P.; et al. No Evolution in the IR-Radio Relation for IR-luminous Galaxies at z < 2 in the COSMOS Field. *Astrophys. J. Lett.* **2010**, *714*, L190–L195. [CrossRef]
491. Bourne, N.; Dunne, L.; Ivison, R.J.; Maddox, S.J.; Dickinson, M.; Frayer, D.T. Evolution of the far-infrared-radio correlation and infrared spectral energy distributions of massive galaxies over z = 0–2. *Mon. Not. R. Astron. Soc.* **2011**, *410*, 1155–1173. [CrossRef]
492. Murphy, E.J. The Far-Infrared-Radio Correlation at High Redshifts: Physical Considerations and Prospects for the Square Kilometer Array. *Astrophys. J.* **2009**, *706*, 482–496. [CrossRef]
493. Vollmer, B.; Gassmann, B.; Derrière, S.; Boch, T.; Louys, M.; Bonnarel, F.; Dubois, P.; Genova, F.; Ochsenbein, F. The SPECFIND V2.0 catalogue of radio cross-identifications and spectra. SPECFIND meets the Virtual Observatory. *Astropart. Phys.* **2010**, *511*, A53. [CrossRef]
494. Vollmer, B.; Davoust, E.; Dubois, P.; Genova, F.; Ochsenbein, F.; van Driel, W. A method for determining radio continuum spectra and its application to large surveys. *Astropart. Phys.* **2005**, *431*, 1177–1187. [CrossRef]
495. Vollmer, B.; Soida, M.; Dallant, J. Deciphering the radio-star formation correlation on kpc scales. II. The integrated infrared-radio continuum and star formation-radio continuum correlations. *Astropart. Phys.* **2022**, *667*, A30. [CrossRef]
496. Lisenfeld, U.; Voelk, H.J.; Xu, C. A quantitative model of the FIR/radio correlation for normal late-type galaxies. *Astropart. Phys.* **1996**, *306*, 677. [CrossRef]
497. Lisenfeld, U.; Völk, H.J. On the radio spectral index of galaxies. *Astropart. Phys.* **2000**, *354*, 423–430. [CrossRef]
498. Helou, G.; Bicay, M.D. A Physical Model of the Infrared-to-Radio Correlation in Galaxies. *Astrophys. J.* **1993**, *415*, 93. [CrossRef]
499. Niklas, S.; Beck, R. A new approach to the radio-far infrared correlation for non-calorimeter galaxies. *Astropart. Phys.* **1997**, *320*, 54–64.
500. Lacki, B.C.; Thompson, T.A.; Quataert, E. The Physics of the Far-infrared-Radio Correlation. I. Calorimetry, Conspiracy, and Implications. *Astrophys. J.* **2010**, *717*, 1–28. [CrossRef]
501. Pfrommer, C.; Werhahn, M.; Pakmor, R.; Girichidis, P.; Simpson, C.M. Simulating radio synchrotron emission in star-forming galaxies: Small-scale magnetic dynamo and the origin of the far-infrared-radio correlation. *Mon. Not. R. Astron. Soc.* **2022**, *515*, 4229–4264. [CrossRef]
502. Pfrommer, C.; Pakmor, R.; Simpson, C.M.; Springel, V. Simulating Gamma-Ray Emission in Star-forming Galaxies. *Astrophys. J. Lett.* **2017**, *847*, L13. [CrossRef]
503. Werhahn, M.; Pfrommer, C.; Girichidis, P.; Winner, G. Cosmic rays and non-thermal emission in simulated galaxies—II. γ-ray maps, spectra, and the far-infrared-γ-ray relation. *Mon. Not. R. Astron. Soc.* **2021**, *505*, 3295–3313. [CrossRef]
504. Werhahn, M.; Pfrommer, C.; Girichidis, P. Cosmic rays and non-thermal emission in simulated galaxies—III. Probing cosmic-ray calorimetry with radio spectra and the FIR-radio correlation. *Mon. Not. R. Astron. Soc.* **2021**, *508*, 4072–4095. [CrossRef]
505. Wang, X.; Fields, B.D. Are starburst galaxies proton calorimeters? *Mon. Not. R. Astron. Soc.* **2018**, *474*, 4073–4088. [CrossRef]
506. Zhang, Y.; Peng, F.K.; Wang, X.Y. Interpreting the Relation between the Gamma-Ray and Infrared Luminosities of Star-forming Galaxies. *Astrophys. J.* **2019**, *874*, 173. [CrossRef]
507. Strong, A.W.; Porter, T.A.; Digel, S.W.; Jóhannesson, G.; Martin, P.; Moskalenko, I.V.; Murphy, E.J.; Orlando, E. Global Cosmic-ray-related Luminosity and Energy Budget of the Milky Way. *Astrophys. J. Lett.* **2010**, *722*, L58–L63. [CrossRef]
508. Evoli, C.; Gaggero, D.; Grasso, D.; Maccione, L. Common Solution to the Cosmic Ray Anisotropy and Gradient Problems. *Phys. Rev. Lett.* **2012**, *108*, 211102. [CrossRef]
509. Casse, F.; Lemoine, M.; Pelletier, G. Transport of cosmic rays in chaotic magnetic fields. *Phys. Rev. D* **2001**, *65*, 023002. [CrossRef]
510. Pakmor, R.; Pfrommer, C.; Simpson, C.M.; Springel, V. Galactic Winds Driven by Isotropic and Anisotropic Cosmic-Ray Diffusion in Disk Galaxies. *Astrophys. J. Lett.* **2016**, *824*, L30. [CrossRef]

511. Wang, C.Y.; Lo, Y.Y.; Ko, C.M. MHD Simulations of Parker Instability Undergoing Cosmic-Ray Diffusion. *arXiv* **2010**, arXiv:1011.0162. [CrossRef]
512. Ruszkowski, M.; Yang, H.Y.K.; Zweibel, E. Global Simulations of Galactic Winds Including Cosmic-ray Streaming. *Astrophys. J.* **2017**, *834*, 208. [CrossRef]
513. Lopez-Rodriguez, E.; Mao, S.A.; Beck, R.; Borlaff, A.S.; Ntormousi, E.; Tassis, K.; Dale, D.A.; Roman-Duval, J.; Subramanian, K.; Martin-Alvarez, S.; et al. Extragalactic Magnetism with SOFIA (SALSA Legacy Program). IV. Program Overview and First Results on the Polarization Fraction. *Astrophys. J.* **2022**, *936*, 92. [CrossRef]
514. Pattle, K.; Gear, W.; Redman, M.; Smith, M.W.L.; Greaves, J. Submillimetre observations of the two-component magnetic field in M82. *Mon. Not. R. Astron. Soc.* **2021**, *505*, 684–688. [CrossRef]
515. Whitmore, B.C.; Chandar, R.; Schweizer, F.; Rothberg, B.; Leitherer, C.; Rieke, M.; Rieke, G.; Blair, W.P.; Mengel, S.; Alonso-Herrero, A. The Antennae Galaxies (NGC 4038/4039) Revisited: Advanced Camera for Surveys and NICMOS Observations of a Prototypical Merger. *Astron. J.* **2010**, *140*, 75–109. [CrossRef]
516. Lopez-Rodriguez, E.; Borlaff, A.S.; Beck, R.; Reach, W.T.; Mao, S.A.; Ntormousi, E.; Tassis, K.; Martin-Alvarez, S.; Clark, S.E.; Dale, D.A.; et al. Extragalactic Magnetism with SOFIA (SALSA Legacy Program): The Magnetic Fields in the Multiphase Interstellar Medium of the Antennae Galaxies. *Astrophys. J. Lett.* **2023**, *942*, L13. [CrossRef]
517. Fletcher, A.; Beck, R.; Shukurov, A.; Berkhuijsen, E.M.; Horellou, C. Magnetic fields and spiral arms in the galaxy M51. *Mon. Not. R. Astron. Soc.* **2011**, *412*, 2396–2416. [CrossRef]
518. Barnes, J.E.; Hernquist, L. Dynamics of interacting galaxies. *Annu. Rev. Astron. Astrophys.* **1992**, *30*, 705–742. [CrossRef]
519. Socrates, A.; Davis, S.W.; Ramirez-Ruiz, E. The Eddington Limit in Cosmic Rays: An Explanation for the Observed Faintness of Starbursting Galaxies. *Astrophys. J.* **2008**, *687*, 202–215. [CrossRef]
520. Crocker, R.M.; Krumholz, M.R.; Thompson, T.A. Cosmic rays across the star-forming galaxy sequence—I. Cosmic ray pressures and calorimetry. *Mon. Not. R. Astron. Soc.* **2021**, *502*, 1312–1333. [CrossRef]
521. Crocker, R.M.; Krumholz, M.R.; Thompson, T.A. Cosmic rays across the star-forming galaxy sequence—II. Stability limits and the onset of cosmic ray-driven outflows. *Mon. Not. R. Astron. Soc.* **2021**, *503*, 2651–2664. [CrossRef]
522. Huang, X.; Davis, S.W. The launching of cosmic ray-driven outflows. *Mon. Not. R. Astron. Soc.* **2022**, *511*, 5125–5141. [CrossRef]
523. Heintz, E.; Zweibel, E.G. Galaxies at a Cosmic Ray Eddington Limit. *Astrophys. J.* **2022**, *941*, 78. [CrossRef]
524. Abdo, A.A.; Ackermann, M.; Ajello, M.; Atwood, W.B.; Axelsson, M.; Baldini, L.; Ballet, J.; Barbiellini, G.; Bastieri, D.; Bechtol, K.; et al. Detection of Gamma-Ray Emission from the Starburst Galaxies M82 and NGC 253 with the Large Area Telescope on Fermi. *Astrophys. J. Lett.* **2010**, *709*, L152–L157. [CrossRef]
525. Xi, S.Q.; Zhang, H.M.; Liu, R.Y.; Wang, X.Y. GeV γ-Ray Emission from M33 and Arp 299. *Astrophys. J.* **2020**, *901*, 158. [CrossRef]
526. Xing, Y.; Wang, Z. Identifying the Gamma-ray Emission of the Nearby Galaxy M83. *arXiv* **2023**, arXiv:2304.00229. [CrossRef]
527. Acero, F.; Aharonian, F.; Akhperjanian, A.G.; Anton, G.; Barres de Almeida, U.; Bazer-Bachi, A.R.; Becherini, Y.; Behera, B.; Bernlöhr, K.; Bochow, A.; et al. Detection of Gamma Rays from a Starburst Galaxy. *Science* **2009**, *326*, 1080. [CrossRef]
528. Acciari, V.A. et al. [VERITAS Collaboration]. A connection between star formation activity and cosmic rays in the starburst galaxy M82. *Nature* **2009**, *462*, 770–772. [CrossRef]
529. Abdalla, H. et al. [H. E. S. S. Collaboration]. The starburst galaxy NGC 253 revisited by H.E.S.S. and Fermi-LAT. *Astropart. Phys.* **2018**, *617*, A73. [CrossRef]
530. Shimono, N.; Totani, T.; Sudoh, T. Prospects of newly detecting nearby star-forming galaxies by the Cherenkov Telescope Array. *Mon. Not. R. Astron. Soc.* **2021**, *506*, 6212–6222. [CrossRef]
531. Zhang, S.; Wang, Q.D.; Ji, L.; Smith, R.K.; Foster, A.R.; Zhou, X. Spectral Modeling of the Charge-exchange X-ray Emission from M82. *Astrophys. J.* **2014**, *794*, 61. [CrossRef]
532. Wu, K.; Li, K.J.; Owen, E.R.; Ji, L.; Zhang, S.; Branduardi-Raymont, G. Charge-exchange emission and cold clumps in multiphase galactic outflows. *Mon. Not. R. Astron. Soc.* **2020**, *491*, 5621–5635. [CrossRef]
533. Lopez, L.A.; Mathur, S.; Nguyen, D.D.; Thompson, T.A.; Olivier, G.M. Temperature and Metallicity Gradients in the Hot Gas Outflows of M82. *Astrophys. J.* **2020**, *904*, 152. [CrossRef]
534. Lopez, S.; Lopez, L.A.; Nguyen, D.D.; Thompson, T.A.; Mathur, S.; Bolatto, A.D.; Vulic, N.; Sardone, A. X-ray Properties of NGC 253's Starburst-driven Outflow. *Astrophys. J.* **2023**, *942*, 108. [CrossRef]
535. Perna, M.; Arribas, S.; Catalán-Torrecilla, C.; Colina, L.; Bellocchi, E.; Fluetsch, A.; Maiolino, R.; Cazzoli, S.; Hernán Caballero, A.; Pereira Santaella, M.; et al. MUSE view of Arp220: Kpc-scale multi-phase outflow and evidence for positive feedback. *Astropart. Phys.* **2020**, *643*, A139. [CrossRef]
536. Barker, S.; de Grijs, R.; Cerviño, M. Star cluster versus field star formation in the nucleus of the prototype starburst galaxy M 82. *Astropart. Phys.* **2008**, *484*, 711–720. [CrossRef]
537. Chevalier, R.A.; Clegg, A.W. Wind from a starburst galaxy nucleus. *Nature* **1985**, *317*, 44–45. [CrossRef]
538. Völk, H.J.; Aharonian, F.A.; Breitschwerdt, D. The Nonthermal Energy Content and Gamma-Ray Emission of Starburst Galaxies and Clusters of Galaxies. *Space Sci. Rev.* **1996**, *75*, 279–297. [CrossRef]
539. Bolatto, A.D.; Warren, S.R.; Leroy, A.K.; Walter, F.; Veilleux, S.; Ostriker, E.C.; Ott, J.; Zwaan, M.; Fisher, D.B.; Weiss, A.; et al. Suppression of star formation in the galaxy NGC 253 by a starburst-driven molecular wind. *Nature* **2013**, *499*, 450–453. [CrossRef]
540. Leroy, A.K.; Bolatto, A.D.; Ostriker, E.C.; Rosolowsky, E.; Walter, F.; Warren, S.R.; Donovan Meyer, J.; Hodge, J.; Meier, D.S.; Ott, J.; et al. ALMA Reveals the Molecular Medium Fueling the Nearest Nuclear Starburst. *Astrophys. J.* **2015**, *801*, 25. [CrossRef]

541. Mitsuishi, I.; Yamasaki, N.Y.; Takei, Y. An X-ray Study of the Galactic-Scale Starburst-Driven Outflow in NGC 253. *Publ. Astron. Soc. Jpn.* **2013**, *65*, 44. [CrossRef]
542. Yoast-Hull, T.M.; Gallagher, J.S.; Zweibel, E.G. Cosmic rays, γ-rays, and neutrinos in the starburst nuclei of Arp 220. *Mon. Not. R. Astron. Soc.* **2015**, *453*, 222–228. [CrossRef]
543. Barcos-Muñoz, L.; Aalto, S.; Thompson, T.A.; Sakamoto, K.; Martín, S.; Leroy, A.K.; Privon, G.C.; Evans, A.S.; Kepley, A. Fast, Collimated Outflow in the Western Nucleus of Arp 220. *Astrophys. J. Lett.* **2018**, *853*, L28. [CrossRef]
544. Lacki, B.C.; Thompson, T.A. Diffuse Hard X-ray Emission in Starburst Galaxies as Synchrotron from Very High Energy Electrons. *Astrophys. J.* **2013**, *762*, 29. [CrossRef]
545. Yoast-Hull, T.M.; Everett, J.E.; Gallagher, J.S., III; Zweibel, E.G. Winds, Clumps, and Interacting Cosmic Rays in M82. *Astrophys. J.* **2013**, *768*, 53. [CrossRef]
546. Lacki, B.C.; Thompson, T.A.; Quataert, E.; Loeb, A.; Waxman, E. On the GeV and TeV Detections of the Starburst Galaxies M82 and NGC 253. *Astrophys. J.* **2011**, *734*, 107. [CrossRef]
547. Behrens, E.; Mangum, J.G.; Holdship, J.; Viti, S.; Harada, N.; Martín, S.; Sakamoto, K.; Muller, S.; Tanaka, K.; Nakanishi, K.; et al. Tracing Interstellar Heating: An ALCHEMI Measurement of the HCN Isomers in NGC 253. *Astrophys. J.* **2022**, *939*, 119. [CrossRef]
548. Buckman, B.J.; Linden, T.; Thompson, T.A. Cosmic rays and magnetic fields in the core and halo of the starburst M82: Implications for galactic wind physics. *Mon. Not. R. Astron. Soc.* **2020**, *494*, 2679–2705. [CrossRef]
549. Downes, D.; Solomon, P.M. Rotating Nuclear Rings and Extreme Starbursts in Ultraluminous Galaxies. *Astrophys. J.* **1998**, *507*, 615–654. [CrossRef]
550. Kennicutt, R.C., Jr. The Global Schmidt Law in Star-forming Galaxies. *Astrophys. J.* **1998**, *498*, 541–552. [CrossRef]
551. González-Alfonso, E.; Fischer, J.; Bruderer, S.; Müller, H.S.P.; Graciá-Carpio, J.; Sturm, E.; Lutz, D.; Poglitsch, A.; Feuchtgruber, H.; Veilleux, S.; et al. Excited OH^+, H_2O^+, and H_3O^+ in NGC 4418 and Arp 220. *Astropart. Phys.* **2013**, *550*, A25. [CrossRef]
552. Persic, M.; Rephaeli, Y.; Arieli, Y. Very-high-energy emission from M 82. *Astropart. Phys.* **2008**, *486*, 143–149. [CrossRef]
553. Paglione, T.A.D.; Abrahams, R.D. Properties of nearby Starburst Galaxies Based on their Diffuse Gamma-Ray Emission. *Astrophys. J.* **2012**, *755*, 106. [CrossRef]
554. Domingo-Santamaría, E.; Torres, D.F. High energy γ-ray emission from the starburst nucleus of NGC 253. *Astropart. Phys.* **2005**, *444*, 403–415. [CrossRef]
555. Rephaeli, Y.; Arieli, Y.; Persic, M. High-energy emission from the starburst galaxy NGC 253. *Mon. Not. R. Astron. Soc.* **2010**, *401*, 473–478. [CrossRef]
556. Heesen, V.; Beck, R.; Krause, M.; Dettmar, R.J. Cosmic rays and the magnetic field in the nearby starburst galaxy NGC 253. I. The distribution and transport of cosmic rays. *Astropart. Phys.* **2009**, *494*, 563–577. [CrossRef]
557. Heesen, V.; Krause, M.; Beck, R.; Dettmar, R.J. Cosmic rays and the magnetic field in the nearby starburst galaxy NGC 253. II. The magnetic field structure. *Astropart. Phys.* **2009**, *506*, 1123–1135. [CrossRef]
558. Heesen, V.; Beck, R.; Krause, M.; Dettmar, R.J. Cosmic rays and the magnetic field in the nearby starburst galaxy NGC 253 III. Helical magnetic fields in the nuclear outflow. *Astropart. Phys.* **2011**, *535*, A79. [CrossRef]
559. de Cea del Pozo, E.; Torres, D.F.; Rodriguez Marrero, A.Y. Multimessenger Model for the Starburst Galaxy M82. *Astrophys. J.* **2009**, *698*, 1054–1060. [CrossRef]
560. Ha, J.H.; Ryu, D.; Kang, H. Modeling of Cosmic-Ray Production and Transport and Estimation of Gamma-Ray and Neutrino Emissions in Starburst Galaxies. *Astrophys. J.* **2021**, *907*, 26. [CrossRef]
561. Yoast-Hull, T.M.; Gallagher, J.S., III; Aalto, S.; Varenius, E. γ-Ray emission from Arp 220: Indications of an active galactic nucleus. *Mon. Not. R. Astron. Soc.* **2017**, *469*, L89–L93. [CrossRef]
562. Hung, C.L.; Sanders, D.B.; Casey, C.M.; Koss, M.; Larson, K.L.; Lee, N.; Li, Y.; Lockhart, K.; Shih, H.Y.; Barnes, J.E.; et al. A Comparison of the Morphological Properties between Local and z $\sim$1 Infrared Luminous Galaxies: Are Local and High-z (U)LIRGs Different? *Astrophys. J.* **2014**, *791*, 63. [CrossRef]
563. Larson, K.L.; Sanders, D.B.; Barnes, J.E.; Ishida, C.M.; Evans, A.S.; U, V.; Mazzarella, J.M.; Kim, D.C.; Privon, G.C.; Mirabel, I.F.; et al. Morphology and Molecular Gas Fractions of Local Luminous Infrared Galaxies as a Function of Infrared Luminosity and Merger Stage. *Astrophys. J.* **2016**, *825*, 128. [CrossRef]
564. Lonsdale, C.J.; Farrah, D.; Smith, H.E. Ultraluminous Infrared Galaxies. In *Astrophysics Update 2*; Mason, J.W., Ed.; Springer: Berlin/Heidelberg, Germany, 2006; p. 285. [CrossRef]
565. Pérez-Torres, M.; Mattila, S.; Alonso-Herrero, A.; Aalto, S.; Efstathiou, A. Star formation and nuclear activity in luminous infrared galaxies: An infrared through radio review. *Astron. Astrophys. Rev.* **2021**, *29*, 2. [CrossRef]
566. Palladino, A.; Fedynitch, A.; Rasmussen, R.W.; Taylor, A.M. IceCube neutrinos from hadronically powered gamma-ray galaxies. *J. Cosmol. Astropart. Phys.* **2019**, *2019*, 004. [CrossRef]
567. He, H.N.; Wang, T.; Fan, Y.Z.; Liu, S.M.; Wei, D.M. Diffuse PeV neutrino emission from ultraluminous infrared galaxies. *Phys. Rev. D* **2013**, *87*, 063011. [CrossRef]
568. Aartsen, M.G. et al. [IceCube Collaboration]. Characteristics of the diffuse astrophysical electron and tau neutrino flux with six years of IceCube high energy cascade data. *arXiv* **2020**, arXiv:2001.09520. [CrossRef]

569. Abbasi, R.; Ackermann, M.; Adams, J.; Aguilar, J.A.; Ahlers, M.; Ahrens, M.; Alispach, C.; Alves, A.A.; Amin, N.M.; Andeen, K.; et al. IceCube high-energy starting event sample: Description and flux characterization with 7.5 years of data. *Phys. Rev. D* **2021**, *104*, 022002. [CrossRef]
570. Abbasi, R.; Ackermann, M.; Adams, J.; Aguilar, J.A.; Ahlers, M.; Ahrens, M.; Alameddine, J.M.; Alispach, C.; Alves, A.A., Jr.; Amin, N.M.; et al. Improved Characterization of the Astrophysical Muon-neutrino Flux with 9.5 Years of IceCube Data. *Astrophys. J.* **2022**, *928*, 50. [CrossRef]
571. Ackermann, M.; Ajello, M.; Albert, A.; Atwood, W.B.; Baldini, L.; Ballet, J.; Barbiellini, G.; Bastieri, D.; Bechtol, K.; Bellazzini, R.; et al. Resolving the Extragalactic γ -Ray Background above 50 GeV with the Fermi Large Area Telescope. *Phys. Rev. Lett.* **2016**, *116*, 151105. [CrossRef]
572. Bechtol, K.; Ahlers, M.; Di Mauro, M.; Ajello, M.; Vandenbroucke, J. Evidence against Star-forming Galaxies as the Dominant Source of Icecube Neutrinos. *Astrophys. J.* **2017**, *836*, 47. [CrossRef]
573. Murase, K.; Guetta, D.; Ahlers, M. Hidden Cosmic-Ray Accelerators as an Origin of TeV-PeV Cosmic Neutrinos. *Phys. Rev. Lett.* **2016**, *116*, 071101. [CrossRef] [PubMed]
574. Vereecken, M.; de Vries, K.D. Obscured pp-channel neutrino sources. *arXiv* **2020**, arXiv:2004.03435. [CrossRef]
575. Hollenbach, D.; Kaufman, M.J.; Neufeld, D.; Wolfire, M.; Goicoechea, J.R. The Chemistry of Interstellar OH^+, H_2O^+, and H_3O^+: Inferring the Cosmic-Ray Ionization Rates from Observations of Molecular Ions. *Astrophys. J.* **2012**, *754*, 105. [CrossRef]
576. González-Alfonso, E.; Fischer, J.; Bruderer, S.; Ashby, M.L.N.; Smith, H.A.; Veilleux, S.; Müller, H.S.P.; Stewart, K.P.; Sturm, E. Outflowing OH^+ in Markarian 231: The Ionization Rate of the Molecular Gas. *Astrophys. J.* **2018**, *857*, 66. [CrossRef]
577. Simpson, J.M.; Swinbank, A.M.; Smail, I.; Alexander, D.M.; Brandt, W.N.; Bertoldi, F.; de Breuck, C.; Chapman, S.C.; Coppin, K.E.K.; da Cunha, E.; et al. An ALMA Survey of Submillimeter Galaxies in the Extended Chandra Deep Field South: The Redshift Distribution and Evolution of Submillimeter Galaxies. *Astrophys. J.* **2014**, *788*, 125. [CrossRef]
578. Dole, H.; Le Floc'h, E.; Pérez-González, P.G.; Papovich, C.; Egami, E.; Lagache, G.; Alonso-Herrero, A.; Engelbracht, C.W.; Gordon, K.D.; Hines, D.C.; et al. Far-infrared Source Counts at 70 and 160 Microns in Spitzer Deep Surveys. *Astrophys. J. Suppl.* **2004**, *154*, 87–92. [CrossRef]
579. Le Floc'h, E.; Aussel, H.; Ilbert, O.; Riguccini, L.; Frayer, D.T.; Salvato, M.; Arnouts, S.; Surace, J.; Feruglio, C.; Rodighiero, G.; et al. Deep Spitzer 24 μm COSMOS Imaging. I. The Evolution of Luminous Dusty Galaxies—Confronting the Models. *Astrophys. J.* **2009**, *703*, 222–239. [CrossRef]
580. Blain, A.W.; Smail, I.; Ivison, R.J.; Kneib, J.P.; Frayer, D.T. Submillimeter galaxies. *Phys. Rep.* **2002**, *369*, 111–176. [CrossRef]
581. Indriolo, N.; Bergin, E.A.; Falgarone, E.; Godard, B.; Zwaan, M.A.; Neufeld, D.A.; Wolfire, M.G. Constraints on the Cosmic-Ray Ionization Rate in the z $\sim$ 2.3 Lensed Galaxies SMM J2135-0102 and SDP 17b from Observations of OH^+ and H_2O^+. *Astrophys. J.* **2018**, *865*, 127. [CrossRef]
582. Danielson, A.L.R.; Swinbank, A.M.; Smail, I.; Bayet, E.; van der Werf, P.P.; Cox, P.; Edge, A.C.; Henkel, C.; Ivison, R.J. ^{13}CO and C^{18}O emission from a dense gas disc at z = 2.3: Abundance variations, cosmic rays and the initial conditions for star formation. *Mon. Not. R. Astron. Soc.* **2013**, *436*, 2793–2809. [CrossRef]
583. Falgarone, E.; Zwaan, M.A.; Godard, B.; Bergin, E.; Ivison, R.J.; Andreani, P.M.; Bournaud, F.; Bussmann, R.S.; Elbaz, D.; Omont, A.; et al. Large turbulent reservoirs of cold molecular gas around high-redshift starburst galaxies. *Nature* **2017**, *548*, 430–433. [CrossRef]
584. French, K.D.; Yang, Y.; Zabludoff, A.; Narayanan, D.; Shirley, Y.; Walter, F.; Smith, J.D.; Tremonti, C.A. Discovery of Large Molecular Gas Reservoirs in Post-starburst Galaxies. *Astrophys. J.* **2015**, *801*, 1. [CrossRef]
585. French, K.D.; Zabludoff, A.I.; Yoon, I.; Shirley, Y.; Yang, Y.; Smercina, A.; Smith, J.D.; Narayanan, D. Why Post-starburst Galaxies Are Now Quiescent. *Astrophys. J.* **2018**, *861*, 123. [CrossRef]
586. Rowlands, K.; Wild, V.; Nesvadba, N.; Sibthorpe, B.; Mortier, A.; Lehnert, M.; da Cunha, E. The evolution of the cold interstellar medium in galaxies following a starburst. *Mon. Not. R. Astron. Soc.* **2015**, *448*, 258–279. [CrossRef]
587. Alatalo, K.; Lisenfeld, U.; Lanz, L.; Appleton, P.N.; Ardila, F.; Cales, S.L.; Kewley, L.J.; Lacy, M.; Medling, A.M.; Nyland, K.; et al. Shocked POststarburst Galaxy Survey. II. The Molecular Gas Content and Properties of a Subset of SPOGs. *Astrophys. J.* **2016**, *827*, 106. [CrossRef]
588. Watson, D.; Christensen, L.; Knudsen, K.K.; Richard, J.; Gallazzi, A.; Michałowski, M.J. A dusty, normal galaxy in the epoch of reionization. *Nature* **2015**, *519*, 327–330. [CrossRef]
589. Laporte, N.; Ellis, R.S.; Witten, C.E.C.; Roberts-Borsani, G. Resolving ambiguities in the inferred star formation histories of intense [O III] emitters in the reionization Era. *Mon. Not. R. Astron. Soc.* **2023**, *523*, 3018–3024. [CrossRef]
590. Lanz, L.; Stepanoff, S.; Hickox, R.C.; Alatalo, K.; French, K.D.; Rowlands, K.; Nyland, K.; Appleton, P.N.; Lacy, M.; Medling, A.; et al. Are Active Galactic Nuclei in Post-starburst Galaxies Driving the Change or Along for the Ride? *Astrophys. J.* **2022**, *935*, 29. [CrossRef]
591. Smercina, A.; Smith, J.D.T.; Dale, D.A.; French, K.D.; Croxall, K.V.; Zhukovska, S.; Togi, A.; Bell, E.F.; Crocker, A.F.; Draine, B.T.; et al. After the Fall: The Dust and Gas in E+A Post-starburst Galaxies. *Astrophys. J.* **2018**, *855*, 51. [CrossRef]
592. Papadopoulos, P.P. A Cosmic-ray-dominated Interstellar Medium in Ultra Luminous Infrared Galaxies: New Initial Conditions for Star Formation. *Astrophys. J.* **2010**, *720*, 226–232. [CrossRef]
593. Yokoyama, S.L.; Ohira, Y. Resistive heating induced by streaming cosmic rays around a galaxy in the early Universe. *Mon. Not. R. Astron. Soc.* **2023**, *523*, 3671–3677. [CrossRef]

594. Owen, E.R. Cosmic rays as a feedback agent in primordial galactic ecosystems. *arXiv* **2022**, arXiv:2212.06469. [CrossRef]
595. Tumlinson, J.; Peeples, M.S.; Werk, J.K. The Circumgalactic Medium. *Annu. Rev. Astron. Astrophys.* **2017**, *55*, 389–432. [CrossRef]
596. Putman, M.E.; Peek, J.E.G.; Joung, M.R. Gaseous Galaxy Halos. *Annu. Rev. Astron. Astrophys.* **2012**, *50*, 491–529. [CrossRef]
597. Faucher-Giguere, C.A.; Oh, S.P. Key Physical Processes in the Circumgalactic Medium. *arXiv* **2023**, arXiv:2301.10253. [CrossRef]
598. Girichidis, P.; Naab, T.; Hanasz, M.; Walch, S. Cooler and smoother—The impact of cosmic rays on the phase structure of galactic outflows. *Mon. Not. R. Astron. Soc.* **2018**, *479*, 3042–3067. [CrossRef]
599. Werk, J.K.; Prochaska, J.X.; Tumlinson, J.; Peeples, M.S.; Tripp, T.M.; Fox, A.J.; Lehner, N.; Thom, C.; O'Meara, J.M.; Ford, A.B.; et al. The COS-Halos Survey: Physical Conditions and Baryonic Mass in the Low-redshift Circumgalactic Medium. *Astrophys. J.* **2014**, *792*, 8. [CrossRef]
600. Chen, H.W.; Helsby, J.E.; Gauthier, J.R.; Shectman, S.A.; Thompson, I.B.; Tinker, J.L. An Empirical Characterization of Extended Cool Gas Around Galaxies Using Mg II Absorption Features. *Astrophys. J.* **2010**, *714*, 1521–1541. [CrossRef]
601. Prochaska, J.X.; Weiner, B.; Chen, H.W.; Mulchaey, J.; Cooksey, K. Probing the Intergalactic Medium/Galaxy Connection. V. On the Origin of Lyα and O VI Absorption at z < 0.2. *Astrophys. J.* **2011**, *740*, 91. [CrossRef]
602. Tumlinson, J.; Thom, C.; Werk, J.K.; Prochaska, J.X.; Tripp, T.M.; Katz, N.; Davé, R.; Oppenheimer, B.D.; Meiring, J.D.; Ford, A.B.; et al. The COS-Halos Survey: Rationale, Design, and a Census of Circumgalactic Neutral Hydrogen. *Astrophys. J.* **2013**, *777*, 59. [CrossRef]
603. Keeney, B.A.; Stocke, J.T.; Pratt, C.T.; Davis, J.D.; Syphers, D.; Danforth, C.W.; Shull, J.M.; Froning, C.S.; Green, J.C.; Penton, S.V.; et al. A Galaxy Redshift Survey Near HST/COS AGN Sight Lines. *Astrophys. J. Suppl.* **2018**, *237*, 11. [CrossRef]
604. *Gas Accretion onto Galaxies*; Astrophysics and Space Science Library; Springer: London, UK, 2017; Volume 430. [CrossRef]
605. Thom, C.; Tumlinson, J.; Werk, J.K.; Prochaska, J.X.; Oppenheimer, B.D.; Peeples, M.S.; Tripp, T.M.; Katz, N.S.; O'Meara, J.M.; Ford, A.B.; et al. Not Dead Yet: Cool Circumgalactic Gas in the Halos of Early-type Galaxies. *Astrophys. J. Lett.* **2012**, *758*, L41. [CrossRef]
606. Berg, M.A.; Howk, J.C.; Lehner, N.; Wotta, C.B.; O'Meara, J.M.; Bowen, D.V.; Burchett, J.N.; Peeples, M.S.; Tejos, N. The Red Dead Redemption Survey of Circumgalactic Gas about Massive Galaxies. I. Mass and Metallicity of the Cool Phase. *Astrophys. J.* **2019**, *883*, 5. [CrossRef]
607. Butsky, I.S.; Fielding, D.B.; Hayward, C.C.; Hummels, C.B.; Quinn, T.R.; Werk, J.K. The Impact of Cosmic Rays on Thermal Instability in the Circumgalactic Medium. *Astrophys. J.* **2020**, *903*, 77. [CrossRef]
608. Butsky, I.S.; Nakum, S.; Ponnada, S.B.; Hummels, C.B.; Ji, S.; Hopkins, P.F. Constraining cosmic ray transport with observations of the circumgalactic medium. *Mon. Not. R. Astron. Soc.* **2023**, *521*, 2477–2483. [CrossRef]
609. Field, G.B. Thermal Instability. *Astrophys. J.* **1965**, *142*, 531. [CrossRef]
610. Putman, M.E.; Staveley-Smith, L.; Freeman, K.C.; Gibson, B.K.; Barnes, D.G. The Magellanic Stream, High-Velocity Clouds, and the Sculptor Group. *Astrophys. J.* **2003**, *586*, 170–194. [CrossRef]
611. McCourt, M.; Sharma, P.; Quataert, E.; Parrish, I.J. Thermal instability in gravitationally stratified plasmas: Implications for multiphase structure in clusters and galaxy haloes. *Mon. Not. R. Astron. Soc.* **2012**, *419*, 3319–3337. [CrossRef]
612. Sharma, P.; McCourt, M.; Quataert, E.; Parrish, I.J. Thermal instability and the feedback regulation of hot haloes in clusters, groups and galaxies. *Mon. Not. R. Astron. Soc.* **2012**, *420*, 3174–3194. [CrossRef]
613. Voit, G.M.; Donahue, M.; Bryan, G.L.; McDonald, M. Regulation of star formation in giant galaxies by precipitation, feedback and conduction. *Nature* **2015**, *519*, 203–206. [CrossRef]
614. Salem, M.; Bryan, G.L.; Corlies, L. Role of cosmic rays in the circumgalactic medium. *Mon. Not. R. Astron. Soc.* **2016**, *456*, 582–601. [CrossRef]
615. Sharma, P.; Parrish, I.J.; Quataert, E. Thermal Instability with Anisotropic Thermal Conduction and Adiabatic Cosmic Rays: Implications for Cold Filaments in Galaxy Clusters. *Astrophys. J.* **2010**, *720*, 652–665. [CrossRef]
616. Kempski, P.; Quataert, E. Thermal instability of halo gas heated by streaming cosmic rays. *Mon. Not. R. Astron. Soc.* **2020**, *493*, 1801–1817. [CrossRef]
617. Hopkins, P.F.; Chan, T.K.; Garrison-Kimmel, S.; Ji, S.; Su, K.Y.; Hummels, C.B.; Kereš, D.; Quataert, E.; Faucher-Giguère, C.A. But what about...: Cosmic rays, magnetic fields, conduction, and viscosity in galaxy formation. *Mon. Not. R. Astron. Soc.* **2020**, *492*, 3465–3498. [CrossRef]
618. Buck, T.; Pfrommer, C.; Pakmor, R.; Grand, R.J.J.; Springel, V. The effects of cosmic rays on the formation of Milky Way-mass galaxies in a cosmological context. *Mon. Not. R. Astron. Soc.* **2020**, *497*, 1712–1737. [CrossRef]
619. Dekel, A.; Birnboim, Y. Galaxy bimodality due to cold flows and shock heating. *Mon. Not. R. Astron. Soc.* **2006**, *368*, 2–20. [CrossRef]
620. Dekel, A.; Birnboim, Y.; Engel, G.; Freundlich, J.; Goerdt, T.; Mumcuoglu, M.; Neistein, E.; Pichon, C.; Teyssier, R.; Zinger, E. Cold streams in early massive hot haloes as the main mode of galaxy formation. *Nature* **2009**, *457*, 451–454. [CrossRef]
621. Kereš, D.; Katz, N.; Weinberg, D.H.; Davé, R. How do galaxies get their gas? *Mon. Not. R. Astron. Soc.* **2005**, *363*, 2–28. [CrossRef]
622. Kereš, D.; Katz, N.; Fardal, M.; Davé, R.; Weinberg, D.H. Galaxies in a simulated ΛCDM Universe—I. Cold mode and hot cores. *Mon. Not. R. Astron. Soc.* **2009**, *395*, 160–179. [CrossRef]
623. Roberts-Borsani, G.W.; Saintonge, A. The prevalence and properties of cold gas inflows and outflows around galaxies in the local Universe. *Mon. Not. R. Astron. Soc.* **2019**, *482*, 4111–4145. [CrossRef]

624. Ceverino, D.; Dekel, A.; Bournaud, F. High-redshift clumpy discs and bulges in cosmological simulations. *Mon. Not. R. Astron. Soc.* **2010**, *404*, 2151–2169. [CrossRef]
625. Emonts, B.H.C.; Lehnert, M.D.; Yoon, I.; Mandelker, N.; Villar-Martín, M.; Miley, G.K.; De Breuck, C.; Pérez-Torres, M.A.; Hatch, N.A.; Guillard, P. A cosmic stream of atomic carbon gas connected to a massive radio galaxy at redshift 3.8. *Science* **2023**, *379*, 1323–1326. [CrossRef]
626. Mandelker, N.; Nagai, D.; Aung, H.; Dekel, A.; Birnboim, Y.; van den Bosch, F.C. Instability of supersonic cold streams feeding galaxies - IV. Survival of radiatively cooling streams. *Mon. Not. R. Astron. Soc.* **2020**, *494*, 2641–2663. [CrossRef]
627. Martin, D.C.; Matuszewski, M.; Morrissey, P.; Neill, J.D.; Moore, A.; Cantalupo, S.; Prochaska, J.X.; Chang, D. A giant protogalactic disk linked to the cosmic web. *Nature* **2015**, *524*, 192–195. [CrossRef]
628. Daddi, E.; Valentino, F.; Rich, R.M.; Neill, J.D.; Gronke, M.; O'Sullivan, D.; Elbaz, D.; Bournaud, F.; Finoguenov, A.; Marchal, A.; et al. Three Lyman-α-emitting filaments converging to a massive galaxy group at z = 2.91: Discussing the case for cold gas infall. *Astropart. Phys.* **2021**, *649*, A78. [CrossRef]
629. Dijkstra, M.; Loeb, A. Lyα blobs as an observational signature of cold accretion streams into galaxies. *Mon. Not. R. Astron. Soc.* **2009**, *400*, 1109–1120. [CrossRef]
630. Rosdahl, J.; Blaizot, J. Extended Lyα emission from cold accretion streams. *Mon. Not. R. Astron. Soc.* **2012**, *423*, 344–366. [CrossRef]
631. Pandya, V.; Somerville, R.S.; Anglés-Alcázar, D.; Hayward, C.C.; Bryan, G.L.; Fielding, D.B.; Forbes, J.C.; Burkhart, B.; Genel, S.; Hernquist, L.; et al. First Results from SMAUG: The Need for Preventative Stellar Feedback and Improved Baryon Cycling in Semianalytic Models of Galaxy Formation. *Astrophys. J.* **2020**, *905*, 4. [CrossRef]
632. Nelson, D.; Genel, S.; Vogelsberger, M.; Springel, V.; Sijacki, D.; Torrey, P.; Hernquist, L. The impact of feedback on cosmological gas accretion. *Mon. Not. R. Astron. Soc.* **2015**, *448*, 59–74. [CrossRef]
633. Hopkins, P.F.; Chan, T.K.; Ji, S.; Hummels, C.B.; Kereš, D.; Quataert, E.; Faucher-Giguère, C.A. Cosmic ray driven outflows to Mpc scales from L $_*$ galaxies. *Mon. Not. R. Astron. Soc.* **2021**, *501*, 3640–3662. [CrossRef]
634. Su, K.Y.; Hopkins, P.F.; Hayward, C.C.; Faucher-Giguère, C.A.; Kereš, D.; Ma, X.; Orr, M.E.; Chan, T.K.; Robles, V.H. Cosmic rays or turbulence can suppress cooling flows (where thermal heating or momentum injection fail). *Mon. Not. R. Astron. Soc.* **2020**, *491*, 1190–1212. [CrossRef]
635. Schawinski, K.; Urry, C.M.; Simmons, B.D.; Fortson, L.; Kaviraj, S.; Keel, W.C.; Lintott, C.J.; Masters, K.L.; Nichol, R.C.; Sarzi, M.; et al. The green valley is a red herring: Galaxy Zoo reveals two evolutionary pathways towards quenching of star formation in early- and late-type galaxies. *Mon. Not. R. Astron. Soc.* **2014**, *440*, 889–907. [CrossRef]
636. Laporte, N.; Meyer, R.A.; Ellis, R.S.; Robertson, B.E.; Chisholm, J.; Roberts-Borsani, G.W. Probing cosmic dawn: Ages and star formation histories of candidate z $\geq$ 9 galaxies. *Mon. Not. R. Astron. Soc.* **2021**, *505*, 3336–3346. [CrossRef]
637. Gronke, M.; Oh, S.P. The growth and entrainment of cold gas in a hot wind. *Mon. Not. R. Astron. Soc.* **2018**, *480*, L111–L115. [CrossRef]
638. Huang, X.; Jiang, Y.f.; Davis, S.W. Cosmic-Ray-driven Multiphase Gas Formed via Thermal Instability. *Astrophys. J.* **2022**, *931*, 140. [CrossRef]
639. Fujita, A.; Martin, C.L.; Mac Low, M.M.; New, K.C.B.; Weaver, R. The Origin and Kinematics of Cold Gas in Galactic Winds: Insight from Numerical Simulations. *Astrophys. J.* **2009**, *698*, 693–714. [CrossRef]
640. Cooper, J.L.; Bicknell, G.V.; Sutherland, R.S.; Bland-Hawthorn, J. Three-dimensional simulations of a starburst wind. *Astrophys. Space Sci.* **2007**, *311*, 99–103. [CrossRef]
641. Zhang, D. A Review of the Theory of Galactic Winds Driven by Stellar Feedback. *Galaxies* **2018**, *6*, 114. [CrossRef]
642. Murray, N.; Ménard, B.; Thompson, T.A. Radiation Pressure from Massive Star Clusters as a Launching Mechanism for Super-galactic Winds. *Astrophys. J.* **2011**, *735*, 66. [CrossRef]
643. Gronke, M.; Oh, S.P.; Ji, S.; Norman, C. Survival and mass growth of cold gas in a turbulent, multiphase medium. *Mon. Not. R. Astron. Soc.* **2022**, *511*, 859–876. [CrossRef]
644. Lyutikov, M. Magnetic draping of merging cores and radio bubbles in clusters of galaxies. *Mon. Not. R. Astron. Soc.* **2006**, *373*, 73–78. [CrossRef]
645. Li, Z.; Hopkins, P.F.; Squire, J.; Hummels, C. On the survival of cool clouds in the circumgalactic medium. *Mon. Not. R. Astron. Soc.* **2020**, *492*, 1841–1854. [CrossRef]
646. Breitschwerdt, D.; McKenzie, J.F.; Voelk, H.J. Galactic winds. I-Cosmic ray and wave-driven winds from the Galaxy. *Astropart. Phys.* **1991**, *245*, 79–98.
647. Uhlig, M.; Pfrommer, C.; Sharma, M.; Nath, B.B.; Enßlin, T.A.; Springel, V. Galactic winds driven by cosmic ray streaming. *Mon. Not. R. Astron. Soc.* **2012**, *423*, 2374–2396. [CrossRef]
648. Booth, C.M.; Agertz, O.; Kravtsov, A.V.; Gnedin, N.Y. Simulations of Disk Galaxies with Cosmic Ray Driven Galactic Winds. *Astrophys. J. Lett.* **2013**, *777*, L16. [CrossRef]
649. Salem, M.; Bryan, G.L. Cosmic ray driven outflows in global galaxy disc models. *Mon. Not. R. Astron. Soc.* **2014**, *437*, 3312–3330. [CrossRef]
650. Wiener, J.; Pfrommer, C.; Oh, S.P. Cosmic ray-driven galactic winds: Streaming or diffusion? *Mon. Not. R. Astron. Soc.* **2017**, *467*, 906–921. [CrossRef]

651. Chan, T.K.; Kereš, D.; Hopkins, P.F.; Quataert, E.; Su, K.Y.; Hayward, C.C.; Faucher-Giguère, C.A. Cosmic ray feedback in the FIRE simulations: Constraining cosmic ray propagation with GeV γ-ray emission. *Mon. Not. R. Astron. Soc.* **2019**, *488*, 3716–3744. [CrossRef]
652. Samui, S.; Subramanian, K.; Srianand, R. Cosmic ray driven outflows from high-redshift galaxies. *Mon. Not. R. Astron. Soc.* **2010**, *402*, 2778–2791. [CrossRef]
653. Farber, R.; Ruszkowski, M.; Yang, H.Y.K.; Zweibel, E.G. Impact of Cosmic-Ray Transport on Galactic Winds. *Astrophys. J.* **2018**, *856*, 112. [CrossRef]
654. Armillotta, L.; Ostriker, E.C.; Jiang, Y.F. Cosmic-Ray Transport in Varying Galactic Environments. *Astrophys. J.* **2022**, *929*, 170. [CrossRef]
655. Yu, B.P.B.; Owen, E.R.; Pan, K.C.; Wu, K.; Ferreras, I. Outflows from starburst galaxies with various driving mechanisms and their X-ray properties. *Mon. Not. R. Astron. Soc.* **2021**, *508*, 5092–5113. [CrossRef]
656. Gronke, M.; Girichidis, P.; Naab, T.; Walch, S. The Imprint of Cosmic Ray Driven Outflows on Lyman-α Spectra. *Astrophys. J. Lett.* **2018**, *862*, L7. [CrossRef]
657. Mao, S.A.; Ostriker, E.C. Galactic Disk Winds Driven by Cosmic Ray Pressure. *Astrophys. J.* **2018**, *854*, 89. [CrossRef]
658. Recchia, S.; Blasi, P.; Morlino, G. Cosmic ray-driven winds in the Galactic environment and the cosmic ray spectrum. *Mon. Not. R. Astron. Soc.* **2017**, *470*, 865–881. [CrossRef]
659. Fujita, A.; Mac Low, M.M. Cosmic ray driven outflows in an ultraluminous galaxy. *Mon. Not. R. Astron. Soc.* **2018**, *477*, 531–538. [CrossRef]
660. Jacob, S.; Pakmor, R.; Simpson, C.M.; Springel, V.; Pfrommer, C. The dependence of cosmic ray-driven galactic winds on halo mass. *Mon. Not. R. Astron. Soc.* **2018**, *475*, 570–584. [CrossRef]
661. Peschken, N.; Hanasz, M.; Naab, T.; Wóltański, D.; Gawryszczak, A. The angular momentum structure of CR-driven galactic outflows triggered by stream accretion. *Mon. Not. R. Astron. Soc.* **2021**, *508*, 4269–4281. [CrossRef]
662. Peschken, N.; Hanasz, M.; Naab, T.; Wóltański, D.; Gawryszczak, A. The phase structure of cosmic ray driven outflows in stream fed disc galaxies. *Mon. Not. R. Astron. Soc.* **2023**, *522*, 5529–5545. [CrossRef]
663. Quataert, E.; Thompson, T.A.; Jiang, Y.F. The physics of galactic winds driven by cosmic rays I: Diffusion. *Mon. Not. R. Astron. Soc.* **2022**, *510*, 1184–1203. [CrossRef]
664. Hopkins, P.F.; Chan, T.K.; Squire, J.; Quataert, E.; Ji, S.; Kereš, D.; Faucher-Giguère, C.A. Effects of different cosmic ray transport models on galaxy formation. *Mon. Not. R. Astron. Soc.* **2021**, *501*, 3663–3669. [CrossRef]
665. Quataert, E.; Jiang, Y.F.; Thompson, T.A. The physics of galactic winds driven by cosmic rays—II. Isothermal streaming solutions. *Mon. Not. R. Astron. Soc.* **2022**, *510*, 920–945. [CrossRef]
666. Bai, X.N. Toward First-principles Characterization of Cosmic-Ray Transport Coefficients from Multiscale Kinetic Simulations. *Astrophys. J.* **2022**, *928*, 112. [CrossRef]
667. Ko, C.M.; Ramzan, B.; Chernyshov, D.O. Outflows in the presence of cosmic rays and waves with cooling. *Astropart. Phys.* **2021**, *654*, A63. [CrossRef]
668. Modak, S.; Quataert, E.; Jiang, Y.F.; Thompson, T.A. Cosmic-Ray Driven Galactic Winds from the Warm Interstellar Medium. *arXiv* **2023**, arXiv:2302.03701. [CrossRef]
669. Hopkins, P.F.; Butsky, I.S.; Panopoulou, G.V.; Ji, S.; Quataert, E.; Faucher-Giguère, C.A.; Kereš, D. First predicted cosmic ray spectra, primary-to-secondary ratios, and ionization rates from MHD galaxy formation simulations. *Mon. Not. R. Astron. Soc.* **2022**, *516*, 3470–3514. [CrossRef]
670. Girichidis, P.; Pfrommer, C.; Pakmor, R.; Springel, V. Spectrally resolved cosmic rays—II. Momentum-dependent cosmic ray diffusion drives powerful galactic winds. *Mon. Not. R. Astron. Soc.* **2022**, *510*, 3917–3938. [CrossRef]
671. Müller, A.L.; Romero, G.E.; Roth, M. High-energy processes in starburst-driven winds. *Mon. Not. R. Astron. Soc.* **2020**, *496*, 2474–2481. [CrossRef]
672. Peretti, E.; Morlino, G.; Blasi, P.; Cristofari, P. Particle acceleration and multimessenger emission from starburst-driven galactic winds. *Mon. Not. R. Astron. Soc.* **2022**, *511*, 1336–1348. [CrossRef]
673. Chisholm, J.; Tremonti, C.A.; Leitherer, C.; Chen, Y.; Wofford, A.; Lundgren, B. Scaling Relations Between Warm Galactic Outflows and Their Host Galaxies. *Astrophys. J.* **2015**, *811*, 149. [CrossRef]
674. Heckman, T.M.; Borthakur, S. The Implications of Extreme Outflows from Extreme Starbursts. *Astrophys. J.* **2016**, *822*, 9. [CrossRef]
675. Chisholm, J.; Tremonti, C.A.; Leitherer, C.; Chen, Y. The mass and momentum outflow rates of photoionized galactic outflows. *Mon. Not. R. Astron. Soc.* **2017**, *469*, 4831–4849. [CrossRef]
676. Oppenheimer, B.D.; Davé, R.; Kereš, D.; Fardal, M.; Katz, N.; Kollmeier, J.A.; Weinberg, D.H. Feedback and recycled wind accretion: Assembling the z = 0 galaxy mass function. *Mon. Not. R. Astron. Soc.* **2010**, *406*, 2325–2338. [CrossRef]
677. Bertone, S.; De Lucia, G.; Thomas, P.A. The recycling of gas and metals in galaxy formation: Predictions of a dynamical feedback model. *Mon. Not. R. Astron. Soc.* **2007**, *379*, 1143–1154. [CrossRef]
678. Marinacci, F.; Fraternali, F.; Nipoti, C.; Binney, J.; Ciotti, L.; Londrillo, P. Galactic fountains and the rotation of disc-galaxy coronae. *Mon. Not. R. Astron. Soc.* **2011**, *415*, 1534–1542. [CrossRef]
679. Zhang, S.; Cai, Z.; Xu, D.; Shimakawa, R.; Arrigoni Battaia, F.; Prochaska, J.X.; Cen, R.; Zheng, Z.; Wu, Y.; Li, Q.; et al. Inspiraling streams of enriched gas observed around a massive galaxy 11 billion years ago. *Science* **2023**, *380*, 494–498. [CrossRef]

680. Cen, R.; Ostriker, J.P. Where Are the Baryons? II. Feedback Effects. *Astrophys. J.* **2006**, *650*, 560–572. [CrossRef]
681. Nelson, D.; Kauffmann, G.; Pillepich, A.; Genel, S.; Springel, V.; Pakmor, R.; Hernquist, L.; Weinberger, R.; Torrey, P.; Vogelsberger, M.; et al. The abundance, distribution, and physical nature of highly ionized oxygen O VI, O VII, and O VIII in IllustrisTNG. *Mon. Not. R. Astron. Soc.* **2018**, *477*, 450–479. [CrossRef]
682. Bertone, S.; Vogt, C.; Enßlin, T. Magnetic field seeding by galactic winds. *Mon. Not. R. Astron. Soc.* **2006**, *370*, 319–330. [CrossRef]
683. Donnert, J.; Dolag, K.; Lesch, H.; Müller, E. Cluster magnetic fields from galactic outflows. *Mon. Not. R. Astron. Soc.* **2009**, *392*, 1008–1021. [CrossRef]
684. Arámburo-García, A.; Bondarenko, K.; Boyarsky, A.; Nelson, D.; Pillepich, A.; Sokolenko, A. Magnetization of the intergalactic medium in the IllustrisTNG simulations: The importance of extended, outflow-driven bubbles. *Mon. Not. R. Astron. Soc.* **2021**, *505*, 5038–5057. [CrossRef]
685. Oppenheimer, B.D.; Davé, R. Mass, metal, and energy feedback in cosmological simulations. *Mon. Not. R. Astron. Soc.* **2008**, *387*, 577–600. [CrossRef]
686. Anglés-Alcázar, D.; Faucher-Giguère, C.A.; Kereš, D.; Hopkins, P.F.; Quataert, E.; Murray, N. The cosmic baryon cycle and galaxy mass assembly in the FIRE simulations. *Mon. Not. R. Astron. Soc.* **2017**, *470*, 4698–4719. [CrossRef]
687. Christensen, C.R.; Davé, R.; Governato, F.; Pontzen, A.; Brooks, A.; Munshi, F.; Quinn, T.; Wadsley, J. In-N-Out: The Gas Cycle from Dwarfs to Spiral Galaxies. *Astrophys. J.* **2016**, *824*, 57. [CrossRef]
688. Girichidis, P.; Naab, T.; Walch, S.; Hanasz, M.; Mac Low, M.M.; Ostriker, J.P.; Gatto, A.; Peters, T.; Wünsch, R.; Glover, S.C.O.; et al. Launching Cosmic-Ray-driven Outflows from the Magnetized Interstellar Medium. *Astrophys. J. Lett.* **2016**, *816*, L19. [CrossRef]
689. Jana, R.; Gupta, S.; Nath, B.B. Role of cosmic rays in the early stages of galactic outflows. *Mon. Not. R. Astron. Soc.* **2020**, *497*, 2623–2640. [CrossRef]
690. Ji, S.; Kereš, D.; Chan, T.K.; Stern, J.; Hummels, C.B.; Hopkins, P.F.; Quataert, E.; Faucher-Giguère, C.A. Virial shocks are suppressed in cosmic ray-dominated galaxy haloes. *Mon. Not. R. Astron. Soc.* **2021**, *505*, 259–273. [CrossRef]
691. Butsky, I.S.; Werk, J.K.; Tchernyshyov, K.; Fielding, D.B.; Breneman, J.; Piacitelli, D.R.; Quinn, T.R.; Sanchez, N.N.; Cruz, A.; Hummels, C.B.; et al. The Impact of Cosmic Rays on the Kinematics of the Circumgalactic Medium. *Astrophys. J.* **2022**, *935*, 69. [CrossRef]
692. Chan, T.K.; Kereš, D.; Gurvich, A.B.; Hopkins, P.F.; Trapp, C.; Ji, S.; Faucher-Giguère, C.A. The impact of cosmic rays on dynamical balance and disc-halo interaction in L$\star$ disc galaxies. *Mon. Not. R. Astron. Soc.* **2022**, *517*, 597–615. [CrossRef]
693. Ipavich, F.M. Galactic winds driven by cosmic rays. *Astrophys. J.* **1975**, *196*, 107–120. [CrossRef]
694. Simpson, C.M.; Pakmor, R.; Marinacci, F.; Pfrommer, C.; Springel, V.; Glover, S.C.O.; Clark, P.C.; Smith, R.J. The Role of Cosmic-Ray Pressure in Accelerating Galactic Outflows. *Astrophys. J. Lett.* **2016**, *827*, L29. [CrossRef]
695. Bustard, C.; Zweibel, E.G.; D'Onghia, E.; Gallagher, J. S., I.; Farber, R. Cosmic-Ray-driven Outflows from the Large Magellanic Cloud: Contributions to the LMC Filament. *Astrophys. J.* **2020**, *893*, 29. [CrossRef]
696. Gupta, S.; Sharma, P.; Mignone, A. A numerical approach to the non-uniqueness problem of cosmic ray two-fluid equations at shocks. *Mon. Not. R. Astron. Soc.* **2021**, *502*, 2733–2749. [CrossRef]
697. Semenov, V.A.; Kravtsov, A.V.; Diemer, B. Entropy-conserving Scheme for Modeling Nonthermal Energies in Fluid Dynamics Simulations. *Astrophys. J. Suppl.* **2022**, *261*, 16. [CrossRef]
698. Hopkins, P.F.; Squire, J.; Butsky, I.S.; Ji, S. Standard self-confinement and extrinsic turbulence models for cosmic ray transport are fundamentally incompatible with observations. *Mon. Not. R. Astron. Soc.* **2022**, *517*, 5413–5448. [CrossRef]
699. Girichidis, P.; Werhahn, M.; Pfrommer, C.; Pakmor, R.; Springel, V. Spectrally resolved cosmic rays—III. Dynamical impact and properties of the circumgalactic medium. *arXiv* **2023**, arXiv:2303.03417. [CrossRef]
700. Werhahn, M.; Girichidis, P.; Pfrommer, C.; Whittingham, J. Gamma-ray emission from spectrally resolved cosmic rays in galaxies. *arXiv* **2023**, arXiv:2301.04163. [CrossRef]
701. Lazarian, A.; Xu, S. Damping of Alfvén Waves in MHD Turbulence and Implications for Cosmic Ray Streaming Instability and Galactic Winds. *Front. Phys.* **2022**, *10*, 702799. [CrossRef]
702. Zweibel, E.G. The microphysics and macrophysics of cosmic rays. *Phys. Plasmas* **2013**, *20*, 055501. [CrossRef]
703. Hopkins, P.F.; Squire, J.; Chan, T.K.; Quataert, E.; Ji, S.; Kereš, D.; Faucher-Giguère, C.A. Testing physical models for cosmic ray transport coefficients on galactic scales: Self-confinement and extrinsic turbulence at ∼GeV energies. *Mon. Not. R. Astron. Soc.* **2021**, *501*, 4184–4213. [CrossRef]
704. Lazarian, A. Damping of Alfvén Waves by Turbulence and Its Consequences: From Cosmic-ray Streaming to Launching Winds. *Astrophys. J.* **2016**, *833*, 131. [CrossRef]
705. Bai, X.N.; Ostriker, E.C.; Plotnikov, I.; Stone, J.M. Magnetohydrodynamic Particle-in-cell Simulations of the Cosmic-Ray Streaming Instability: Linear Growth and Quasi-linear Evolution. *Astrophys. J.* **2019**, *876*, 60. [CrossRef]
706. Holcomb, C.; Spitkovsky, A. On the Growth and Saturation of the Gyroresonant Streaming Instabilities. *Astrophys. J.* **2019**, *882*, 3. [CrossRef]
707. van Marle, A.J.; Casse, F.; Marcowith, A. Three-dimensional simulations of non-resonant streaming instability and particle acceleration near non-relativistic astrophysical shocks. *Mon. Not. R. Astron. Soc.* **2019**, *490*, 1156–1165. [CrossRef]
708. Hopkins, P.F.; Butsky, I.S.; Ji, S.; Kereš, D. A simple sub-grid model for cosmic ray effects on galactic scales. *Mon. Not. R. Astron. Soc.* **2023**. [CrossRef]

709. Cherenkov Telescope Array Consortium.; Acharya, B.S.; Agudo, I.; Al Samarai, I.; Alfaro, R.; Alfaro, J.; Alispach, C.; Alves Batista, R.; Amans, J.P.; Amato, E.; et al. *Science with the Cherenkov Telescope Array*; World Scientific Publishing Co Pte Ltd.: Singapore, 2019. [CrossRef]
710. Huentemeyer, P.; BenZvi, S.; Dingus, B.; Fleischhack, H.; Schoorlemmer, H.; Weisgarber, T. The Southern Wide-Field Gamma-Ray Observatory (SWGO): A Next-Generation Ground-Based Survey Instrument. *Bull. Am. Astron. Soc.* **2019**, *51*, 109. [CrossRef]
711. Tomsick, J.; Zoglauer, A.; Sleator, C.; Lazar, H.; Beechert, J.; Boggs, S.; Roberts, J.; Siegert, T.; Lowell, A.; Wulf, E.; et al. The Compton Spectrometer and Imager. *Bull. Am. Astron. Soc.* **2019**, *51*, 98. [CrossRef]
712. Tomsick, J. et al. [COSI Collaboration]. The Compton Spectrometer and Imager Project for MeV Astronomy. In Proceedings of the 37th International Cosmic Ray Conference, Berlin, Germany, 15–22 July 2021; Sissa Medialab srl Partita IVA: Trieste, Italy, 2022; Volume 395, p. 652. [CrossRef]
713. Adrián-Martínez, S.; Ageron, M.; Aharonian, F.; Aiello, S.; Albert, A.; Ameli, F.; Anassontzis, E.; Andre, M.; Androulakis, G.; Anghinolfi, M.; et al. Letter of intent for KM3NeT 2.0. *J. Phys. Nucl. Phys.* **2016**, *43*, 084001. [CrossRef]
714. Avrorin, A.D. et al. [Baikal-GVD Collaboration]. Neutrino Telescope in Lake Baikal: Present and Future. *arXiv* **2019**, arXiv:1908.05427.
715. Krumholz, M.R.; Crocker, R.M.; Sampson, M.L. Cosmic ray interstellar propagation tool using Itô Calculus (CRIPTIC): Software for simultaneous calculation of cosmic ray transport and observational signatures. *Mon. Not. R. Astron. Soc.* **2022**, *517*, 1355–1380. [CrossRef]
716. Hanasz, M.; Strong, A.W.; Girichidis, P. Simulations of cosmic ray propagation. *Living Rev. Comput. Astrophys.* **2021**, *7*, 2. [CrossRef] [PubMed]
717. Zweibel, E.G. The Role of Pressure Anisotropy in Cosmic-Ray Hydrodynamics. *Astrophys. J.* **2020**, *890*, 67. [CrossRef]
718. Ji, S.; Squire, J.; Hopkins, P.F. Numerical study of cosmic ray confinement through dust resonant drag instabilities. *Mon. Not. R. Astron. Soc.* **2022**, *513*, 282–295. [CrossRef]